Co-occurrence of microplastics and microparticles containing heavy metals in sea-surface microlayer in Osaka Bay, Japan

周, 密

(Degree)
博士（海事科学）

(Date of Degree)
2025-03-25

(Date of Publication)
2026-03-01

(Resource Type)
doctoral thesis

(Report Number)
甲第9236号

(URL)
https://hdl.handle.net/20.500.14094/0100496517

Doctoral Dissertation

Co-occurrence of microplastics and microparticles containing heavy metals in sea-surface microlayer in Osaka Bay, Japan

(大阪湾の海表面マイクロ層におけるマイクロプラスチックおよび重金属含有微粒子の残留)

January, 2025

Graduate School of Maritime Sciences
Kobe University, Japan

Mi Zhou

周　密

Contents

Preface

The production and consumption of plastic materials have maintained rapid growth in the past decades. The domestic and industrial plastic wastes are discharged and accumulate in land and aquatic ecosystems, and substantial amounts of plastics end up in marine environment through waterways. Plastic particles that are less than 5 mm in diameter are identified as microplastics. Microplastics widely exist and spread in the sea surface, water column and sediment in marine environment worldwide. Kinds of chemical additives in the polymeric matrix of microplastics can be released into surrounding water and cause endocrine disruptors to marine organisms. Moreover, microplastics are prone to adsorb persistent organic pollutants and heavy metals, and act as vehicles of toxic chemicals in the aquatic environment. Once ingested by marine organisms, the potential ecotoxicity in the microplastics can be transferred through the food chain via bioaccumulation, which may eventually threaten human health.

In addition to being able to adsorb metals from the surrounding water environment, some paint-related microplastics also contain metal additives such as pigments or biocides. It is noteworthy that heavy metals are stable and persistent in environmental ecosystems, and they have been considered as one of the most serious pollutants due to their persistence, bioaccumulation and high toxicity. Although some of heavy metals such as copper (Cu), zinc (Zn) and iron (Fe) acting as essential micronutrients for plants and animals are naturally occurring in the environment, they can be toxic once their concentrations are elevated. Compared with the dissovled metals, heavy metals storged in the particulate matters are prone to be transferrred widely. Especially for microparticles containing heavy metals (metal MPs), they are easily ingested by marine organisms due to their tiny sizes. Eventually, heavy metals may gradually accumulate in the human body through food chains and may generate repercussions. Therefore, except for microplastics, metal MPs are also particulate contaminants that cannot be ignored in the marine environment.

Significantly, paint-related microparticls not only contain heavy metals such as biocides or pigment, but also have polymeric matrix, which determines that they have the characteristics of both microplastics and metal particles. Thus, paint-related microparticles can be considered as a special kind of microplastics containing heavy metals. However, compared with microplastics with similar sizes, paint particles exhibit higher chemical toxicity due to their greater mobility of toxic metal ions and higher concentration of hazardous inorganic additives in the matrix. Noteboly, Cu and Zn are mainly used as biocides in contemporary antifouling paints. Meanwhile, the epoxy, alkyd and acrylic resins are always used as binders in the polymeric matrix of antifouling paints. Antifouling paints are applied on the surface of ships and marine structures to prevent marine organisms such as barnacles and algae adhering, which can reduce navigation resistance and save fuel. For antifouling paint particles (APPs), once they are induced into marine environment, their toxic biocides can be released from the polymeric matrix and generate toxicity to marine organisms. In view of this, the residue of APPs in aquatic environment should be paid more attention.

Although the occurrence and distribution of microplastics in the water column and sediment in the aquatic environment worldwide have been investigated widely, there is relatively little research on the pollution of microplastics in the sea-surface microlayer (S-SML) with a thickness of 50–100 μm uppermost layer. Microplastics are prone to accumulate in the S-SML due to the seawater surface tension and then be transferred to

the atmosphere and water column, which can cause more widespread pollution. Moreover, the residues of APPs containing Cu-Zn-based biocides with stronger toxicity in the marine environment except for the North Atlantic Ocean are still unknown. The assesment of paint-related microparticles in most of the relevant researches is just based on the analysis of polymer types, while the identification on heavy metals therein are always neglected. Therefore, the investigation on the co-occurrence of microplastics and metal MPs in surface seawater can reveal the pollution loads of organic polymers and heavy metals in aquatic environment, and APPs can also be identified based on the analysis on metals and polymers simultaneously, which can highlight the paint-related pollution source of microplastics and provide some theoretical guidance for controlling microplastics pollution.

Based on the above background and our previous studies, the co-occurrence of microplastics and metal MPs in S-SML and bulk water (1 m depth) among different sampling zones including coastal area, navigation routes and center in Osaka Bay in Japan was investigated. In this study, the microplastics, paint particles and particles containing metals are identified as "microplastics (MPs)". The main purposes of this thesis are focused on the following subjects:

1. To assess the occurrence, abundance, spatial distribution, polymer types and sizes of microplastics in all sampling sites to reveal the microplastics pollution status in the surface seawaer in Osaka Bay.
2. To estimate the disparity of microplastics loads among different sampling zones to explore their sources related to shipping activities and marine paints.
3. To investigate the metal types, abundance, spatial distribution and sizes of metal MPs to reflect the pollution status of particulate heavy metals in surface seawater in Osaka Bay.
4. To identify the polymer types of metal MPs to detect the paint-related microplastics and measure the concentrations for Cu and Zn in metal MPs to explore their association with APPs.
5. To create a new highly reliable and accurate method to quantify Cu and Zn in microparticles, which can be used in further related researches.
6. To analysis the correlation between the microparticles with different metal types and microplastics with different polymer types to reveal the diverse sources of these microplastics and metal MPs.
7. To verify the generation of APPs from antifouling paints and investigate the effect of accelerated weathering process of ultraviolet C on the exfoliation and decomposition of APPs.

Chapter I
Introduction

1.1 Microplastics

Microplastics (less than 5mm) pollution in marine environment, firstly highlighted in 1970s, has nowadays become a global concern, due to microplastics small sizes, enormous abundance, ubiquitous distribution, bioavailability and the latent menace they pose to ecosystem [1]. Presence of microplastics is a ubiquitous problem in terrestrial and aquatic ecosystems. Once introduced into aquatic environment by wind transport, stormwater runoff, drainage and sewage system, plastic debris can be transported offshore and enter oceanic gyres by surface currents and winds, which leads to 80% of terrigenous plastic waste accumulating in marine environment [2,3]. For instance, at least 79 thousand tons of ocean plastics are floating inside an area of 1.6 million km^2 at the Great Pacific Garbage Patch (GPGP), where microplastics account for 8% of total mass [4]. Besides residual of primary microplastics with microscopic sizes such as resin pellets and microbeads used in cosmetics and air-blasting media [5,6], secondary microplastics are continuously generated from the breakdown of larger plastic debris due to UV irradiation, mechanical forces and biological processes and they also end up in marine ecosystems [7]. Compared to macroplastics, microplastics can exudate more toxic additives due to larger specific surfaces and fuller exposure in seawater, and they can more vigorously transmit hazardous chemicals to biota [8]. Additionally, microplastics are prone to adsorb persistent organic pollutants (POPs) from surrounding water medium [9]. Once these microplastics are ingested by all kinds of aquatic fauna, they may bioaccumulate and biomagnify via the food web [10]. Microplastics have been discovered in a diversity of seafood items and even in human faeces and blood clots [11,12], as such it can be assumed that humans are exposed to microplastics through their diet. This exposure may compromise fecundity and other somatic processes and potentially threaten to human health [13].

1.2 Paint-related microparticles

Microplastics are synthetic materials composed by polymers and additives [14], and paint particles also contain consistent components with backbones of polymers such as alkyd, epoxy and acrylic resins [15]. Nevertheless, paint particles are always excluded from the category of microplastics due to the omission of paint in marine litter guidelines [16]. Only recently the International Union for the Conservation of Nature (IUCN) did confirm that marine coatings and antifouling paints are also potential sources of marine microplastics [17]. Noteworthy, compared with microplastics with similar sizes, paint particles exhibit higher chemical toxicity due to their greater mobility of toxic metal ions and higher concentration of hazardous inorganic additives in the matrix [18]. The occurrence of floating paint particles in surface seawater has also been reported over the past decade. Paint fragments with a size range of 0.3–23 mm presented a total abundance approximately 30 times higher than that of plastics in the sea surface waters around the Antarctic Peninsula; red paint fragments deriving from hulls were the most abundant [19]. In addition, among the total microplastics in the surface seawater, micro-sized paint particles accounted for 28.42% in the Goiana Estuary of Brazil [20], 7.7% in the Mediterranean Sea [21], 12% around oceanic islands of the Western Tropical Atlantic Ocean [22], 55.45% in the Sinop Sarikum Coast of the Southern Black Sea [23], 25.8% in the Chabahar Bay, Gulf of Oman [24], 33% in the

South China Sea [25] and 15.21% in the Jiangsu coastal area in China [26], respectively. These micro-sized paint particles are mostly suspected to originate from the boat maintenance and cleaning. Moreover, marine traffic and shipping activities seem to produce higher amounts of antifouling and marine paint-related microparticles (MPs). Abundant micro-sized Polymethyl Methacrylate (PMMA) resins have been detected in navigation routes, at the shipping lane in the northwestern region of the German Bight, with a concentration of 1032 ppt in surface seawater, accounting for 83% of total microplastics [27]. Massive amounts of micro-sized alkyd resins have also been found in the southern coast of Korea, with an abundance of 171 items/L in sea-surface microlayer (S-SML), accounting for 81% of total measured microplastics [28]. These paint-related PMMA and alkyd resins in shipping lane may originate from antifouling and marine paints applied on ship hulls.

1.3 Antifouling and marine paints

Biofouling is the undesirable accumulation of micro-organisms, plants and animals on artificial surfaces immersed in water. It is more serious in marine environment because that more than 2500 organisms have been reported in marine fouling communities, which include bacteria, micro-algae, macro-algae, sea-grass, crustacean, and so on. In marine environment, the biofouling caused by these organisms can occur on ships and other submerged structures such as hydropower station, cooling water system for electric power plant, some pipes and cables under water and so on. As shown in Fig.1-1, biofouling inevitably occurs on ship hull bottom during navigation, which leads to the higher frictional resistance and fuel consumption. A 1mm thick layer of algal slime can increase hull friction and fuel consumption by 80% and 17%, respectively [29]. In view of this, antifouling paints are applied on hull bottom to prevent fouling organisms attaching, which can reduce friction resistance and fuel consumption during navigating. Other marine paints such as anticorrosive paints are also used on hull surface to protect metallic substrate from being corroded by seawater. In addition, some marine paints are used on superstructure and upside of ships to matin beauty and gloss.

Many heavy metals are related to antifouling and marine paints. For marine paints, Titanium (Ti), Barium (Ba), Chromium (Cr), Fe, Tin (Sn) and Lead (Pb) are commonly used in pigments, and Cr is also used in anticorrosive agents [15]. For antifouling paints, Cu and Zn are used as biocides to prevent fouling and attachment of marine organisms on hulls [30]- as such it is safe to assume that they reflect the occurrence of antifouling paint particles (APPs). Cu, Zn, Silver (Ag), Cadmium (Cd), Cr, Nickel (Ni), Pb, Sn and Manganese (Mn) have all been detected in antifouling paint residues collected from the hard-standings of a marine leisure boat facility in Plymouth, UK [31]. In Singapore's coastal environment, Zn was the most abundant metal and it most likely originated from the antifouling paint from boats [32]. Given the greater surface area exposed to aqueous medium when in particulate form, metals are predicted to leach from APPs more rapidly [33], which can undoubtedly cause sustained ecotoxicity to aquatic organisms.

Before navigation After navigation

Fig.1-1 Fouled hulls due to biofouling during navigation
(By Fukae Maru Ship Captain Yano)

1.4 Biocides in antifouling paints

As shown in Fig.1-2, total 361 antifouling paint products exist in Japanese antifouling paint market until 2023, among them 277 products (77%), 201 products (56%) and 40 products (11%) contain copper oxide (Cu_2O), copper pyrithione (CuPT) and Zinc pyrithione (ZnPT) as biocides, respectively [34]. Besides, although other biocides including Pyridine triphenylborane, DCOIT (Sea Nine 211), Diuron, Tralopyril (ECONEA), Zineb, Copper thiocyanate (CuSCN), 2,4,5,6-Tetrachloroisophthalonitrile and Medetomidine are also used in antifouling paint formula in Japan, their occurrence frequency is always relatively low (always less than 1%). Moreover, until 2022, in the antifouling paint market worldwide, the occurrence frequency of antifouling paint products containing Cu_2O, CuPT and ZnPT as biocides accounted for 76.1%, 28.8% and 16.7%, respectively [35]. Compared to other biocides, Cu and Zn-based biocides are mostly widely used in antifouling paints in both Japan and other countries. Indeed, Cu_2O has already been identified as a biocide frequently used in antifouling paints [36]. Different from the proportion of biocides in the Japanese antifouling paint market, Zineb, DCOIT, CuSCN, Irgarol, zinc oxide (ZnO), tralopyril, dichlofluanid, copper flake accounted for 11.5%, 9.3%, 8.8%, 4.5%, 4.1%, 3.9%, 3.7%, 2.7%, 1.9% and 1.6% respectively in the use of biocides in antifouling paint products worldwide [35]. In addition, thiram, cupric oxide (CuO), tolylfluanid, tributyltin methacrylate, chlorothalonil, ziram, terbutryn, medetomidine, tributyltin oxide, TCMS Piridina, N-ethyl-2-melthylbenzenesulfonamide and cupric acetate accounted for less than 1% in the frequency of occurrence for biocides in the antifouling paint market worldwide.

In general, there is a main Cu-or-Zn-based biocide along with one or more organic biocides as mentioned above, and these organic biocides act as booster biocides to enhance the toxicity of the metal-based biocides [37]. Therefore, Cu and Zn in some microparticles with polymeric matrix may reflect the biocides component and these microplastics containing Cu and Zn may be identified as APPs.

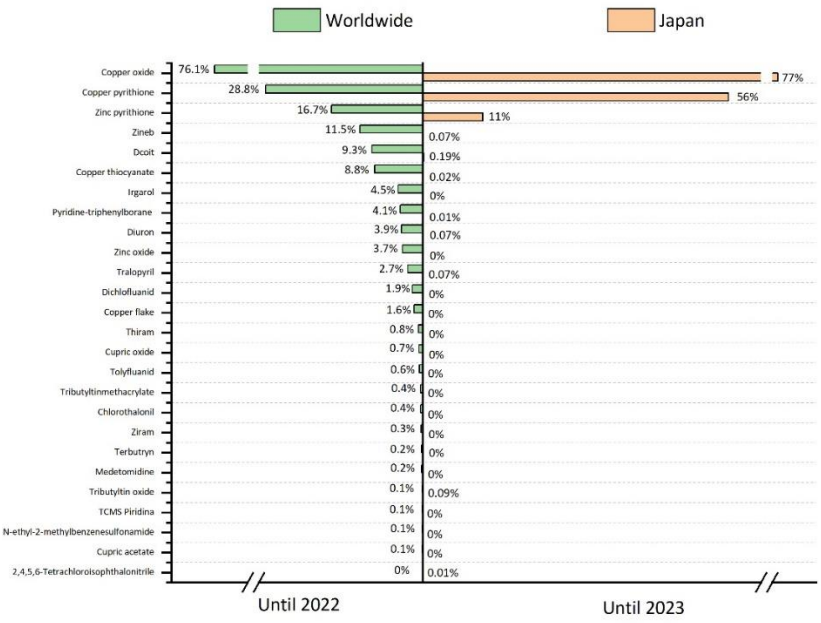

Fig.1-2 The frequency of occurrence (%) for biocides used in antifouling paint products [35]

1.5 Weathering of microplastics and APPs

The weathering processes of microplastics mainly include mechanical fragmentation, photo-degradation, thermal-degradation, and biodegradation [38]. In water column, mechanical fragmentation of microplastics originates from the abrasion and disintegration forces that resulted from their interaction with waves and tide action. Significantly, the photo-degradation is the major weathering process for most microplastics, and the ultraviolet (UV) fraction of light irradiation plays a key role in this weathering process. UV radiation with a wavelength of 290–400 nm in sunlight has enough energy (299–412 kJ/mol) to break the C–C bond (284–368 kJ/mol) and the C–H bond (381–410 kJ/mol) for most plastics. The photo-aging causes the formation of a brittle surface of microplastics, which can accelerate the fragmentation rate after the action of physical forces. Thus, the weathered microplastics always break into more particles with decreased particle sizes. The formation of cracks and fragments in the weathered microplastics provides a larger contact area for chemicals with oxygen or for the aqueous solution, which can promote the chemical leaching of additives from polymeric matrix. These released additives mainly include endocrine disrupting chemicals such as phthalate and bisphenols and produce negative impact on marine organisms [39].

Similarly, APPs also undergo the same weathering process as microplastics, especially the UV weathering. The accelerated weathering process by UV-C have induced the change of chemical properties in polymeric binders of APPs, including the release of volatile components and the formation of hydrophilic groups, which likely impaired the binder's structure then resulted in the increased leaching of metals in freshwater conditions [40]. Compared with non-weathered ones, the concentration of heavy metals was several times higher in the leachates of weathered APPs and contributed to the increased toxicity to the green algae *raphidocelis subcapitata* [41].

1.6 Leaching of biocides from APPs

Once introduced into water environment, APPs can persist in water column and sediment, and the release of biocides is a continuous process. For metallic biocides in APPs, the majority of Cu and Zn is bound in the polymeric matrix in oxidic form (Cu_2O, ZnO), while hydrophobic organic complexes, such as ziram, zineb and Cu- and Zn-pyrithione, are often added as booster co-biocides. The leaching of total Cu and Zn from a composite of discarded antifouling paint residues has been studied over a period of 75 h. Among the discarded APPs samples, hydrophobic Cu and Zn accounted for about 0.15% and 1.4% of the total concentrations for Cu and Zn, respectively. For the leaching of total Cu and Zn from APPs, there is a relatively short period of rapid release (within 20 h) followed by a more protracted period of slower release, finally after 75 h, about 10% of Cu and 5% of Zn had been released from the original antifouling paint composite into the aqueous phase, Cu is more soluble than Zn and is released more rapidly. For the leaching of hydrophobic Cu from APPs, after 75 h, between 1% (light–dark condition) and 2% (constant darkness condition) of total Cu released into sea water was of a hydrophobic nature, which suggested that hydrophobic Cu is released more readily than the principal inorganic form of the metal (Cu_2O or CuCNS). Regarding Zn, hydrophobic forms were observed when the paint sea water suspensions were exposed to light–dark cycles and accounted for about 10% of total aqueous Zn after 75 h, while the hydrophobic Zn was not detected throughout the dark cycles, which may result from the relative stabilities and trans-chelation of metal pyrithione complexes. As a consequence, in shaded, turbid or interstitial environments of coastal waters impacted by boat maintenance activities, Cu pyrithione is predicted to be more long lasting than Zn pyrithione [42].

Prior to 1989, tributyltin (TBT) had been the most effective biocides in antifouling paints, while its usage brought about severe environmental consequences, then it was banded for use until 2003. Later, TBT was succeeded by copper-based antifouling paints, and kinds of organic booster biocides have been introduced to fortify performance of copper-based antifoulants. A wide range of compounds are used as the organic booster biocides in antifouling paints, including, Irgarol 1051, diuron, SeaNine 211, and dichlofluanid [43]. These compounds are directly released from the paint surface into the water and persist according to their physico-chemical properties and the conditions of the environment to which they are released. Iragrol 1051 does not easily degrade [44] and is extremely persistent with a half-life over 226 days under anaerobic conditions, thus Iragrol in sediments always persist [45]. Although Diuron also shows to be extremely persistent in seawater, it degraded much quicker under anaerobic conditions with a half-life of 14 days in marine sediments at 15°C [45]. SeaNine 211 and dichlofluanid were found to completely degrade within 24 h and their anaerobic half-lives were less than 0.5 days, while they degraded at a much slower rate when associated with paint particles [45]. A leaching experiment revealed that a considerable amount of Dichlofluanid (ca. 24 μg/L) leached from 0.4 g/L of APP after the first hour, followed by a marked decline in the amount measured in the water over time, almost degrading after 24 h in seawater, affording less of an environmental threat to non-target organisms [46]. Considering the rapid degradation and less acute toxicity, Dichlofluanid could be considered a good booster biocide in antifouling paint [46].

1.7 Ecotoxicity of microplastics and APPs

Freshwater macro-invertebrates and fish have been reported to ingest microplastics with subsequent trophic transfer to higher predators, including transfer to predatory birds. Physical and chemical damage to aquatic organisms caused by microplastics exposure can result in lethal and sublethal effects on aquatic food web consumers. As a lower trophic aquatic specie commonly found in aquatic environments, microalgae are prone to suffer from the negative effects of microplastics. Microplastics deposition can reduce development of microalgal tissues [47], and positive correlations exist between microplastics concentrations and decreased microalgal growth [48]. The chlorophyll *a* content and photosynthetic activity of *Skeletonema costatum* decreased after exposed to PVC microspheres [49]. The photosynthetic activity of *Chlorella vulgaris*, *Thalassiosira pseudonana*, and *Dunaliella tertiolecta* decreased after exposed to polystyrene microplastics for 72 h [50]. Furthermore, incidental ingestion of microplastics by the other higher trophic aquatic consumers also occurred. Microplastics between 0.01 and 1 mm were found in gut epithelia of *Daphnia magna* and were deposited in lipid storage droplets, disrupting filtration in this crustacean [51]. Increased damage and mortality also occurred after microplastics exposure for long periods in seals, dolphins, and sea snakes [52]. DNA damage was also observed in rainbow trout that ingested microplastics [52]. Moreover, trophic transfer of bio-accumulated microplastics may cause food web toxicity including human health hazards. Microplastics present in marine organisms may cause human health impacts through consumption [53]. The biochemical mechanism of microplastics toxicity may include alteration of lipid metabolism, interaction of reactive oxygen species in the bloodstream, formation of gut barriers, and dysbiosis of gut-inhabiting microbiota [54–56]. In addition, trophic transfer of microfiber microplastics in indoor and outdoor environments may be deposited and translocated into the human tissues [57].

In contemporary antifouling paint formulations, copper-based compounds such as cuprous oxide (Cu_2O) and copper thiocyanate (CuSCN) are used as biocides with supplementation of booster biocides including Irgarol 1051, Sea Nine 211, Diuron, Chlorothalonil, and other metallic compounds like zinc pyrithione (ZnPT) and copper pyrithione (CuPT) to control Cu resistant fouling organisms. These biocides are intended to be environmentally less harmful compared to the organotin biocides such as tributyltin (TBT). However, the problems of toxicity on several marine species are still remained. These biocides were found to be toxic for some algae, invertebrates and fishes. For Cu-based biocides, it can inhibit growth of *Chlorella vulgaris* and *Dunaliella tertiolecta* when Cu concentration is about 4 µg/L and 600 µg/L respectively [58]. Molluscs are moderately sensible to copper oxides such as CuO and Cu_2O when their concentrations are between 1 and 2 mg/L [59]. After 96 h of exposure, copper reduces survival of Pagrus major by 50% at a low concentration 84.4 µg/L [60]. For Irgarol 1051, its toxicity towards photosynthesis of periphyton, for algal reproduction of *S. vacuolatus* and for growth of *Selenastrum capricornutum* and *Enteromorpha Intestinalis* is particularly high [61]. For Sea Nine 211, it shows high toxicity on algae of *Enteromorpha intestinalis*, *Fucus serratus* and *Scenedesmus vacuolatus* even at low concentration, and it also affects the embryonic development and larval growth of invertebrates of both *M. edulis* and *P. lividu* at very low concentrations. For Diuron, it is very toxic to the growth of the marine algae such *Chaetoceros Gracilis*, *Selenastrum capricornutum* and *Chlorella vulgaris*, and is quite toxic to invertebrates such as

juvenile oysters of *Crassostrea virginica* and for embryos of *Paracentrotus lividus*. For Chlorothalonil, it is the most toxic compound to the early developmental stages of three species of marine invertebrates: *Paracentrotus lividus*, *Ciona intestinalis* and *Mytilus edulis*, many crustacean species have been found to be very sensitive to Chlorothalonil such as *Amphiascus tenuiremis*, *Penaeus duorarum*, *Ceriodaphnia dubia* and *Daphnia magna*, and Chlorothalonil has a high toxicity for salmoniform fish in the Galaxiidae family including *Galaxias auratus*, *Galaxias maculates* and *Galaxias truttaceus*. For ZnPT, it appears to be very toxic to algae of *Chaetoceros Gracilis* because only 3.2 µg/L can inhibit their growth, and also shows toxicity to juvenile (physiologically immature/undeveloped) *Elasmopus rapax* and toy shrimps *Heptacarpus futilirostris* even at low concentration [61]. In total, Diuron and Irgarol 1051 seem to be the less harmful to the environment, while Chlorothalonil and Sea Nine 211 are seen to be more toxic.

1.8 Sea surface microlayer

The sea-surface microlayer (S-SML) with a thickness of 50–100 µm in the uppermost layer of the ocean is the interface between the atmosphere and sublayer water [32]. Microparticles in the S-SML can be transferred into the upper marine air through bubbles [62] or sink into the deeper water column or into sediments due to biofouling [63]. Meanwhile, due to the water surface tension and the sticky microgel produced by microbial activity [64], microparticles are prone to accumulate in the S-SML. However, due to the relatively high requirements in time, cost, and equipment for collecting samples from the S-SML, compared with the collection of water column and sediments, investigations on microparticles in the S-SML are few in Japan and worldwide. Considering that microparticles in S-SML may cause widespread pollution between the atmosphere and water environment, the abundance and distribution of microparticles in S-SML should be paid more attention.

1.9 Purpose and main work of this research

Microplastics originate from the release of plastic microbeads during industrial production and the fragmentation of plastic litters that are discharged from the domestic plastic products. Meanwhile, as a special type of microplastics, APPs always fall off from the hull bottom of ships during the process of navigating activities in sea areas and the cleaning and maintenance in shipyards. Once introduced into marine environment, the chemical additives in microplastics and biocides in APPs can leach from polymeric matrix then enter aquatic environment continuously, which can produce toxicity on marine organism including algae, invertebrates and fishes. The UV radiation and abrasion from waves can accelerate the weathering of microplastics and APPs, which can result in their size reduction and abundance increase of these microparticles. These weathered microparticles with smaller sizes are more easily ingested by marine organisms, and they can also generate more rapid leaching of toxic additives and biocides due to their high specific surface area.

Although microplastics have been detected in water column and sediments in seawater worldwide, the investigation and detection on APPs in marine environment is limited. Moreover, researches on anthropogenic microparticles pollution in S-SML where abundant microplastics and APPs are prone to accumulate is still given less attention. In view of this, Osaka Bay, which connects the waters of western Japan and

may reflect its pollution in general, was selected to evaluate the anthropogenic microparticles pollution in both S-SML and bulk water (1 m depth) among coastal area, navigation routes and center of bay. We aimed to (1) investigate the abundance, polymer types, metal types, size ranges and spatial distribution of microplastics and microparticles containing heavy metals in surface seawater in Osaka Bay; (2) identify APPs from these anthropogenic microparticles based on the detection of both polymer types and metal concentrations for Cu and Zn in one microparticle; (3) establish a new reliable and accurate method to measure concentrations for Cu and Zn in one microparticle and provide some new ideas and reference values for further related studies; (4) firstly focused on the co-occurrence of microplastics and microparticles containing metals to reveal their antifouling paints and marine coatings-related sources.

To realize these aims, firstly, the general introduction was given. The histories and current status of enviornmental researches on microplastics and APPs were reviewed. The process of weathering of polymeric matrix and leaching of additivies of microplastics were introduced. Especially, the chemical component, ecotoxicity of additives and biocides in microplastics and APPs were also summarized.

Secondly, the S-SML and bulk water samples in 8 sampling sites among differnet sampling zones including coastal area, navigation routes and center in Osaka Bay were collected from September to June from 2021 to 2023. These surface seawater samples were fitered and processed to obatin anthropogenic microparticles.

Thirdly, the abundance and polymer types of these microplastics with differnet size ranges were observed and counted by the Fourier Transform Infrared Spectrometer (μ-FTIR) and the discrepancy of spatial distribution of microplastics was analyzed. The abundance and metal types of microparticles conatining metals with differnet size ranges were observed and counted by the X-Ray Fluorescence Spectrometry (μ-XRF), and the polymer types of some of these microparticles containing metals were identified by the μ-FTIR. The μ-FTIR spectra of some microplastics and microparticles containing metals were compared with that of commercial marine and antifouling paint particles.

Fourthly, calibration curves obtained from standard paint particles containing different Cu and Zn concentrations with different particle sizes were firstly established. For standard paint particles, this calibration curves reflected the relationship between their fluorescence X-ray intensity (measured by μ-XRF) and their concentrations for Cu and Zn (measured by flameless atomic absorption spectrophotometry (FLAAS)). Considering that these standard paint particles made with commercial antifouling paint have the similar acrylic polymeric matrix with that of Cu-Zn-based microparticles in Osaka Bay, the quantification of Cu and Zn in these microparticles according to the calibration curves is more reliable and accurate.

Fifthly, the principal component analysis and correlation analysis on polymer and metal types of these microplastics and microparticles containing metals were conducted to explore the diverse sources, especially the paint-related sources.

Finally, the antifouling paints on Q235 steel discs were weathered by UVC with different periods, then immersed into rotating artificial seawater. The occurrence and abundance APPs fell off from these painted-samples were observed by μ-XRF, and the concentration of dissolved Cu and Zn leached from APPs in the artificial seawater were measured by the FLAAS.

Chapter II
Microplastics floating in Sea-Surface Microlayer in Osaka Bay, Japan

2.1 Introduction

The production and consumption of plastic materials have maintained rapid growth in the past decades. Plastics have become indispensable due to their versatility, lightweight, low cost, durability, and pliability. Plastic products like plastic bottles, films, packages and containers have been widely used in daily life. These domestic and industrial plastic waste are discharged and accumulate in land and aquatic ecosystems, and substantial amounts of plastics end up in marine environment through waterways. Plastic debris gradually break down into microplastics under a series of weathering conditions including ultraviolet irradiation, abrasion and erosion of waves and biological pollution [3]. Plastic particles that are less than 5 mm in diameter are identified as microplastics [3]. Microplastics widely exist and spread in sea surface [28], water column [26] and sediment [7] in marine environment from nearshore to offshore across the oceans worldwide.

Additives such as plasticizers, flame retardants and stabilizers are more likely to be released from microplastics due to their small size and high surface area. These additives in microplastics have been proved to cause endocrine disruptors to marine organisms [65]. Moreover, microplastics are prone to be clung by persistent organic pollutants (POPs) including polychlorinated, biphenyls (PCBs), polycyclic aromatic hydrocarbons (PAHs), and polybrominated diphenyl ethers (PBDEs) due to their hydrophobic nature [66] and adsorb heavy metals such as copper, lead and nickel [67,68] from the surrounding waters. Therefore, except the hazardous plastic additivities, microplastics can also act as vehicles of toxic chemicals in aquatic environment. Evidence shows that microplastics can be ingested by invertebrates, fish, seabirds, turtles, mammals, and other organisms [69] and cause blockage of metabolic channels mainly including alimentary tract and gut, physical damages, reduced appetite, altered feeding behavior and fatigue which can hinder the growth, development, and reproduction of these marine life [70]. Significantly, the potential toxicity of microplastic can be transmitted through the food chain via bioaccumulation [10], and may eventually accumulate in the human body through seafood consumption, drinking water, and air exposure, thereby threatening human health [71]. In view of this, the investigation on the microplastics pollution situation in Osaka Bay is the prerequisite for evaluating the negative impact of microplastics on marine organisms and even humans in Japan. However, there is relatively little research on the pollution of microplastics in seawater in Osaka Bay. Thus, this study focused on microplastics in the S-SML that may yield extensive and severe microplastics pollution.

In relevant researches on microplastics in surface seawater, it was noted in relevant investigations where manta trawl nets (330 μm mesh) or neuston trawl nets (300 μm mesh) were used for sampling that large-size microplastics (>300 μm) were always detected because smaller microplastics less than 330 μm could not be captured. For instance, microplastics in surface seawater in the South China Sea were found to be around 0.045 ± 0.093 items/m^3 when a bongo net (333 um mesh) was used; however, this was changed to 2569 ± 1770 items/m^3 when a pump was used [72]. In the latter

case, smaller-size fractions (<0.3 mm) contributed 92% of the total microplastics load [72]. Even though tiny microplastics (<50 μm) are significantly abundant [73] and pose a higher risk of being incorporated into organisms' tissues [13] than larger microplastics, few studies identify and evaluate them [57]. Thus, these tiny microplastics have been ignored in many studies due to high-tech instrument requirements and time-consuming determination [74], which can lead to a serious underestimation of microplastics loads in the environment and their corresponding risks [75]. As such, microplastics of 10–53 μm size were especially collected and analyzed in this study.

For evaluating the microplastics pollution status in Osaka Bay in Japan, the present study sought to (1) assess the occurrence and distribution of microplastics loads according to different depths in the water column (S-SML and bulk water) (2) estimate the disparity of microplastics loads among different sampling zones such as navigation routes, coastal area and bay center; (3) investigate the abundance, spatial distribution, polymer types, size distribution and sources of these microplastics. This study can be of significance in providing data on microplastics fate and distribution in a regional or global scale and it can also provide some theoretical guidance for controlling microplastics' pollution. To our knowledge this is the first research on the microplastics pollution in the S-SML in Osaka Bay.

2.2 Materials and Methods

2.2.1 Sampling sites

Osaka Bay, located in western Japan, is connected to the enclosed sea area of Harimanada through the Akashi Strait in the northwest. Eastward water transport always prevails in the Seto Inland Sea due to westerly winds, and significant tidal currents with a complex dynamic mechanism are formed at Akashi Strait, which leads to the contamination of Osaka Bay by the transport of pollutants through this strait [76]. Meanwhile, cyclonic circulation at Osaka Bay both in summer and in winter can also provide impetus to water conveyance from Kii Strait in the southeast finally to the Pacific [77]. Coupled with domestic and industrial activities from international trade ports, large industrial centers and coastal industrial cities in Hanshin Industrial Zone around Osaka Bay, this situation has led to the formation of terrestrial and marine plastic debris arising from the whole of western Japan, which is then exported towards the Pacific.

The sampling sites at Osaka Bay included 3 sampling zones (Fig.2-1 and Tab.2-1); S1, S2 and S3 are located in the coastal area, S4, S5, S6 and S7 are located in shipping navigation routes, and S8 is the center of Osaka Bay. The 4 sampling sites on shipping navigation routes were identified according to Fig.S1.

Tab.2-1 Sampling date, sites, weather and water temperature

Date	Sampling site	Latitude	Longitude	Weather	S-SML water temperature (℃)	Bulk water temperature (℃)
	3	34°38.085'N	135°26.748'E	Sunny	26.6 (10 cm depth)	26.4
15/9/2021	7	34°37.662'N	135°22.834'E	Cloudy	26 (10 cm depth)	26.0
	5	34°35.639'N	135°14.259'E	Cloudy	28.4	28.1
	8	34°33.308'N	135°12.590'E	Sunny	19.3	20.1
15/11/2021	4	34°35.014'N	135°08.558'E	Sunny	19.2	20.3
	1	34°38.310'N	135°10.361'E	Sunny	18.4	18.2
	5	34°35.669'N	135°13.980'E	Cloudy	15.3	15.4
6/12/2021	6	34°38.355'N	135°17.157'E	Cloudy	16.8	16.6
	2	34°40.430'N	135°23.542'E	Sunny	16.9	16.4
11/1/2022	8	34°33.322'N	135°12.575'E	Rainy	10.3	16.0
	5	34°35.602'N	135°14.030'E	Sunny	34.0	30.0
5/9/2022	7	34°37.558'N	135°22.965'E	Sunny	32.5	30.5
	3	34°37.987'N	135°26.942'E	Rainy	31.0	30.2
	5	34°35.553'N	135°13.926'E	Cloudy	23.7	24.6
5/10/2022	6	34°39.121'N	135°16.477'E	Cloudy	24.0	24.8
	2	34°40.298'N	135°25.529'E	Cloudy	24.1	24.5
	8	34°33.848'N	135°12.253'E	Sunny	24.2	22.6
24/10/2022	4	34°34.962'N	135°08.546'E	Sunny	23.7	23.3
	1	34°38.449'N	135°10.496'E	Sunny	22.7	22.7
	7	34°37.472'N	135°22.878'E	Sunny	20.6	20.2
7/11/2022	3	34°38.012'N	135°26.867'E	Sunny	21.6	20.9
	2	34°40.266'N	135°23.535'E	Sunny	22.3	21.2
	4	34°34.962'N	135°08.558'E	Sunny	22.9	21.3
1/6/2023	6	34°38.355'N	135°16.477'E	Cloudy	22.4	21
	7	34°37.662'N	135°22.965'E	Cloudy	21.7	22.7

2.2.2 Field surveys

All water samples were collected from September to June from 2021 to 2023 (Tab.2-1 and 2-2). S-SML was sampled by an electric rotating drum sampler (RDS) with cylindrical drum (diameter 0.25 m, width 0.45 m, surface area 0.353 m^2). Total surface area 212 m^2 of seawater was collected at 20 rotation per minute for 30 min. Meanwhile, bulk water below 1m of sea surface was sampled through a pump (SK-62510, Koshin, Kyoto, Japan) as a contrast substrate. Approximately 10 L seawater samples were collected.

Both S-SML and bulk water samples were filtered by a stainless-steel sieve cascade (φ10cm) (JIS Z 8801, Tokyo Screen, Japan). For the first filtration the sieve was equipped with a 500 μm mesh size filter, the subsequent filtration was performed with a 125 μm mesh size filter, and the final with a 53 μm mesh size filter and then the water was returned to a 10 L tank. Retained microplastics on these sieves with separate size ranges of >500, 125-500 and 53-125 μm respectively, were rinsed into bottles by

ultra-pure water. Microparticles in water samples in tanks were almost less than 53 μm. Water samples in bottles and tanks were sealed and stored on the experimental ship, then carried back to the laboratory.

Tab.2-2 Parameters of water samplings

Date	Sampling site	S-SML volume (kg)	S-SML sampling time (min)	S-SML depth (μm)	Bulk water volume (kg)	S-SML pH	Bulk water pH	S-SML EC (S/m)	Bulk water EC (S/m)	S-SML TOC (ppm)	S-SML DOC (ppm)	Bulk water TOC (ppm)	Bulk water DOC (ppm)
15/9/2021	3	9.5	-	10 (cm)	11.3	7.78	7.81	2.68	3.58	2.84	2.44	2.76	2.30
	7	11.5	-	10 (cm)	10.1	7.95	8.22	3.52	4.43	2.37	2.24	2.32	1.92
15/11/2021	5	10.0	30	47	11.9	8.51	8.43	4.09	4.28	2.90	2.67	2.09	2.08
	8	11.5	30	54	10.7	8.32	8.56	4.89	4.88	3.92	2.81	3.72	2.49
	4	11.8	23	72	11.5	8.11	8.08	4.84	4.85	3.93	1.78	4.06	3.82
	1	11.6	23	71	11.2	7.07	7.98	4.53	4.58	1.96	1.12	3.61	3.51
6/12/2021	5	9.7	30	45	11.9	8.50	8.71	3.70	3.77	46.16	29.73	32.34	22.21
	6	9.9	30	46	12.3	8.16	8.11	3.71	3.63	29.19	23.12	40.82	24.55
	2	10.8	23	66	11.8	7.80	7.85	3.62	3.67	21.31	14.14	47.38	30.02
11/1/2022	8	10.8	40	38	12.2	8.60	8.65	3.35	3.77	15.47	13.82	10.80	9.05
5/9/2022	5	9.0	30	42	9	8.99	9.24	5.01	4.90	33.93	11.91	27.89	2.50
	7	9.3	23	56	9.1	9.37	9.09	3.45	4.53	24.21	5.26	14.49	2.74
	3	10.5	20	74	9.8	9.45	9.06	2.87	3.37	20.71	20.47	8.98	7.45
5/10/2022	5	10.3	22	65	12.2	8.39	8.39	4.90	4.87	0.94	0.25	0.53	0.07
	6	10.6	21	71	12.5	8.48	8.39	4.70	4.79	0.96	0.46	0.63	0.13
	2	11.3	22	72	11	8.80	8.31	3.25	4.45	1.86	1.80	1.06	0.44
24/10/2022	8	10.5	20	74	11.8	8.35	8.34	4.90	4.86	0.67	0.53	0.95	0.56
	4	11.0	18	86	11.3	8.41	8.43	4.92	4.90	0.33	0.14	0.29	0.23
	1	9.8	17	81	10.1	8.63	8.53	4.82	4.79	1.01	0.42	0.30	0.25
7/11/2022	7	11.5	18	90	12.1	8.53	8.56	4.53	4.39	1.05	0.73	0.63	0.36
	3	10.2	18	79	11.6	8.47	8.52	3.29	3.71	1.08	0.81	1.02	0.81
	2	11.3	18	88	11.3	8.22	8.23	4.08	4.51	2.58	1.41	1.47	1.40
1/6/2023	4	11.5	26	87	11.1	8.89	8.87	4.56	2.3	20	1.36	19.5	0.96
	6	11.5	19	78	11.6	9.17	9.24	2.92	4	19.4	1.68	19.7	1.09
	7	11.15	18	86	11.85	9.1	8.81	3.5	4.03	21.7	1.4	2.27	1.28

2.2.3 Laboratory pre-treatment

Microparticles in bottles (with size ranges of 53-125, 125-500 and >500 μm) were filtered through a PTFE filter (POPMF-1000, 10 μm, Wintec, Kobe, Japan) with a diameter of 47mm, and microparticles in tanks (with size < 53 μm) were filtered through PTFE filter (POPMF-1000, 10 μm, Wintec, Kobe, Japan) with diameter of 142mm. The filters with retained microparticles were kept in Petri dishes and dried at 60℃ for 12 h, then 30% H_2O_2 solution was added to the filters to digest organic matter for 1 week. For removing skins and shells of algae and microbe coverings on samples, microparticles with size ranges of 10-53, 53-125, 125-500 and >500 μm on these filters were washed down and filtered through nylon filter with mesh size of 10 μm (#500/520, Tantore), 48 μm (No.305T, AS ONE, Osaka, Japan), 108 μm (No. 150T, AS ONE) and 500 μm (NB-34, AS ONE) respectively. Especially for microparticles of 10-53 μm, this

vacuum filtering process lasted for more than 40 min to make massive algae shells fully air-dried and fixed on a nylon filter, so that microparticles can be completely separated without the disturbance of these residual shells. The microparticles retained on these nylon filters were rinsed apart from the fettered algae shells and filtered through a PTFE filter (H100A013A, ADVANREC, Osaka, Japan, 1 μm, 13 mmφ). Since microparticles of 10-53 μm were easy to clog filter pores when in abundance, they were washed into 100 mL ultra-pure water and then filtered in five times and retained on five filters, rather than just filtered once. Finally, all filters were dried at 60℃ for 12 h and used for microscopic observations. All filtering processes operated in a vacuum filtration system. Microparticles were rinsed by ultra-pure water and filters were dried in the dryer (D-450 FA, AS ONE, Osaka, Japan). The relevant process of water sampling and laboratory treatment is shown in Fig.S2.

2.2.4 Detection and identification of microplastics

Microplastics on filters were observed and counted by Infrared Microscope (AIM-9000, SHI-MAZU, Kyoto, Japan) and their polymer types were analyzed and identified by Fourier Transform Infrared Spectrometer (μ-FTIR: IRTracer-100, SHIMADZU, Kyoto, Japan). For microparticles of >500, 125-500 and 53-125 μm, 1/4 square of filter was chosen and the whole plastic-like particles were detected, then corresponding polymer types and abundances of microplastics were measured and recorded. For microparticles of 10-53 μm, due to their high concentrations and their laborious counting, the particles were counted in three squares of the filter paper only, each of which was randomly assigned from a center, middle, and outer zone of every PTFE filter [78]. One square was 1.6 x 1.8 mm^2 and three squares was approximately 1/9 of the total filtered area (Fig.S3). Microplastics of 10-53 μm on all five filters were counted repetitively in this way. Polymer type of each microplastic could be identified by measuring its transmittance and matching its IR spectrum with that in FTIR polymer spectrum library with a matching degree higher than 70%. All the polymer types found in this study were acrylic resin mainly represented by Polymethyl methacrylate (PMMA), Polypropylene (PP), Polyethylene (PE), Polyester (PET), Polystyrene (PS), Nylon (PA), Polyvinyl chloride (PVC) and others.

For excluding contamination from environmental microplastics such as nylon filters, PS bottles and PE tanks, ultra-pure water was used as the blank water sample to repeat the above processes of treatment and filtration. No microplastics were detected in the blank samples, as such the contamination from the equipment was negligible.

2.2.5 Data analysis

QGIS 3.38.0 (QGIS.ORG, https://qgis.org/ja/site/) was used for mapping sampling sites and Osaka Bay that shown in Fig.2-1. The differences in microplastics abundances in S-SML and the corresponding bulk water below were assessed through the Mann-Whitney U test. In addition, the discrepancy of abundance of microplastics with all polymers and PMMA in S-SML and bulk water among different sampling zones was analysed by one-way ANOVA (Tamhane'sT2 post-hoc test). Simple linear regression was carried out to test the liner relationship between microplastics abundance and size. Pearson correlation analysis was conducted to measure the correlation between microplastics abundance and other factors including polymer types, size ranges of microplastics and depth, pH, salinity, temperature, total organic carbon (TOC) and dissolved organic carbon (DOC) of water sampling. Microplastics sources were summarized by the method of Principle Component Analysis (PCA). The

correspondence analysis was conducted to reveal the relationship among abundances of microplastics with every polymer type, depth, sampling zones and size ranges. All the data analyses were detected by SPSS 19.0 (IBM, New York, NY, USA) and Origin 2021 (OriginLab, Northampton, MA, USA). The curves of polymer spectra were visualized by EZ OMNIC. All the figures were drawn by Excel and Origin 2021.

2.3 Results and Discussion

2.3.1 Spatial distribution of microplastics

As shown in Fig.2-1, microplastics in S-SML and bulk water at Osaka Bay exhibited higher concentrations of microplastics at navigation routes (S4, S5, S6 and S7) than those at coastal area (S1, S2 and S3) and at the center of Bay (S8). Especially in S-SML, microplastics abundance at navigation routes was significantly larger than that at the coastal area (one-way ANOVA Tamhane's T2 post-hoc test, $p<0.05$) and at the center (one-way ANOVA Tamhane's T2 post-hoc test, $p<0.05$).

The average abundance of microplastics at coastal area was 402 ± 179 items/kg (ranging from 104 to 575 items/kg) in S-SML, about 10 times higher than that of 43 ± 16.4 items/kg (ranging from 21.8 to 66.6 items/kg) in bulk water. In addition, the average abundance of microplastics at S1, S2, and S3 was 457 ± 7.78, 373 ± 243 and 390 ± 255 items/kg in S-SML and 48.7 ± 4.67, 43.2 ± 16.4 and 38.5 ± 24.5 items/kg in bulk water, respectively. Little discrepancy of microplastics abundance both in S-SML and bulk water among S1, S2 and S3 indicated a similar microplastics pollution distribution at coastal area.

The average abundance of microplastics at navigation routes was 1360 ± 1050 items/kg in S-SML, about 20 times higher than that of 68.3 ± 49.3 items/kg in bulk water. The maximum abundance among all sampling sites was found at S6, 2310 ± 1390 items/kg in S-SML and 108 ± 73.3 items/kg in bulk water. Other sites at navigation routes had similar microplastics loads. The average abundance of microplastics at S4, S5, and S7 was 1070 ± 1120, 1020 ± 662 and 1040 ± 773 items/kg in S-SML and 56.6 ± 16.2, 71.2 ± 44.8 and 43.9 ± 47.1 items/kg in bulk water, respectively. Most previous studies have shown that microplastics abundances in coastal area were always higher than that in water areas far from shore [18,70, 78, 79], however, in this study, although navigation routes were far from shore, microplastics abundance therein was significantly larger than that at coastal area. We believe that microplastics newly generated in navigation routes had replaced the lost ones due to long-distance transportation from nearshore to further sea areas, which caused that microplastics abundance at navigation routes both in S-SML and bulk water was about 2-4 times larger than that at coastal area. This suggested that the amounts of marine-based microplastics generated during navigation far exceed the amounts originating from land-based microplastics, which is quite different from the widely cited 80% terrestrial- to 20% marine-based microplastics debris ratio for microplastics, as also shown from a study in the German Bight [27]. This may result from generation of particles from antifouling and marine paints during navigating process.

As shown in Fig.2-1, the average abundance of microplastics at the center of the bay (S8) was 261 ± 240 items/kg in S-SML, about 9 times higher than the 33.1 ± 17 items/kg (ranging from 23.4 to 50.9 items/kg) in bulk water. These numbers were the lowest among all sampling sites, and they also reflected the decrease and loss of microplastics from nearshore to offshore.

Fig.2-1 shows the average abundance of microplastics among all different sampling times for every sampling site. However, notably, as shown in Fig.2-2, the

fluctuation in microplastics' abundance among different samplings was extraordinarily large in the S-SML both at S4 (ranging from 342 to 1070 items/kg with a CV of 105%) and S8 (ranging from 62.7 items/kg to 528 items/kg with a CV of 92%). This result may be due to the exchange of seawater through the Akashi Strait in the western side of Osaka Bay. Freshwater inflow from all rivers on lands to the Seto Inland Sea has been reported to be approximately 14 km^3/year (38 × 106 m^3/day) [80], 91% of which corresponding to seawater flows through the Akashi Strait from Harimanada [81]. As such, original microplastics accumulated at S4 and S8 might be diluted by freshwater flows and then transported to the eastern part of Osaka Bay, which led to the relatively lower microplastics' abundances. In total, among all sampling sites, microplastics' abundance in the S-SML always showed larger CV values and presented more intense fluctuation than that in bulk water. At the bay center, where all seawater circulation can flow through, the CV value was 110% in the S-SML and 36% in bulk water, respectively. Thus, we can formulate a hypothesis that in the highly mobile and easily diffused S-SML, microplastics' abundance constantly changes, and a large fluctuation is noted in the process of long-distance transportation and migration.

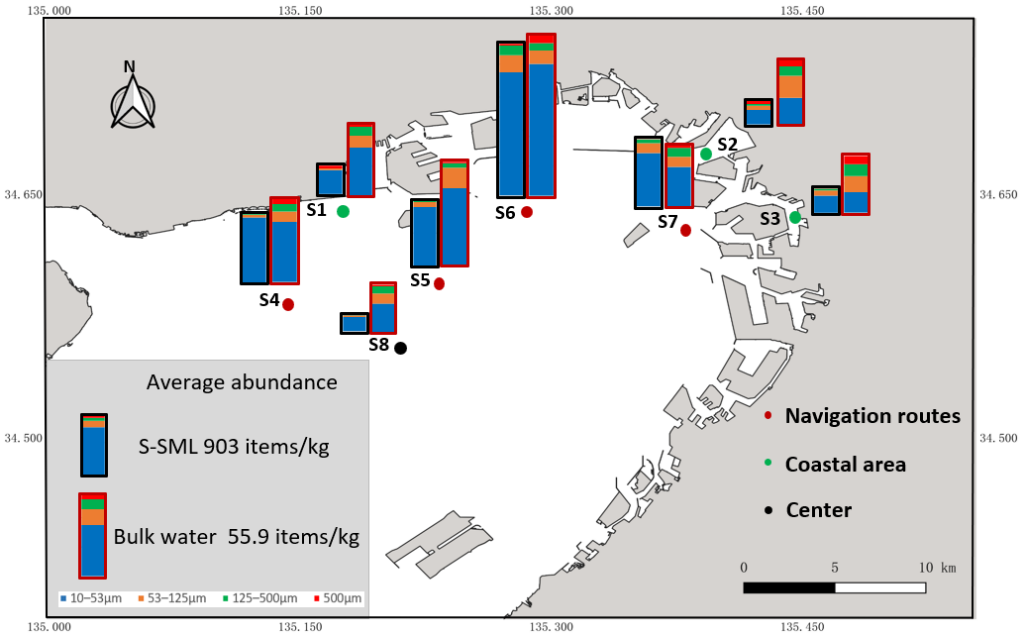

Fig.2-1 Sampling sites and spatial distribution of average MPs abundance

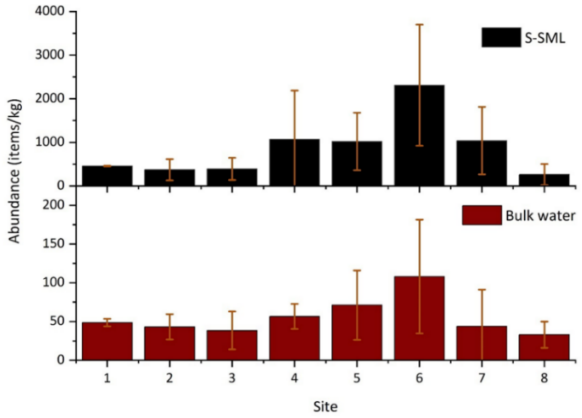

Fig.2-2 Average abundance of microplastics at different sampling sites

2.3.2 Size distribution of microplastics

Microplastics were classified in four size categories: 10–53, 53–125, 125–500, and >500 μm, which accounted for 81.2%, 11.1%, 4.45%, and 3.25% in the S-SML, and for 62.2%, 19.8%, 12%, and 6% in bulk water evenly among all sampling sites, respectively. When distinguishing between substrates, as shown in Fig.2-3 (a), the tiny microplastics (10–53 μm) accounted for 72.1%, 84.6%, and 88.5% of all microplastics in the coastal area, along the navigation routes, and at the bay center, respectively, in the S-SML. In contrast, the tiny microplastics accounted only for 47.4%, 74.4%, and 59.5% for these three zones, respectively, in bulk water. A higher proportion of tiny microplastics (10–53 μm) in the S-SML may result from the accelerated fragmentation of larger microplastics, because weathering forces including wind, biofouling, and UV irradiation are always stronger and more frequent in the S-SML than in deep water [78]. Thus, larger microplastics in the S-SML always undergo a more intensive weathering and break into tiny microplastics more rapidly. In addition, microplastics less than 100 μm in the water column are easily captured by hydrophobic substances such as grease and microbubbles, which then move upwards [82,83], and this may also lead to an increase in tiny microplastics' abundance in the S-SML. It is noteworthy that these exceptionally well floating tiny microplastics (10–53 μm) in the S-SML tend to sink once fouled by algae and invertebrates [3], thus they are transported to the subwater and diffuse the pollution. Hence, further studies should focus on mechanisms of vertical transport of microplastics that can be affected by both intrinsic microplastic buoyancy [84] and hydrodynamic characteristics, including stratification, plume front, and turbulence as well [85]. It should be mentioned that the vertical mixing of plastic particles is probably controlled by wind-induced turbulence, and this leads to a preferential removal of heavier and smaller plastic particles from the sea surface, so traditional surface measurements may have severely underestimated the total plastic content [86]. However, it has been verified that microplastics with a size of 10, 100, and 1000 μm maintain their maximum concentration in the top layer of <1 m [87]. Therefore, in this study, microplastics in bulk water under 1 m from the sea surface may reflect the relatively real microplastics' abundance. In addition, even if the S-SML is disrupted by wind turbulence, it can still be rapidly reformed without depletion of organic matter within 1 min [64]. Therefore, the influence of turbulence on microplastics' abundance in the S-SML can also be excluded in this study.

As shown in Fig.2-3 (b), both in the S-SML and bulk water, as microplastic sizes increased, their relative abundances decreased (simple linear regression, $r^2 = 0.646$, $p < 0.01$ in the S-SML and $r^2 = 0.604$, $p < 0.01$ in bulk water, respectively), which was mostly consistent with previous research results [28]. Microplastics with a size >500 μm were significantly fewer than microplastics of other sizes (one-way ANOVA Tamhane's T2 post hoc test, $p < 0.05$). Microplastics with a size of 10–53 μm were the most abundant compared to microplastics of other size ranges (one-way ANOVA Tamhane's T2 post hoc test, $p < 0.01$) both in the S-SML and in bulk water. Microplastics originating from coastal areas always showed high loads in size ranges larger than 53 μm; this may be because these large microplastics were newly generated and were not yet weathered and broken into smaller fractions. Among the tiny microplastics with a size of 10–53 μm, higher microplastic loads were mainly along navigation routes rather than in the coastal area and at the bay center. These tiny microplastics with larger specific surface areas have increasing sorption capacities, and they can adsorb more pollutants, including persistent organic pollutants (POPs) and endocrine disrupting chemicals, once ingested by organisms, or transported by

circulation over long distances. As such, the threats to marine ecosystems of these tiny microplastics are multiplied.

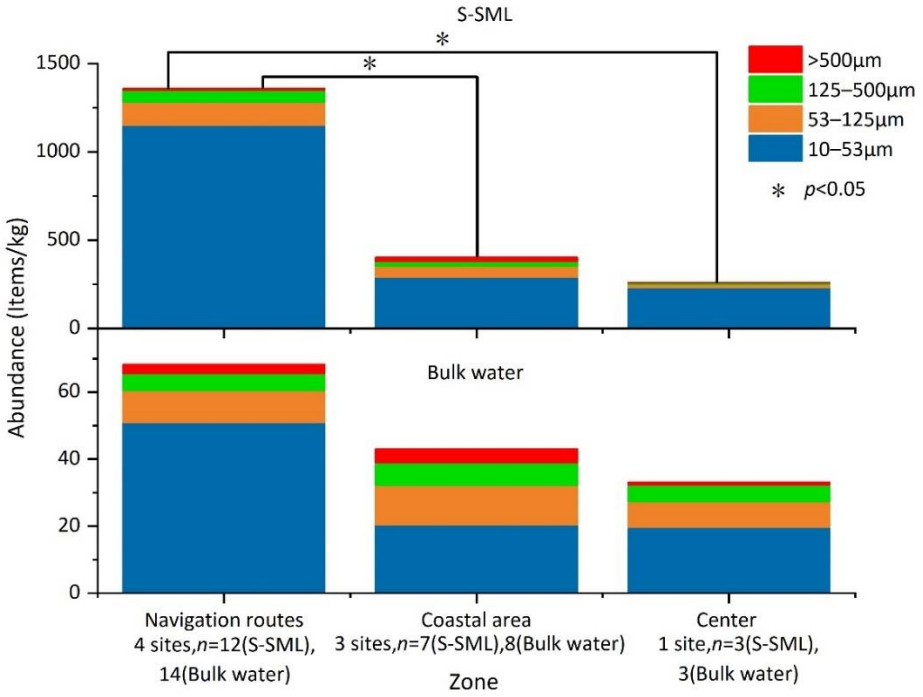

(a)

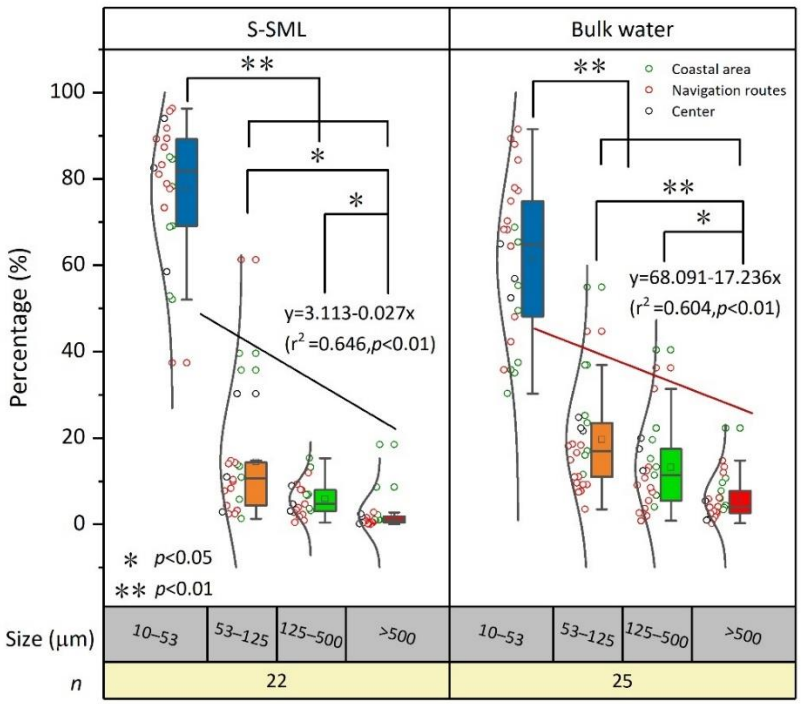

(b)

Fig.2-3 Average abundances of microplastics with different size ranges at different sampling zones (a) and percentage of microplastics with different size ranges at all sampling sites in total (b).

2.3.3 Polymer composition of microplastics

Approximately 11 kinds of polymer types of microplastics were detected at Osaka Bay, i.e., acrylic resins mainly represented by Polymethyl methacrylate (PMMA), Polypropylene (PP), Polyethylene (PE), Polyester (PET), Polystyrene (PS), Nylon (PA), Polyvinyl chloride (PVC), Polyurethane (PU), Polycarbonate (PC), Ethylene-vinyl acetate copolymer (EVA) and Epoxy. Corresponding spectra and pictures observed by μ-FTIR are shown in Fig.2-4 and Fig.2-5. Since abundances of PU, PC EVA and epoxy were relatively few, these four kinds of polymer types were grouped and defined as "others" in this study. Polymethyl methacrylate (PMMA), the most important type of acrylic polymers, is also called acrylic resin [88]. Besides PMMA, other kinds of acrylic polymers were also detected with relatively less abundance by spectra of μ-FTIR, and they were also classified as acrylic resin (PMMA).

As shown in Fig.2-6, PMMA accounted for the highest proportions of microplastics in both S-SML and bulk water, with 95.1% and 45.6%, respectively, followed by PE, PP, PS, PA, PET, others and PVC, which accounted for 1.22%, 1.13%, 0.851%, 0.632%, 0.591%, 0.372% and 0.104% in S-SML, and 16%, 12.8%, 6.99%, 6.56%, 5.88%, 4.27% and 1.9% in bulk water, respectively. In addition, PMMA accounted for 96.8 % in S-SML and 49.8 % in bulk water among all microplastics with 10-53 μm.

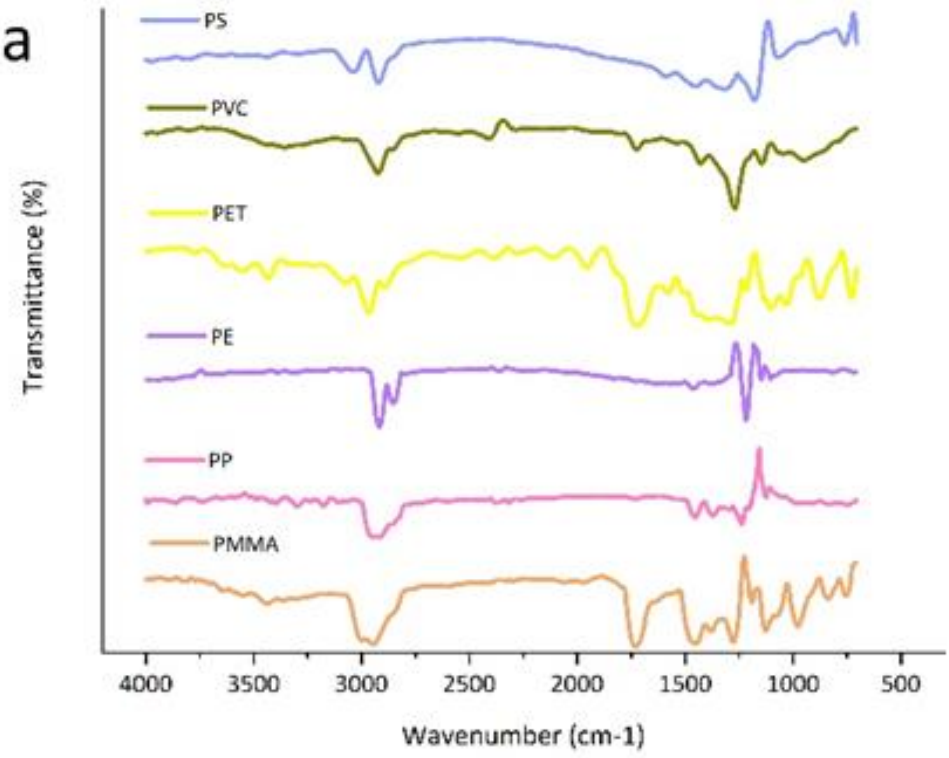

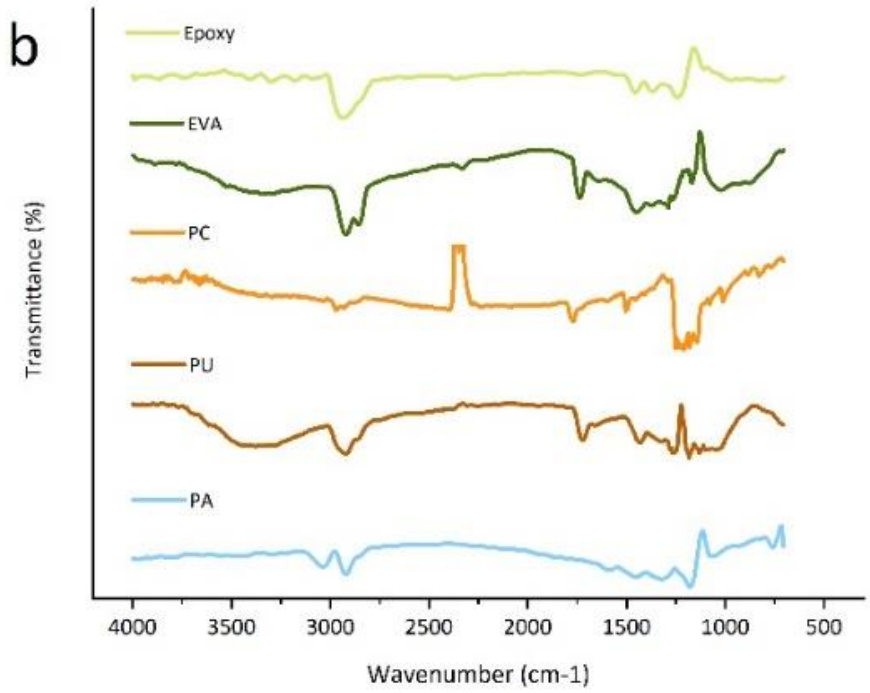

Fig.2-4 μ-FTIR spectra of polymer types of microplastics

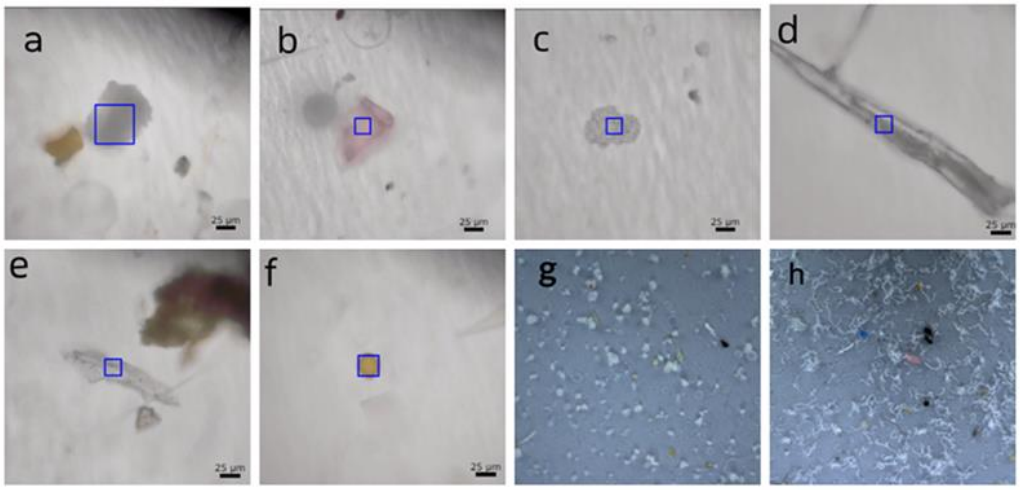

Fig.2-5 Pictures of polymer types of microplastics (a) PMMA (b) PP (c) PE (d) PET (e) PS (f) PA (g) PMMA fragment (h) PMMA fiber

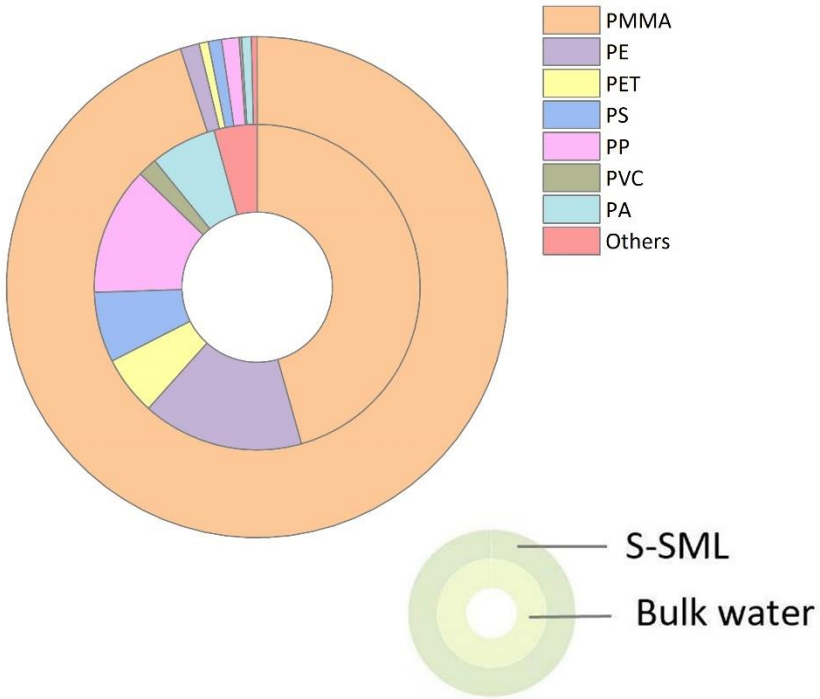

Fig.2-6 Average percentage of every polymer type of microplastics both in S-SML and bulk water

As shown in Fig.2-7, in the S-SML, PMMA dominated all polymer types and accounted for 96.5% (1310 items/kg), 89.9% (362 items/kg), and 88.5% (230 items/kg) along navigation routes, in coastal areas, and at the bay center, respectively. In bulk water, although the percentage of PMMA declined, it was still larger than that of other polymer types and accounted for 49.2% (33.6 items/kg), 36.8% (15.8 items/kg), and 33.7% (11.2 items/kg) at the above sampling zones, respectively. Although the relative density of PMMA is larger than that of the seawater, it still accumulated in the S-SML in large quantities, which can be attributed to the capture capability of the S-SML's tension.

These abnormally high abundances of PMMA were different from the results in other relevant studies which revealed that PP and PE were dominant polymer types in aquatic environments [89]. According to the conclusion of a similar study at the German Bight, PMMA predominated in local major shipping lanes and navigation routes [27]. This study also suggested the antifouling and marine paints on ship hulls were plausible sources for this pollution.

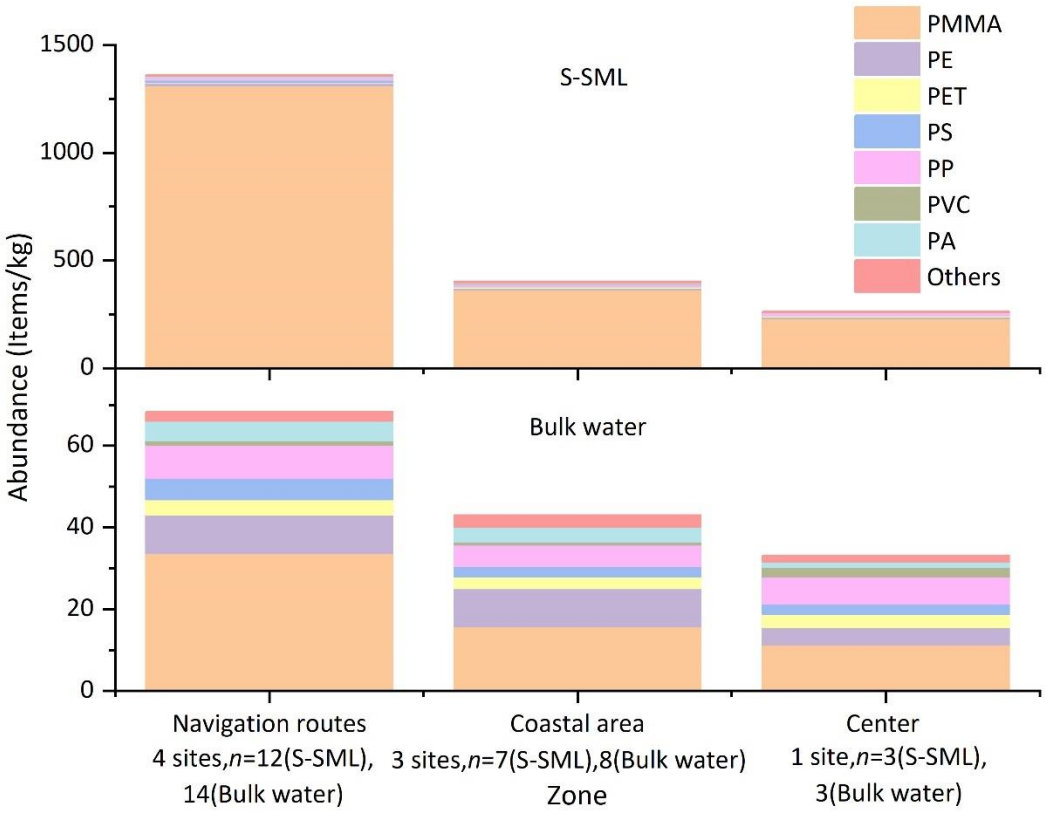

(a)

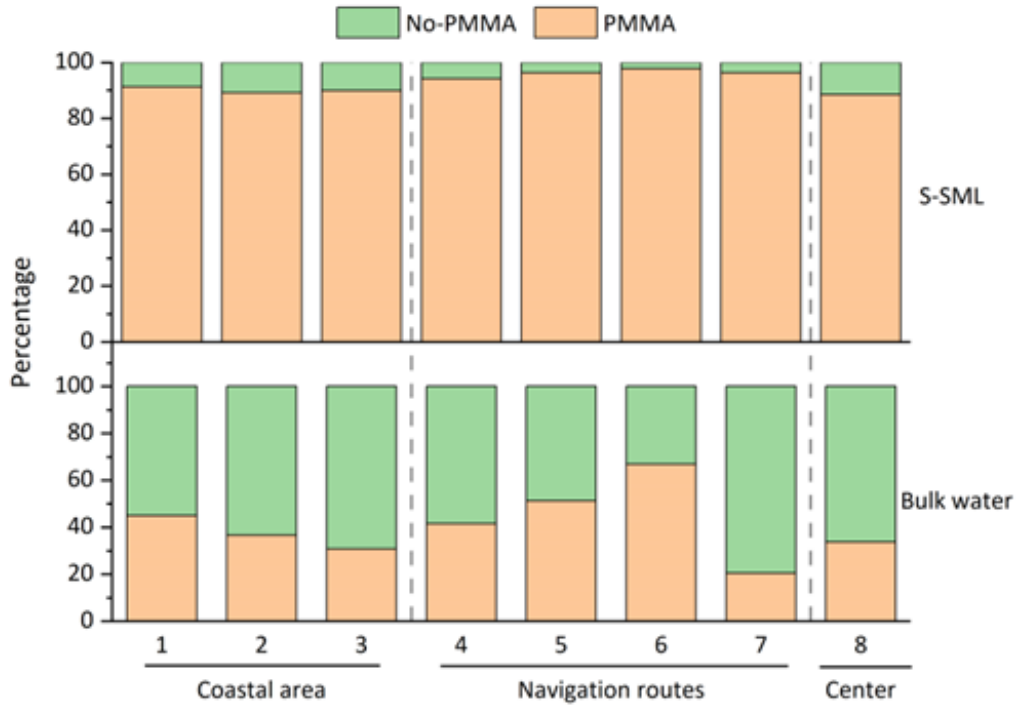

(b)

Fig.2-7 Average abundances of microplastics at different sampling zones with different polymer types (a) and percentage of microplastics with and without PMMA in total (b).

2.3.4 PMMA from marine and antifouling paints

Acrylic polymers such as PMMA stand out among organic coatings because of their non-wettability, chemical inertness, environmental stability, and photostability [90]. Antifouling paint applied on the surface of the hull bottom can prevent the adhesion of fouling organisms and improve speed and reduce fuel consumption for ships. Highly toxic biocides have been incorporated in binders and then are released into water gradually to accomplish antifouling. The use of acrylic resins as binders in antifouling paints can be traced back to 1955 for insoluble matrix or contact paints and to 1974–1985 for self-polishing paints containing tin (TBT-SPC) [91]. Meanwhile, according to the formulas of antifouling paints in Japan, acrylic resins including PMMA were also used as binders [92]. For insoluble matrix or contact antifouling paints, their binders are insoluble in seawater, and pores can be left empty after biocides diffuse out of paint layers, then seawater can spread through these pores and dissolve biocides in deeper binders [91], which may accelerate the abrasion of the honeycomb structure of residual binders with seawater, finally leading to the exfoliation of these acrylic resin fragments without further hydrolysis in a relatively static water column. In addition, for self-polishing antifouling paints that are mainly composed of (meth)acrylic polymer binders [93], as pigments and biocides dissolve faster than the binder hydrolysis, a leached layer is formed at 10–30 μm behind the binder front [94]. Biocides can then be released through a leached layer continuously accompanied by the binder hydrolysis, through which the self-renewing of antifouling paint surface can be achieved [95]. Although (meth)acrylic binders can be soluble in water by hydrolysis of the silyl ester bond [93], for most self-polishing antifouling paints, their antifouling ability mainly depends on the shear of seawater flow and is therefore poor in static seawater [96]. Hence, once the hydrolysis of acrylic binders is prevented by biofilm-covered surfaces, APPs from shipyards by wind and rain runoff may persist in marine environments with a low water flow. In particular, during the navigating process, as hydrolysis occurs, more hydrophilic ester bonds (-COO-) are exposed on the paint surface, which makes the resin on the paint surface brittle and easy to peel off [97]. The friction and collision between the hull and seawater may exacerbate the exfoliation of these resins. Once detached from the hull bottom, these resin fragments can remain in a relatively static water environment without further hydrolysis for a long time, then break into APPs due to UV weathering and biodegradation. By contrast, ships locating in coastal areas are always in a static water environment, and the antifouling paints cannot be hydrolyzed due to the shear of seawater flow; thus, the resins on the surface of paints may not delaminate from the hull bottom. This may lead to a lower APPs' abundance in the coastal area compared to navigation routes. Actually, APPs detected in the coastal area mainly come from ship building and boat cleaning at shipyards.

Besides antifouling paints, PMMA is also widely used in marine paints that are applied on the outboard and superstructure of hulls to maintain beauty and gloss. It is noteworthy that acrylic paints are prone to dehiscing and cracking at low temperatures [98], and it has been verified that some acrylic paints become brittle at 5 ℃with 50% relative humidity (RH) and even at 13 ℃ with a lower RH [99]. Therefore, these PMMA marine paints on upper hulls are also prone to becoming brittle and then falling off from the ship structure when navigating, especially in winter, which can result in abundant white PMMA fragments and fiber residues (shown in Fig.2-4) in the S-SML.

Although microplastics in this study were mainly in the shape of fragments, large quantities of PMMA fibers were found in the S-SML at S2, S3, S6, and S7, and their

abundances were far larger than that of PMMA fragments. Significantly, most of these PMMA fibers were in the size range of 53−125 μm; therefore, they may have originated from UV weathering and wave fragmentation of microplastics with a size of 125−500 μm and >500 μm. If not quickly exchanged with open ocean waters, these PMMA fibers might continuously be broken down and become smaller and more abundant, especially in the local semi enclosed waters at S3 and S7. Thus, PMMA fibers may be deemed to be a special shape of disintegrating vectors through which PMMA fragments decompose from larger sizes to smaller sizes.

To further verify whether PMMA and other acrylic polymers in this study derive from antifouling and marine paints, two kinds of paints (Paint 1 and Paint 2 as shown in Tab.S1) with acrylic polymers as binders were chosen to match with microplastic samples found in Osaka Bay. Paint 1 was used for the outboard and superstructure of hulls to maintain beauty and gloss. As shown in Fig.2-8, the μ-FTIR spectra of sample 1, which belonged to a PMMA fragment in the S-SML, matched with that of paint 1. For sample 1, a peak at 2942 cm^{-1} showed the stretching vibrations of C-H of methylene, a peak at 1731 cm^{-1} attributed to the bending of saturated C=O-, and the asymmetric stretching vibration of ether C-O-C showed between 1300 and 1000 cm^{-1} and had a peak at 1281 cm^{-1}, according to which the polymer type of sample 1 was identified as PMMA. As the μ-FTIR spectra of sample 1 were clearly presented in all PMMA samples and consistent with that of paint 1, these PMMA samples were assumed to originate from marine paints on the upper structures of ships.

Meanwhile, since antifouling paint is one potential source of APPs, the match between microplastic sample and selected paint 2, one kind of antifouling paint, was conducted to verify this hypothesis. As shown in Fig.2-8, sample 2, which was one microplastic fragment in the S-SML, was determined as an acrylic polymer but not as PMMA, and its μ-FTIR spectra showed a significant peak at 2939 cm^{-1} as C-H stretching vibrations, 1714 cm^{-1} as C=O stretching vibrations and 1100, 1204, and 1293 cm^{-1} as C-O-C stretching vibrations, respectively. The μ-FTIR spectra of both sample 2 and paint 2 were consistent, thus pervasive acrylic microplastics represented by sample 2 may derive from antifouling paints. Most notably, the main polymer component in acrylic paints is not just confined to PMMA monomer; other acrylic derivative polymers containing acrylate and methacrylate are also widely used in acrylic paints as binders.

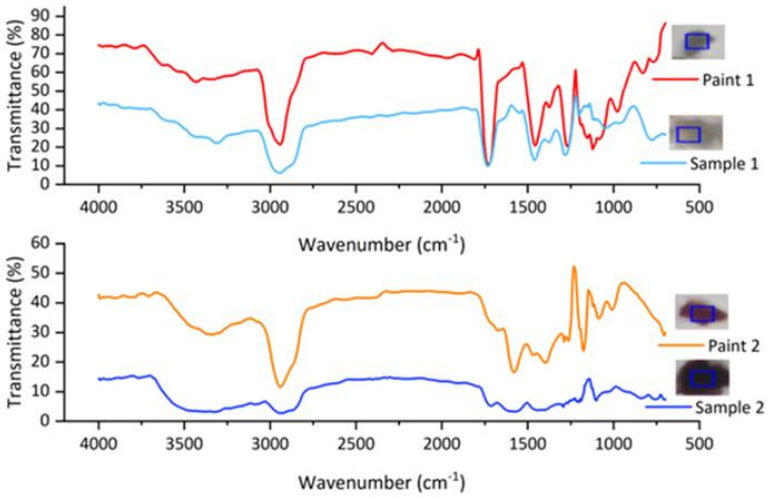

Fig.2-8 FTIR spectra of polymer types from microplastics at Osaka Bay and selected marine and antifouling paints

To exclude the possibility that abundant PMMA microplastics were generated from the experimental ship, antifouling paints were obtained from the bottom hull of the experimental ship and analyzed by μ-FTIR with a spectral result of polyamide 6: poly(ethylene-co-propylene) 4:1, i.e., a blend of PA 6 and PP-PE with a ratio of 4:1, as shown in Fig.2-9. Approximate transmittance values at peaks of spectral reflected a similar weathering degree for both microplastic samples in bulk water and antifouling paints on the experimental ship. As such, some microplastics of the polymer type PA 6:PE-PP 4:1 with small abundances could only come from antifouling paint on the experimental ship. Given that PA has been used in the manufacturing of antifouling paint to modify surfaces for reducing bacterial adhesion [100], different from traditional PA fibers from the laundry of textiles and clothes, PA fragments found in this study may also come from marine coatings.

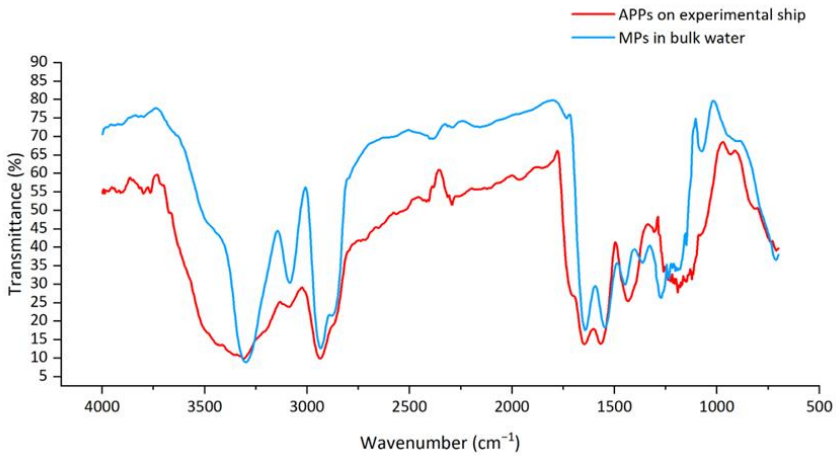

Fig.2-9 FTIR spectra of APPs on experimental ship and microplastics in bulk water

2.3.5 Difference between PMMA and non-PMMA microplastics

As shown in Fig.2-10, in S-SML, the average abundance of PMMA microplastics was 1310 items/kg along navigation routes, 362 items/kg in the coastal area, and 230 items/kg at the bay center, respectively, while 33.6 items/kg, 15.8 items/kg, and 11.2 items/kg were found in corresponding zones, respectively, in bulk water. PMMA microplastics with a size of 10–53 μm contributed the most in both S-SML (85.4% along navigation routes, 75% in the coastal area, and 93% at the bay center) and in bulk water (80.1% along the navigation routes, 47.2% in the coastal area, and 77.3% at the bay center). Especially in the S-SML, the abundance of PMMA microplastics with a size of 10–53 μm along the navigation routes was significantly higher than that in the coastal area (one-way ANOVA Tamhane's T2 post-hoc test, $p < 0.05$) and at the bay center (one-way ANOVA Tamhane's T2 post hoc test, $p < 0.05$). Also, the PMMA abundances of all size ranges were higher along the navigation routes than in the coastal area (one-way ANOVA Tamhane's T2 post hoc test, $p < 0.05$) and at the bay center (one-way ANOVA Tamhane's T2 post hoc test, $p < 0.05$). However, no significant differences in PMMA abundance were found in bulk water for all sampling zones. The abnormally high PMMA abundance along the navigation routes clearly shows that shipping activities brought about massive acrylic marine and antifouling paint particles and produced large amounts of PMMA microplastics with a size of 10–53 μm in the S-SML that may persist along the shipping lanes for months and years.

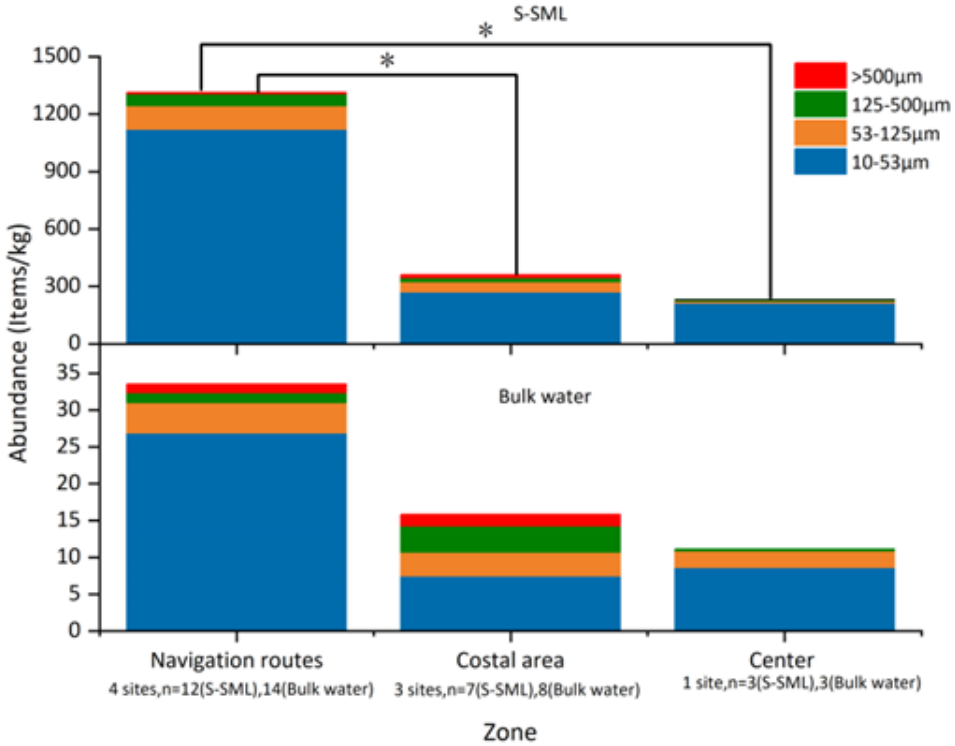

Fig.2-10 Average abundances of PMMA microplastics with different size ranges at different sampling zones

Although the PMMA microplastics abundance in the S-SML was significantly larger than that in bulk water, as shown in Fig.2-11, microplastics that did not belong in the PMMA category (non-PMMA) exhibited a similar abundance level of less than 16 items/kg in both S-SML and bulk water. It could also be verified by the correlation analysis in Fig.2-12, that PMMA abundance was negatively correlated with water depth,

while this was not the case for other polymers. As shown in Fig.2-10, PMMA abundance was the determining factor for the significant differences for the total microplastics' abundance between the navigation routes, the coastal area, and the bay center in S-SML. Moreover, in S-SML, PMMA abundance was obviously higher than that of non-PMMA polymers among three sampling zones. Compared with PMMA, non-PMMA polymers slightly contributed to all polymer types' loads both in S-SML and in bulk water. To some extent, the PMMA abundance can even reflect the whole microplastics loads in the S-SML. As shown in Fig.2-13, the result of the correspondence analysis showed that PMMA microplastics with a size of 10–53 μm along the navigation routes in the S-SML dominated the whole microplastics loads in Osaka Bay. Considering that factors with some similar characteristics always are more likely gather together with close distance in the correspondence analysis, in Fig.2-13, the converged factors of PMMA, 10-53 μm, navigation routes and S-SML reflected a relatively high microplastics abundance loads.

Among non-PMMA polymers, PP and PE presented higher abundance than other polymers both in S-SML and in bulk water. In addition, PET, PS and PA were also more abundant than PVC in general. As shown in Fig.2-12, for PMMA, PE, PET, PP, PS and PVC, their abundances increased as their size became smaller.

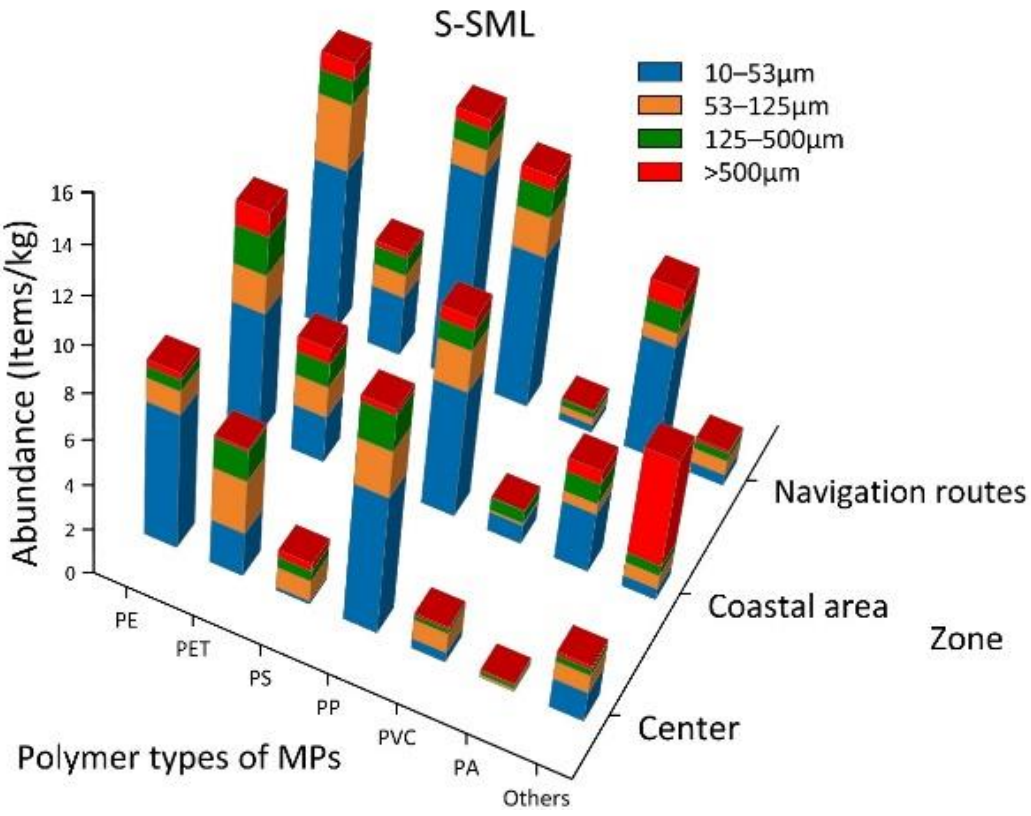

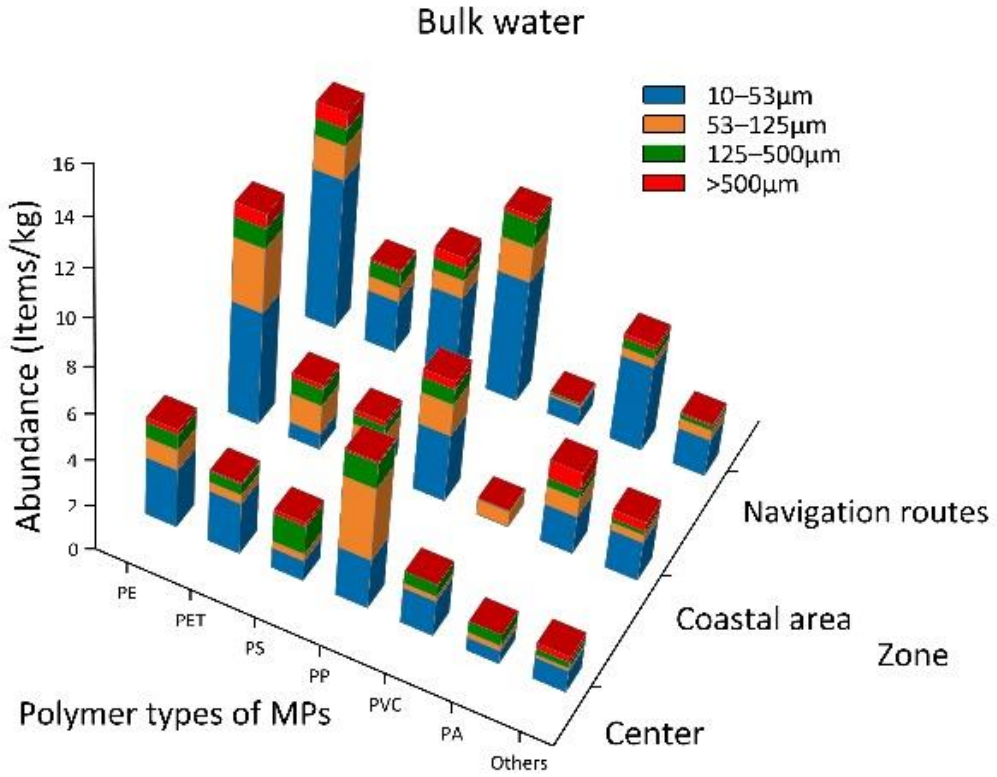

Fig.2-11 Average abundances of non-PMMA microplastics with different size ranges at different sampling zones

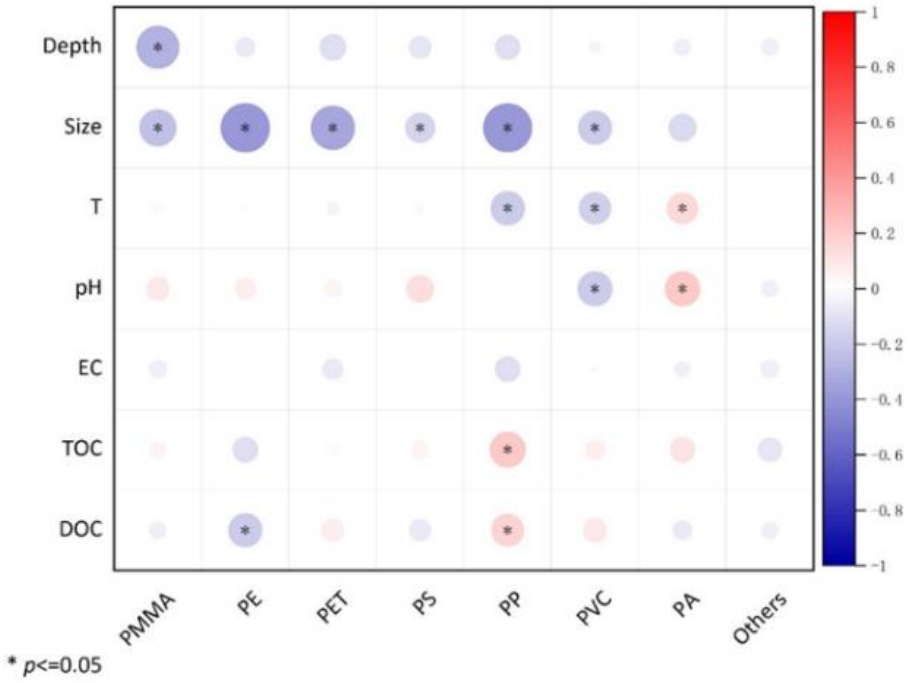

Fig.2-12 Correlation analysis between polymer abundances and seawater and microplastics size factors

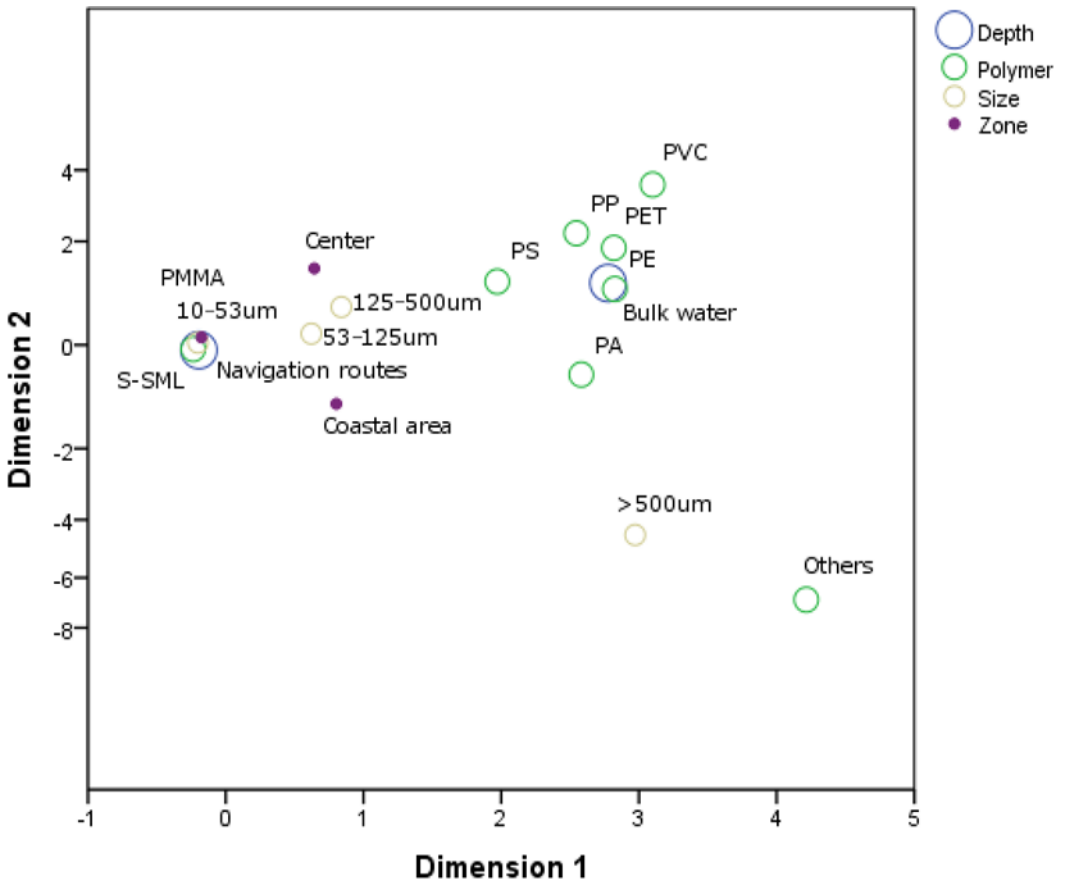

Fig.2-13 Correspondence analysis among depth (S-SML and bulk water), abundance of microplastics of all kinds of polymer, size and sampling zones

2.3.6 Sources of polymer types of microplastics

For assessing the contribution of polymer types of microplastics on polymer abundances and on sampling sites, a principal component analysis (PCA) was performed, and the loadings and 8 sampling sites are shown in Fig.2-14 for the S-SML and bulk water, respectively. For the S-SML, two principal components (several polymers are grouped together due to their similar abundance characteristics and are considered as a principal component) explained 63.1% of the variance in the data, where PC1 contributed 36.5% of the total variance and with positive loadings of PMMA, PA, and PE which have significant variance projection on the X-axis. PC2 contributed 26.6% of the total variance, with positive loadings of PMMA, PP, and PET which have significant variance projection on the Y-axis. For bulk water, two principal components explained 71.4% of the variance in the data, where PC1 contributed 45.4% of the total variance and with positive loadings of PMMA, PP, and PVC which have significant variance projection on the X-axis. PC2 contributed 26% of the total variance, with positive loadings of PE and PS which have significant variance projection on the Y-axis.

According to relevant previous research, sources of all polymer types were categorized as shown in Fig.2-15. Except from marine and antifouling paints, PMMA can also originate from terrestrial paints such as those used in building surfaces, road markings, and so on. In addition, PMMA is also the main component of plexiglass, which is widely used in windows, lamps, and dashboards for everyday use, as well as in the manufacturing of airplanes, vehicles, and instruments. Notably, the United States and Japan have made mandatory provisions in their laws that primary, secondary, and

kindergarten buildings must use plexiglass. Furthermore, PMMA microbeads that are used in cosmetics can enter sewage treatment systems directly and can then be released into aquatic environments as primary microplastics. Occurrence of PP and PE is consistent with their huge global production and wide use in modern life, such as plastic bottles, bags, food packing films, fishing gears, caps and containers due to their low cost and good performance.

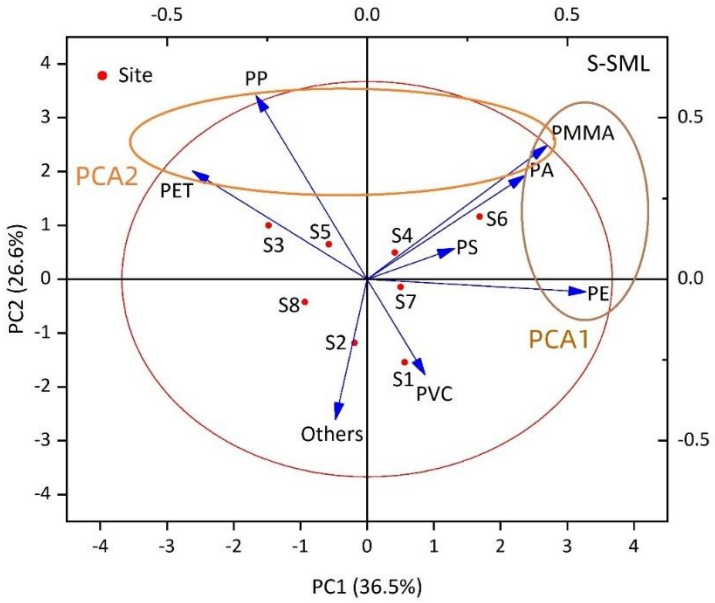

(a)

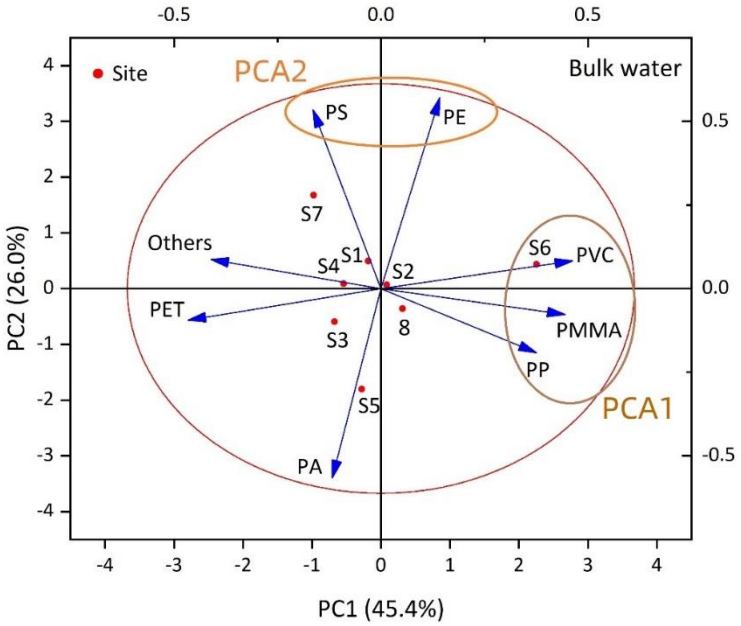

(b)

Fig.2-14 Principal component analysis (PCA) of MPs of all polymer types in S-SML (a) and bulk water (b)

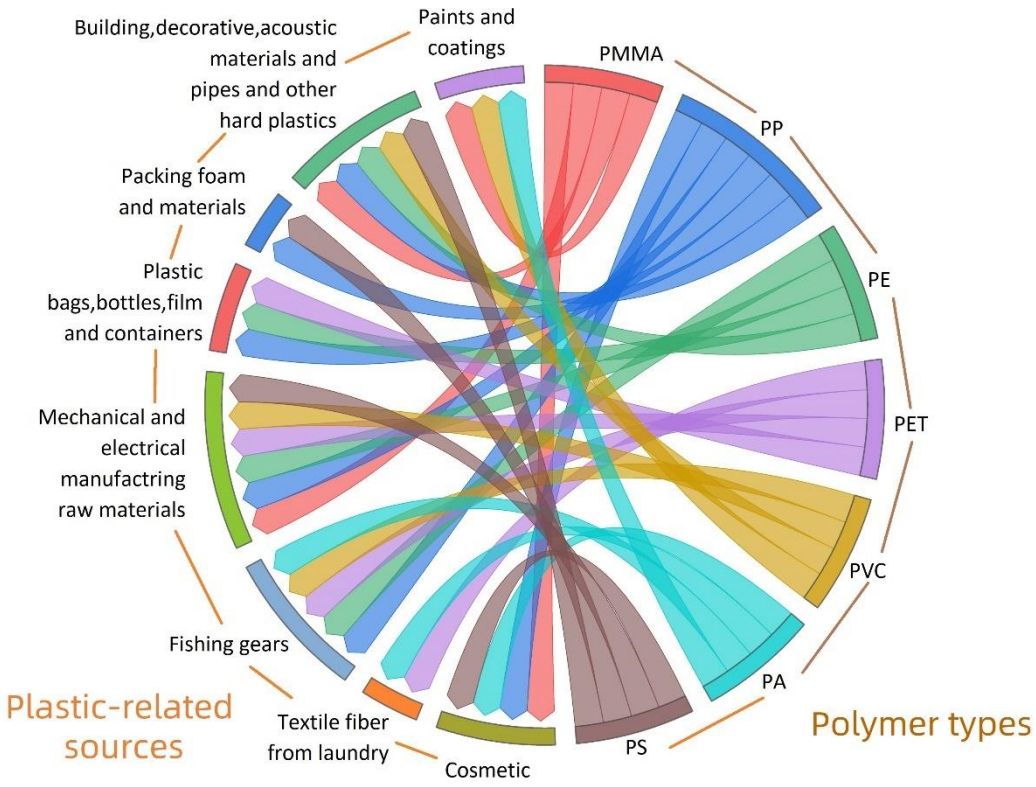

Fig.2-15 Source of microplastics of all polymer types [101–106]

In the S-SML, the strong positive loadings of PA, PE and PMMA on PC 1 mainly reflected the emissions of marine paints and antifouling paints from shipping activities. Site 6 was placed in the direction of the PA loading since it had the highest PA average abundance (14.5 items/kg). In addition, site 6 and site 4—located along navigation routes—were placed in the direction of the PMMA loading because they exhibited the highest PMMA average abundance of 2250 items/kg and 1000 items/kg, respectively, among all sampling sites. Sites 4, 6, and 7 belonging to the navigation routes were aligned on PC1, showing that navigation route sites always generated more paint particles. PC2 was characterized by strong positive loadings of PMMA, PP and PET and showed a linkage with discarded fishing gears generated from fishing activities (fishing nets, ropes, and lines, etc.) according to Fig.2-15. Site 3 and site 5 were aligned on the direction of PET loading because they exhibited the highest average PET abundance of 9.18 items/kg and 5.64 items/kg. The strong negative loadings of PVC and "others" on PC2 may be due to their relatively low "others" had the highest average abundance (11.3 items/kg) at site 2; both site 1 and site 2 abundance, although PVC had the highest average abundance (3.87 items/kg) at site 1 and are located in coastal areas and they had little relationship with fishing activities. To sum up, the PCA in the S-SML seemed to reveal single marine-based MP pollution source due to marine activities including shipping and fishing activities.

In bulk water, PC1 showed the positive loadings of PMMA, PP, and PVC indicating diverse MP pollution sources, which may come from domestic consumption such as plastic packages and containers, building, and decorative materials such as PVC

pipes and other hard plastics. Site 6 on the direction of PVC loading exhibited the highest PVC average abundance of 2.99 items/kg among all sampling sites. PE and PS's positive loadings in PC2 indicated the source of raw materials used in mechanical and electrical manufacturing. PA and PET showed strong negative loadings on PC1 and PC2 because these are fibrous MPs generated from clothes, curtains, and carpets during laundry, which had little relationship with package and building decoration. Site 5 on the direction of PA loading had the highest PA average abundance of 13.1 items/kg among all sampling sites. In total, PCA in bulk water may reflect a complex land-based MP pollution source from daily production and life.

2.3.7 Summary of abundances of microplastics in Osaka Bay

Microplastics were widely distributed in both S-SML and bulk water in Osaka Bay. In the S-SML, the average abundance of microplastics ranged from 261 ± 240 items/kg to 2310 ± 1390 items/kg, with an average abundance of 903 ± 921 items/kg. In bulk water, the average abundance of microplastics ranged from 33.1 ± 17 items/kg to 108 ± 77.3 items/kg, with an average abundance of 55.9 ± 40.4 items/kg. Microplastics' abundance in the S-SML was about 15 times larger than that in bulk water. These are the first abundance-related data available for Osaka Bay.

As shown in Tab.2-3, if 0.45 μm was taken as the minimum size standard, microplastics' abundance in the S-SML in Osaka Bay was much higher than that in Geoje Island [28] and Jinhae Bay in Korea [107] and in Southampton in the UK [108], and microplastics' abundance in bulk water in Osaka Bay was much higher than that in Geojie Island in Korea [28] and Hudson River in US [109]. If 44 μm was taken as the minimum size standard, microplastics' abundance in the S-SML in Osaka Bay was higher than that in Winyah Bay and Charleston Harbor [110] in the US and was similar to that on the Incheon/Kyeonggi Coast in Korea [78], and microplastics' abundance in bulk water was higher than that on the Incheon/Kyeonggi Coast in Korea [78], in the South China Sea [72], in the Terengganu estuary in Malaysia [111], and on the Shore of Rayong in Thailand [112]. Obviously, the abundance of microplastics both in the S-SML and bulk water in Osaka Bay was relatively high in relation to worldwide values.

Tab.2-3 Abundances of microplastics in surface water in the literatures worldwide

S-SML				Bulk water			
Size (μm)	**Country**	**Site**	**MPs abundance (Items/L)**	**Size (μm)**	**Country**	**Site**	**MPs abundance (Items/L)**
>10	Japan	Osaka Bay (This study)	903	>10	Japan	Osaka Bay (This study)	55.9
>0.75	Korea	Geoje Island (Song et al., 2014)	211	>0.75	Korea	Geoje Island (Song et al., 2014)	0.946
>0.75	Korea	Jinhae Bay (Song et al., 2015)	182	>0.45	US	Hudson River (Miller et al., 2017)	0.980
>0.45	UK	Southampton (Stead et al., 2020)	75.4	>50	Malaysia	Terengganu estuary (Taha et al., 2021)	0.546
>53	Japan	Osaka Bay (This study)	170	>53	Japan	Osaka Bay (This study)	21.1
>50	Korea	Incheon/ Kyeonggi Coastal (Chate et al., 2015)	153	>50	Korea	Incheon/ Kyeonggi Coastal (Chate et al., 2015)	1.60
>63	US	Winyah Bay (Gray et al., 2018)	30.8	>44	China	South China Sea (Cai et al., 2018)	2.57
>63	US	Charleston Harbor (Gray et al., 2018)	6.60	>75	Thailand	Shore of Rayong (Prarat et al., 2021)	1.78

2.4 Conclusions

This research highlighted the occurrence and distribution of microplastics pollution in S-SML at Osaka Bay for the first time. Abundant microplastics dominated by the PMMA category were detected both in S-SML and in bulk water with a higher pollution level worldwide. Their concentrations exhibited a distribution trend of larger abundances at navigation routes than that at the coastal area and the bay center, wherein microplastics of 10-53 μm were the most abundant among all size ranges. Considering that microplastics with PMMA and other acrylic polymers retained consistent μ-FTIR spectra with marine and antifouling paints, an abnormally high abundance of microplastics especially PMMA at navigation routes suggested a pollution source from shipping activities. Although microplastics abundance in S-SML was significantly larger than that in bulk water, an abundance of microplastics with other polymers besides PMMA was similar between S-SML and bulk water. As such PMMA was responsible for the large differences in microplastics abundance among navigation routes, coastal waters and bay center. It was also responsible for the significant differences in microplastics concentration between S-SML and bulk water [113].

Chapter III
Microparticles containing heavy metals floating in Sea-Surface Microlayer in Osaka Bay, Japan

3.1 Introduction

Heavy metals are stable and persistent in environmental ecosystems, they have been considered as one of the most serious pollutants due to their persistence, bioaccumulation and high toxicity [114]. Especially, heavy metals are inevitably gathered in ocean from various anthropogenic activities and potentially threaten the health of aquatic organisms [115]. Although some of heavy metals such as copper (Cu), zinc (Zn) and iron (Fe) acting as essential micronutrients for plants and animals are naturally occurring in the environment, they can be toxic once their concentrations are elevated [116]. Noteboly, Cu and Zn are mainly used as biocides in contemporary antifouling paints to eliminate some marine organisms such as barnacles and algae to prevent them from adhering to the surface of ships and marine structures [34], and they are toxic for some algae, invertebrates and fishes. Nonessential metals, such as mercury (Hg), cadmium (Cd), arsenic (As), and lead (Pb) are particularly toxic even in trace amounts [117]. These heavy metals in aquatic environment can be retained in aquatic organisms through bioaccumulation, then accumulate gradually in human body through the consumption of seafood eventually threaten the helath of human beings through food chains [118]. Moreover, those metals have been linked with many diseases, such as nervous system, kidney, and bone diseases [119]. Consequently, heavy metal pollution is considered as a global threat and has been identified as a major environmental problem.

Multiple sources of heavy metals in marine environment include natural and anthropogenic sources, including atmospheric fallout (consisting of both wet and dry deposition), urban sewage, industrial waste, submarine groundwater discharge, and river loadings [120−122]. Various concentrations of Cu, Zn, Pb, Cd, Hg and As in dissolved phase in surface seawater were detected in Jinzhou Bay [123] and in Liaodong Bay [124] in China, respectively. In Singapore's coastal environment, suspended particulate matters were significantly enriched in Cd, Cr, Cu, Ni, Pb and Zn, in S-SML; furthermore, particulate heavy metals were dominant in relation to the dissolved metals. Compared to subsurface mid water column, the highest concentrations of heavy metals both in particulate phase and dissolved phase were mostly observed in the S-SML and bottom water. Zn was the most abundant metal and it most likely originated from the antifouling paint from boats [32].

Among all the heavy metal pollutants, suspended particulate matters are the main sources and play an important role in the transport and storage of potentially hazardous metals [32]. Especially for microparticles containing heavy metals (metal MPs), they are easily ingested by marine organisms due to their tiny sizes. However, there have been a few studies providing some data on metal MPs in seawater in Japan. Therefore, this study focus on the metal MPs floating in S-SML and bulk water to assess their pollution status in surface seawater in Osaka Bay.

Investigation on particulate heavy metals in S-SML can be traced back to 1972; it was found in Narragansett Bay in USA that the enrichment factor of particulate metals (Cu, Fe, and Ni) in S-SML varied from below detection limit to approximately 50 ppb,

when compared to water 20 cm below the surface. These particulate metals in S-SML could also enter the atmosphere and enrich the atmosphere aerosol [125]. In their turn, atmospheric aerosols can be transported many km away depending on the wind and meteorological conditions. As such, anthropogenic particulate metals pollution at remote Antarctic regions due to transportation of aerosols by circumpolar wind had been verified [126]. In view of this, particulate metals transported from S-SML to atmosphere can also cause widespread transmission and pollution. The opposite mechanism can also be noted; S-SML can accumulate particulate metals from atmospheric deposition [32], then these particulate metals can sink and spread into water column and sediment due to gravitational settling. Since abundant microplastics were found in S-SML, much more than in water column, S-SML was also preferentially investigated to research the metal MPs pollution therein.

Considering that microplastics can absorb heavy metals from surrounding water environment, the investigation on metal MPs is helpful to deepen the understanding of the function of microplastics as pollutant carriers and vectors for heavy metals. In addition, given that Cu and Zn may reflect the biocides component from antifouling paints, identifying Cu and Zn in microparticles is also the prerequisite to study and judge the occurrence of APPs in marine environment. Meanwhile, other metal types in microparticles may also reflect the association between metal component and marine paints, which can provide theoretical preparation and basis for the research on paint-related microplastics in seawater. Thus, for all kinds of metal MPs, their sources that are related to antifouling and marine paints from shipping activities should be disccussed particularly.

Considering that abundant microplastics have previously been found in surface seawater in Osaka Bay, metal MPs therein were continued to be investigated to (1) identify the occurrence of metal MPs and their metal types, (2) investigate the abundance, size distribution and sources of these metal MPs in different depths in surface seawater (S-SML and bulk water) and in different marine spatial zones (coastal area, navigation routes and center of the bay), (3) discuss their sources that are related to marine and antifouling paints that are generated from shipping activities. To our knowledge this is the first research on metal MPs in surface seawater in Osaka Bay, which can reflect the pollution of metal MPs in S-SML in recent years.

3.2 Materials and Methods

3.2.1 Metal MPs sampling and processing

The collecting method and laboratory pre-treatment of all microparticles on filters were carried out according to 2.2.2 and 2.2.3. Among these collected microparticles, metal MPs are included. The microparticles were collected during the years 2021–2023 in surface seawater in Osaka Bay described in 2.2.1. An electric rotating drum sampler and pump sampler were used to collect S-SML and bulk water, respectively. Both S-SML and bulk water were sequentially filtered by stainless-steel sieves (φ10 cm) (JIS Z 8801, Tokyo Screen, Japan) with mesh-sizes of 500, 125 and 53 μm, then the waters were returned to a 10 L tank. Microparticles captured on these sieves were rinsed into bottles by UPW. After to laboratory, microparticles in these bottles and tanks were filtered by PTFE filters (POPMF-1000, 10 μm, Wintec, Kobe, Japan) with diameters of 47mm and 142 mm, respectively. Microparticles on filters had been classified by size ranges of 10–53, 53–125, 125–500 and >500 μm. These filters with microparticles of every size range were kept in petri dishes and dried at 60℃ for 12 h, then 30% H_2O_2 solution was added onto these filters to digest organic matter for 1 week. After this, the

microparticles on these filters were rinsed by UPW was filtered through nylon filters with corresponding mesh sizes respectively, and microparticles captured on these nylon filters were rinsed into PTFE filter (H100A013A, ADVANREC, 1 μm, φ13 mm, Wintec, Kobe, Japan) for the last filtering. Finally, all filters were dried at 60℃ for 12 h in an oven (D-450 FA, AS ONE, Osaka, Japan) and used for microscopic observations.

3.2.2 Detection and identification of metal MPs

The microparticles on filters were observed and their metal types were identified by the X-Ray Fluorescence Spectrometry (μ-XRF: XGT-900, HORIBA, Kyoto, Japan). Compared to inductively coupled plasma-mass spectroscopy (ICP-MS) that has been widely used to measure metal elements in seawater in previous relevant studies [32,124], μ-XRF can detect multiple types of metals in one solid particle simultaneously. For microparticles of >500, 125–500 and 53–125 μm, all of them on filters were determined by the μ-XRF and their metal types and corresponding abundances were recorded. For microparticles of 10–53 μm, due to their high abundances and laborious counting, just five squares of the filter were randomly selected, and metal MPs therein were identified and counted as mentioned above. One square was 1.4×1.4 mm^2 and five squares were approximately 1/8 of the total filtered area (78.5 mm^2). The relevant process of water sampling and laboratory treatment is shown in Fig.S4.

3.3 Results and Discussions

3.3.1 Types and potential sources of metal MPs

Through the μ-XRF detection, 7 main kinds of metal components were detected in microparticles both in S-SML and bulk water in Osaka Bay, i.e., Cu, Cu and Zn (Cu-Zn), Zn, Ti, Sn, Fe and Mn or Ni (Fe-Mn-Ni) and Ba. The spectra and figure of each representative metal microparticle are shown in Fig.3-1 and Fig.3-2. These metal MPs may originate from dumping of industrial and household waste from urban drainage [127] and atmospheric deposition[32], but they may also come from the antifouling and marine paints used on boats and ships, especially for Cu and Zn MPs [15]. In addition, microplastics can also adsorb trace metal ions from their surrounding seawater [128]. The accumulation of trace metals onto these microparticles may cause negative impacts on marine life [129], and compared to similarly sized microplastics, paint particles always present higher chemical toxicity due to the presence of hazardous metals [18].

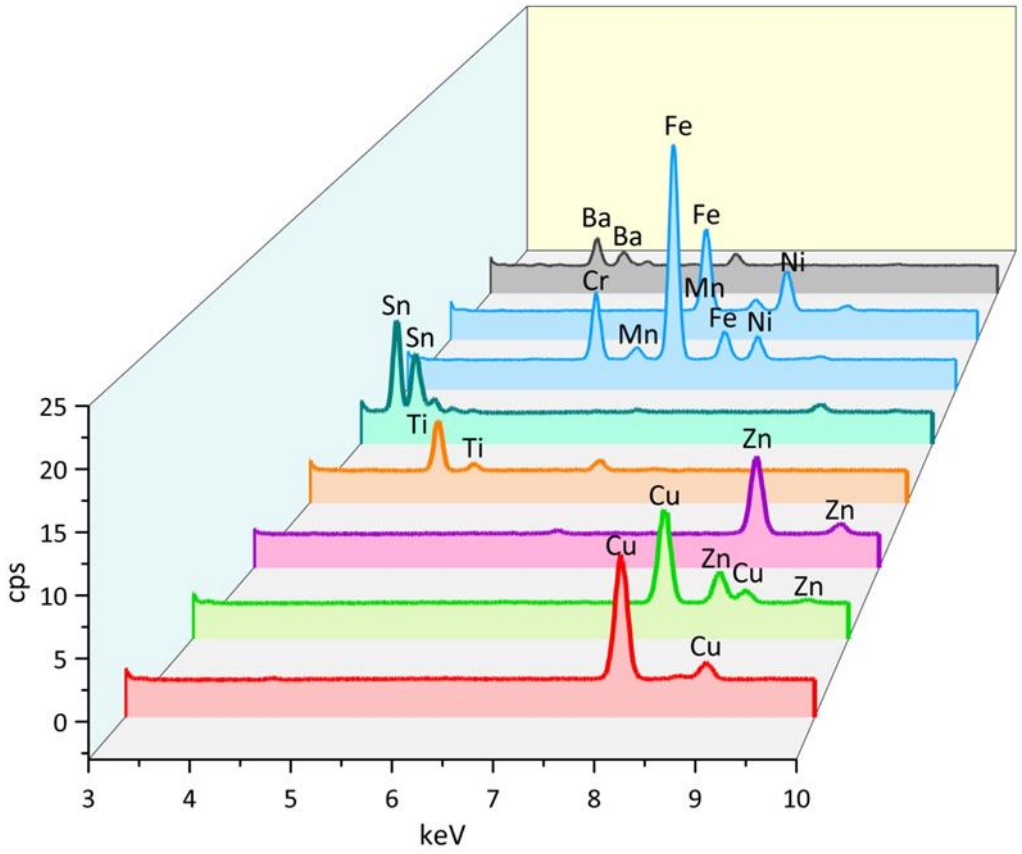

Fig.3-1 Metal element detected in microparticles by μ-XRF spectra (Mono capillary)

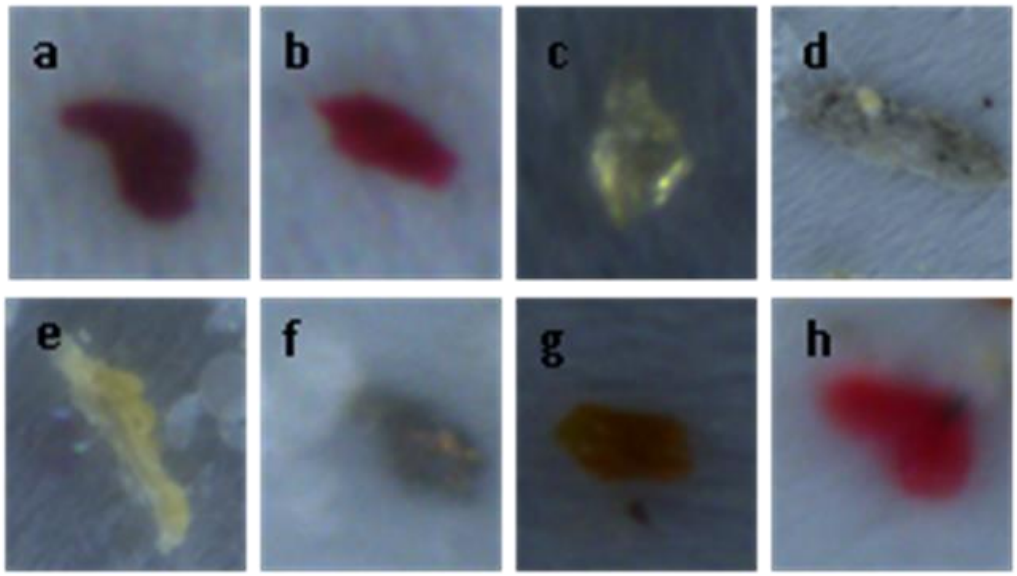

Fig.3-2 μ-XRF picture of microparticles containing various metal components
(a) Cu MP, (b)Cu-Zn MP, (c) Zn MP, (d) Ti MP, (e) Sn MP, (f)Fe-Mn, (g) Fe-Ni MP, (h) Ba MP

3.3.2 Spatial abundance distribution of total metal MPs

As shown in Fig.3-3, metal MPs were detected by μ-XRF at all sampling sites. The average abundance (MPs items in 1 kg seawater) of metal MPs was 38.8 items/kg in S-SML and 54.3 items/kg in bulk water, respectively, while there was no significant difference between them (p>0.05, Mann-Whitney U test). Also, metal MPs abundance was distributed without significant difference between coastal area, navigation routes and center (p>0.05, one-way ANOVA Tamhane's T2 post-hoc test), which indicated that metal MPs have a relatively uniform distribution in abundance in surface seawater in Osaka Bay.

As clearly shown in Fig.3-3, Ti-MPs and Fe-Mn-Ni MPs contributed huge amounts of metal MPs at all sampling sites. Both in S-SML and bulk water, Fe-Mn-Ni MPs abundance was significantly higher than that of Ti MPs (p<0.05, Mann-Whitney U test) and of other metal MPs (p<0.01, Mann-Whitney U test), meanwhile, Ti MPs abundance was also significantly higher than that of Cu, Cu-Zn, Zn, Sn and Ba MPs (p<0.01, Mann-Whitney U test). Fe was the most abundant metal found in metal MPs in this study. This was mostly consistent with previous relevant research in the Bohai Bay in China, where mass concentration of Fe was higher than that of other metals in suspend particulate matter [130].

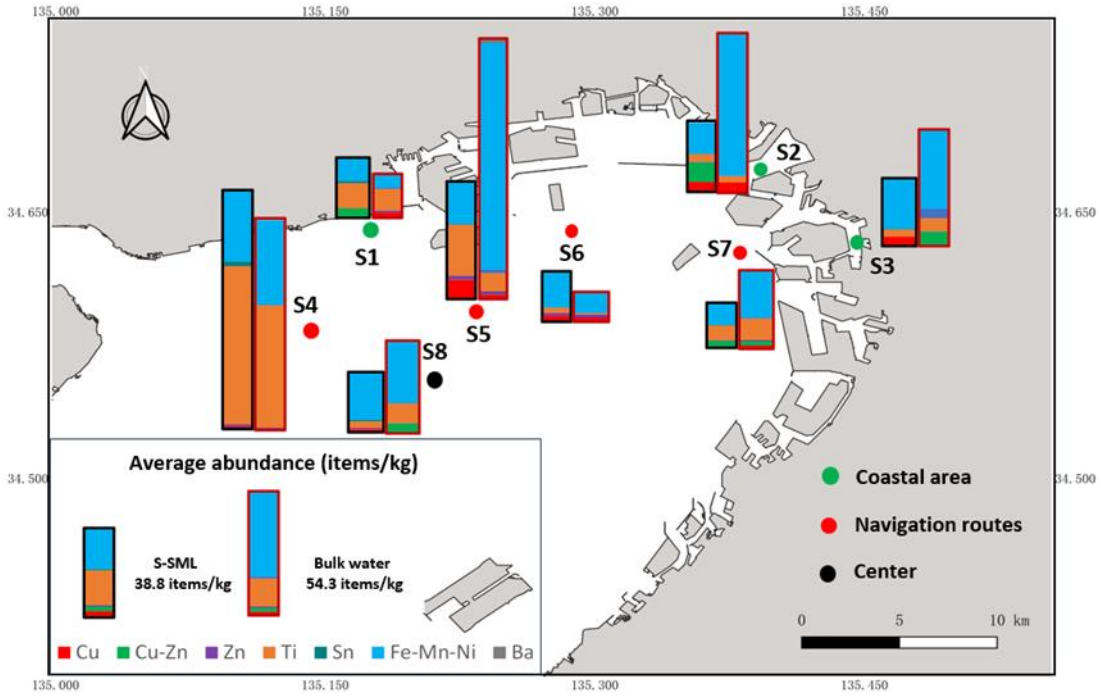

Fig.3-3 Sampling sites and spatial distribution of average abundance of metal MPs

3.3.3 Spatial abundance distribution of every kind of metal MPs

The distribution of average abundance of Cu, Cu-Zn and Zn MPs at different sampling sites is shown in Fig.3-4. The average abundance of Cu, Cu-Zn and Zn MPs was 2.83±5.79, 2.05±5.65, 0.68±1.26 items/kg in S-SML, and 1.6±2.52, 1.72±5, 0.61±1.27 items/kg in bulk water, respectively. In total, Cu and Cu-Zn MPs retained a similar abundance level, and their abundance was about 3 times higher than that of Zn

MPs. Except in S-SML at Site 7 and bulk water at Site 8, Cu MPs were detected in the remaining sampling sites with an average abundance higher than 1 items/kg. The maximum abundance of Cu MPs was found at Site 5 in S-SML with 8.71±15.09 items/kg and at Site 2 in bulk water with 4.75±5.03 items/kg, respectively. For Cu-Zn MPs, the maximum abundance was found at Site 2 in S-SML with 8.53±14.1 items/kg and at Site 3 in bulk water with 7.27±12.4 items/kg, respectively. Among 16 surface water samples collected in both S-SML and bulk water at 8 sites, Cu-Zn MPs were not detected in 7 samples, which reflects the uneven distribution of Cu-Zn MPs. Except for S-SML at Site 1, Zn MPs were detected in all remaining sites and their abundance fluctuated within 1 items/kg among most sites. The maximum abundance of Zn MPs was found at Site 5 in S-SML with 1.71±2.79 items/kg and at Site 6 in bulk water with 1.42±1.91 items/kg, respectively. Zn MPs always exhibited a relatively uniform distribution among all sites. In total, Cu-based MPs always presented a higher abundance level than Zn MPs, which may be related to the widespread application of Cu-based biocides in contemporary formulations of antifouling paints if associated with APPs.

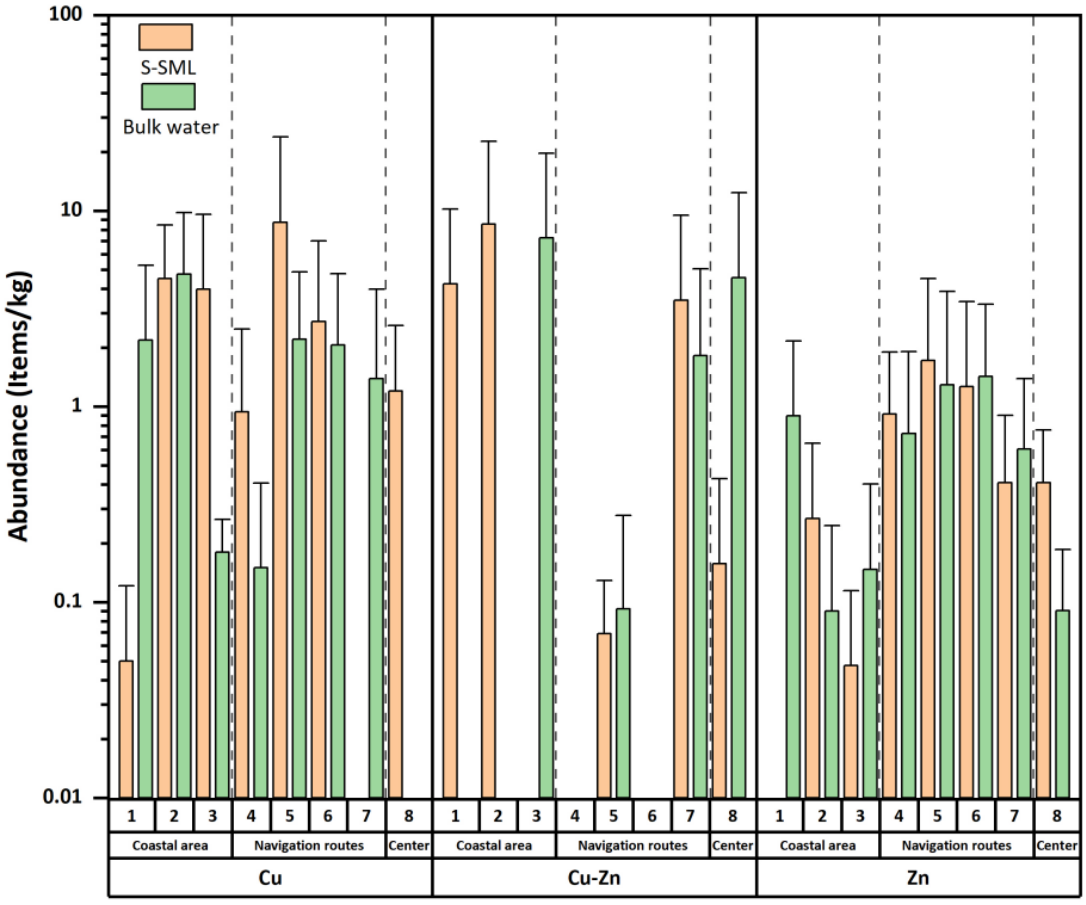

Fig.3-4 The distribution of average abundance of Cu, Cu-Zn and Zn MPs at different sampling sites

The distribution of average abundance of Ti and Fe-Mn-Ni MPs at different sampling sites is shown in Fig.3-5. The average abundance of Ti and Fe-Mn-Ni MPs was 15.9±41, 17.8±19.2 items/kg in S-SML, and 12.1±26, 40±72.5 items/kg in bulk water, respectively. The abundance of Ti MPs and Fe-Mn-Ni MPs retained in a similar level, which was significantly higher than that of other kinds of metal MPs ($p<0.05$).

The maximum abundance of Ti MPs was found at Site 4 with 69.4±108 items/kg in S-SML and 53.5±71.2 items/kg in bulk water, respectively. Ti MPs at most sites presented the abundance fluctuation ranging from 1 to 10 items/kg. If associated with marine paints, compared to Cu, Cu-Zn and Zn MPs that may come from antifouling paints on hull bottom, the wider distribution and higher abundance of Ti MPs may reflect a higher pollution degree of paint particles from superstructure of hulls due to the application of Ti as pigment in marine paints. The maximum abundance of Fe-Mn-Ni MPs was found at Site 4 in S-SML with 30.8±41.7 items/kg and at Site 5 in bulk water with 99.2±180 items/kg, respectively. For Fe-Mn-Ni MPs, they always presented the abundance higher than 10 items/kg at most sites, and they were also prone to deposit and gather with high abundance more than 20 items/kg in bulk water, this may be attributed to their higher metal density with less polymer component. If associated with pollution from shipping activities, the occurrence of these abundant Fe-Mn-Ni MPs in surface seawater may reflect a relatively severe pollution from the metal debris of hull substrate of carbon steel containing main component of Fe. In addition, the heavy fuel oil used as fuel by ship engine may also become a potential source of these Fe-Mn-Ni MPs. Sulfur, V, and Fe are typical components of the fuel [131], and Mn and Ni were also found in the use engine oils [132]. Actually, Fe has been detected in the particulate matters which were transferred from the fuel to the emissions [131]. Once the particulate matters in the exhaust gases from shipping activities enter the seawater through atmospheric deposition, these Fe-Mn-Ni MPs can become a metallic pollution in the marine environment.

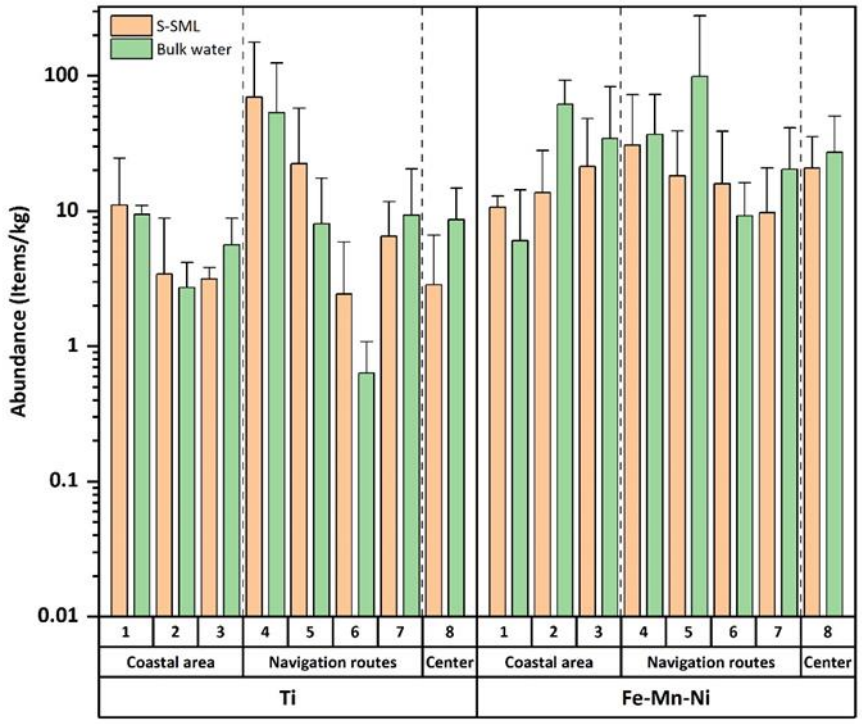

Fig.3-5 The distribution of average abundance of Ti and Fe-Mn-Ni MPs at different sampling sites

The distribution of average abundance of Sn and Ba MPs at different sampling sites are shown in Fig.3-6. The average abundance of Sn and Ba MPs was 0.54±1.26, 0.0386±0.159 items/kg in S-SML, and 0.928±1.78, 0.296±0.814 items/kg in bulk water, respectively. The Sn MPs presented a similar abundance level with Zn MPs. Ba MPs undoubtedly were the fewest among all kinds of metal MPs. The maximum abundance of Sn MPs was found at Site 4 in S-SML with 1.97±3.42 items/kg and at Site 3 in bulk water with 4.25±3.55 items/kg, respectively. The abundance of Sn MPs at most sites were higher than 0.1 items/kg. Among 16 surface water samples collected in both S-SML and bulk water at 8 sites, the occurrence of Ba MPs was verified in 6 samples, and the maximum abundance of Ba MPs were detected at Site 3 in S-SML with 0.38±0.54 items/kg and at Site 5 in bulk water with 1.49±1.74 items/kg. The low occurrence and abundance of Ba MPs may suggest that the pollution from Ba-related pigments and additives in paint and coatings is not prevalent in marine environment if they are associated with paint-related microparticles. Compared to Ba MPs, the higher loads of Sn MPs may reflect the residues of TBT antifouling paint with historical formula if associated with paint microparticles.

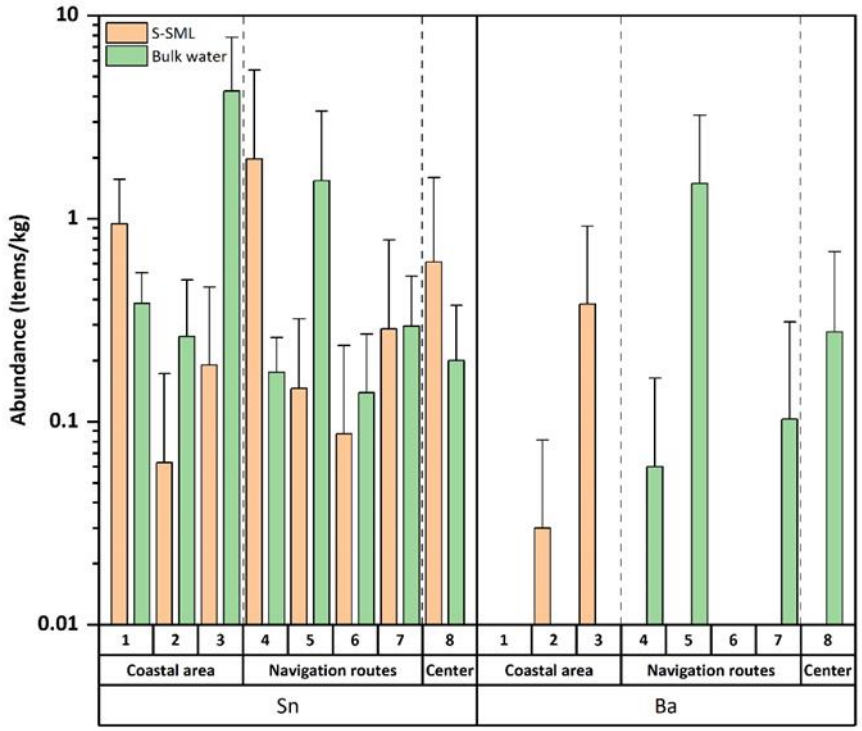

Fig.3-6 The distribution of average abundance of Sn and Ba MPs at different sampling sites

The average abundance of every kind of metal MPs in different sampling zones is shown in Fig.3-7. For all kinds of metal MPs, their abundance in coastal area, navigation routes and center did not show significant differences (p>0.05, one-way ANOVA Tamhane's T2 post-hoc test). However, as shown in Tab.3-1, the abundances of Ti and Fe-Mn-Ni MPs were generally significantly higher than that of other kinds of metal MPs at coastal area and navigation routes (p<0.05, Mann-Whitney U test), which revealed that Ti and Fe-Mn-Ni MPs always presented a higher prevalence state. The sources that are related to antifouling and marine paints are discussed combined with

their abundance at different sampling zones. The similar abundance of Cu MPs among all sampling zones may suggest that APPs generated from ship maintenance in the dry docks on land and navigating activities in marine environment retained homogenic distribution and loads. The abundance of Cu-Zn MPs exhibited irregular distribution and large fluctuations among different sampling zones. In both S-SML and bulk water, Zn MPs and Ti MPs had higher abundance in navigation routes than that in coastal area and center, and this may be related to the higher discharge of Zn-based APPs and Ti-based marine paints due to ship operation and activities. Fe-Mn-Ni MPs in bulk water had a little higher average abundance than that in S-SML among all sampling zones, which may be attributed their trend of settlement due to their high metal density. Sn MPs at all sampling zones retained a stable average abundance. Ba MPs had the least average abundance, and they showed similar loads level with that of Zn MPs in coastal area in S-SML, even a higher average abundance than that of Zn and Sn MPs in bulk water in center. This indicates that Ba MPs have a relatively narrow distribution range and are more inclined to converge in certain specific marine regions.

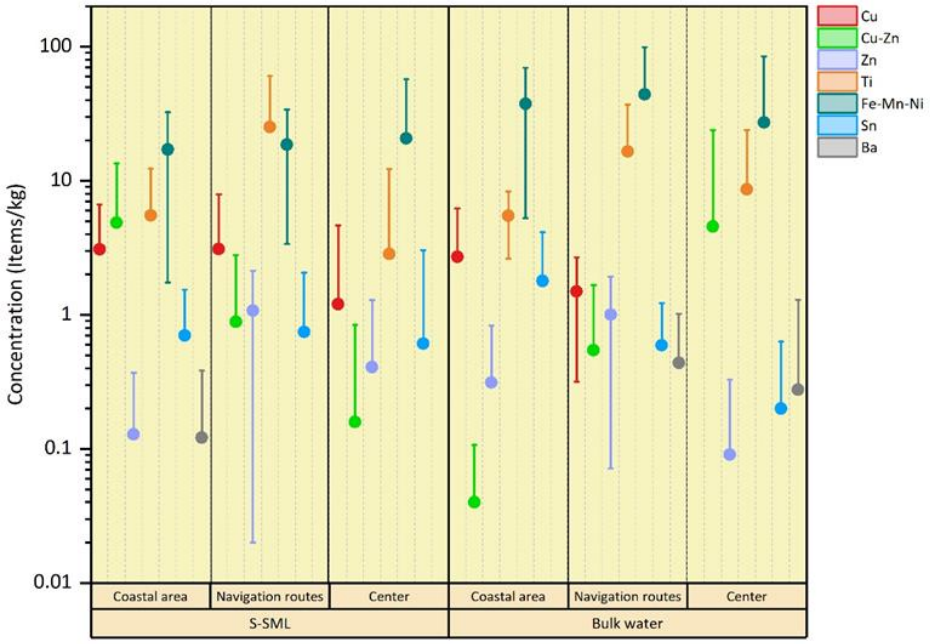

Fig.3-7 The average abundance of every kind of metal MPs at different sampling zones

Tab.3-1 Significance difference between different metal MPs abundance tested by Mann-Whitney U test at different sampling zones

Depth	Zone	Significance difference ($p<0.05$ ✳)					
		Metal MPs	Cu	Cu-Zn	Zn	Sn	Ba
S-SML	Coastal area	Ti			✳	✳	✳
		Fe-Mn-Ni			✳	✳	✳
	Navigation routes	Ti		✳	✳	✳	
		Fe-Mn-Ni	✳	✳	✳	✳	
	Center	Ti					✳
		Fe-Mn-Ni		✳			✳
Bulk water	Coastal area	Ti		✳	✳	✳	
		Fe-Mn-Ni	✳	✳	✳	✳	
	Navigation routes	Ti	✳	✳	✳	✳	✳
		Fe-Mn-Ni	✳	✳	✳	✳	✳
	Center	Ti	✳				
		Fe-Mn-Ni	✳				

3.3.4 Size distribution of metal MPs

The percentage of size ranges for all kinds of metal MPs are shown in Fig.3-8. For Cu, Cu-Zn, Zn, Ti and Fe-Mn-Ni MPs that were mostly associated with paint particles, MPs with size range of 10–53 μm always accounted for more than 80% in total abundance. This may be due to the brittleness of the paint that leads to fragmentation below 50 μm [73]. In addition, there is a gradual breakdown of the floating paint particles into small pieces [28]. In total, except Sn MPs in S-SML and Ba MPs in bulk water, most metal MPs with smaller sizes were always more, which was consistent with the negative correlation between abundance and sizes for microplastics. This illustrates that metal MPs also underwent the same breaking process that microplastics do, due to the UV degradation of the binding polymer and the mechanical disturbance such as wearing and tearing of coatings caused by wave and water flow [18].

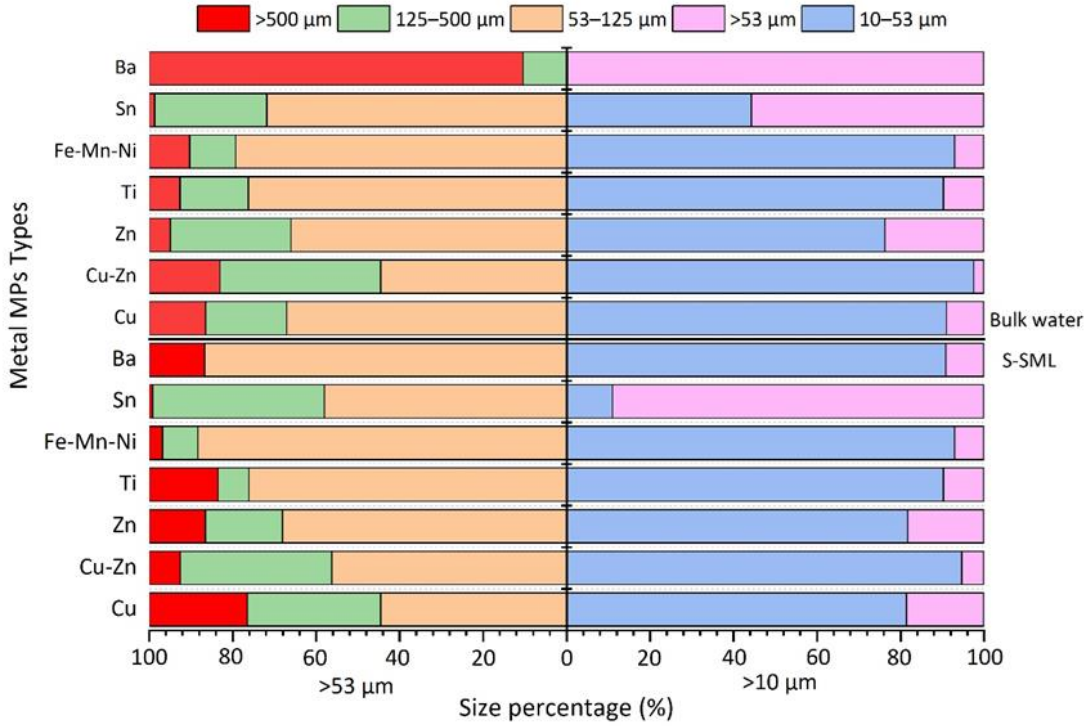

Fig.3-8 Percentage of all types of metal MPs with different sizes in total abundance

3.4 Conclusions

Our research investigated the occurrence, metal types, abundance and distribution of metal MPs in the surface seawater in Osaka Bay for the first time. Cu, Cu-Zn, Zn, Ti, Sn, Fe-Mn-Ni and Ba MPs were detected and they presented relatively uniform distribution in both S-SML and in bulk water among all sampling sites and zones. Metal MPs with a size of 10–53 µm were the most abundant category among all size ranges. The abundances of Fe-Mn-Ni MPs and Ti MPs were significantly higher than that of other types of metal MPs and they prevailed in surface seawater in Osaka Bay. The Cu MPs and Zn MPs also occupied a certain proportion among all metal MPs, although they are suspected to come from antifouling paints during shipping activities, their associations with APPs still needs further confirmation and identification. Sn MPs and Ba MPs presented relatively less abundance than other metal MPs, while their association with marine and antifouling paint should not be neglected.

Chapter IV
Co-occurrence of microplastics and microparticles containing metals especially for Cu and Zn in Sea-Surface Microlayer in Osaka Bay, Japan

4.1 Introduction

Compared with microplastics with similar sizes, paint particles exhibit higher chemical toxicity due to their greater mobility of toxic metal ions and higher concentration of hazardous inorganic additives in the matrix [18]. Therefore, the pollution level and ecological toxicity of paint particles in marine environment should be paid more attention. However, until now, reports on paint particles are not as common as researches on microplastics.

Many microplastics in seawater have been identified as paint particles according to their polymer types [21–26]. Especially for some microplastics with Polymethyl Methacrylate (PMMA) [27] and alkyd resins [28] as polymeric matrix, they have been considered as antifouling paint particles (APPs) because that these polymers are always used as binders in antifouling paints. Actually, except the polymeric binders and matrix, the metallic components are also indispensable in paint particles, such as the Cu or Zn-based biocides in antifouling paints [30] and Ti, Ba, Cr, Fe, Sn and Pb-related pigments in marine paints [15]. However, the assessment of marine microplastics related to ships and marine paints as mentioned above was based on the analysis of polymer types, while the investigation on heavy metals therein was neglected. It is known that polymers such as acrylic, alkyd and epoxy resins are always used as the plastic backbone of marine paints, however, they can also be used in a variety of other plastic products. Therefore, it is important to know whether microplastics originate from marine paints or not; this cannot be assumed just by simply identifying their polymer component and additional metal analysis should follow. Until 2022, 17 items of microparticles containing different metals including Ba, Cu, Cr, Fe, Pb, Sn, Ti and Zn floating in surface seawater in the North Atlantic Ocean were found and their corresponding polymers were detected, among which some alkyd or epoxy-based microparticles containing high concentrations of Cu and Zn were identified as APPs [133]. This provided a more accurate method to distinguish paint microparticles from ordinary microplastics based on the identification of their polymer and metal types.

Given the confirmation of APPs in surface seawater in the North Atlantic Ocean, APPs containing high concentrations of Cu and Zn may have already ingested by marine organisms and caused adverse effects. However, the residues of APPs containing toxic metallic biocides in sea areas except for the North Atlantic Ocean are unknown. Therefore, in this study, microplastics and metal MPs floating in surface seawater in Osaka Bay were investigated to detect paint particles, especially for Cu and Zn MPs which may contain high concentrations of Cu and Zn-based biocides and ecotoxicity. For improving the accuracy of identification on paint-related microplastics, both the polymer types and the metal component with each microparticle were measured to explore the co-occurrence of microplastics and metal MPs in this study. Significantly, the concentrations of Cu and Zn in these Cu and Zn MPs were also measured by a more accurate new method based on the X-Ray Fluorescence Spectrometry (μ-XRF) and the flameless atomic absorption spectrophotometry

(FLAAS). Only acrylic, epoxy or alkyd-based microparticles containing high concentrations of Cu or Zn can be identified as APPs.

Thus, the purpose of this study is to (1) identify the polymer types of these metal MPs to detect the paint-related microplastics and explore their sources, (2) measure the concentrations for Cu and Zn in metal MPs to explore their association with APPs. Significantly, to quantify Cu and Zn concentrations in metal MPs based on μ-XRF and FLAAS, calibration curve obtained from commercial antifouling paints containing different concentrations for Cu and Zn and similar polymeric matrix with that of anthropogenic microparticles in Osaka Bay was established, and highly reliable and accurate Cu and Zn concentrations in metal MPs can be measured by this way, (3) analysis the correlation between the microparticles with different metal types and microplastics with different polymer types to reveal the diverse sources of these microplastics and metal MPs. This study is the first to investigate the co-occurrence patterns of metal MPs and microplastics in the sea-surface microlayer (S-SML), and suggest that the pollution of metal MPs with high concentration for Cu and Zn in S-SML is worth to attention. And the sources of paint-related metal-based microplastics were analyzed, which may contribute to controlling the discharge and transportation of paint-related microplastics into marine environment.

4.2 Materials and Methods

4.2.1 Reagents

All chemicals and reagents were of analytical grade. 30% Hydrogen Peroxide (H_2O_2, Wako Pure Chemical Industries, Ltd., Osaka, Japan) was used to digest organic matters on filter samples. For measuring Cu and Zn content, hydrochloric acid (12M, 35% HCl, Wako Pure Chemical, Osaka, Japan) and nitric acid (13.4 M, 61% HNO_3, Kanto Chemical, Ltd., Osaka, Japan) were diluted with ultrapure water (UPW) to prepare 1 M HCl, 1 M HNO_3 and 0.015 M (= 0.1%) HNO_3, and aqua regia was prepared by mixing 3 parts of HCl (12M, 35%) with 1 part of HNO_3 (13.4M, 61%). The standard Cu solution (Cu1000, 1000 mg/L, Wako Pure Chemical Industries, Ltd., Japan) was diluted to 40, 20, and 10 μg/L (ppb) by 0.1% HNO_3, and the standard Zn solution (Zn 1000, 1000 mg/L, Wako Pure Chemical Industries, Ltd., Japan) was diluted to 3, 1.5, and 0.75 mg/L (ppm) by 0.1% HNO_3 for preparing a calibration curve to be used with flameless atomic absorption spectrometry.

4.2.2 Identification of polymer types for metal MPs

After identified by the μ-XRF as described as 3.2.2, some metal MPs were selected to be observed by Infrared Microscope (AIM-9000, SHIMAZU, Kyoto, Japan, the same position on the filter was used) and their polymer types were detected by the Fourier Transform Infrared Spectrometer (μ-FTIR: IRTracer-100, SHIMADZU, Kyoto, Japan). Filters were observed to detect and count metal MPs for the first time by μ-XRF under full vacuum. Some metal MPs were flown away and lost inevitably due to the violent airflow during vacuum pumping. After the first observation and counting, the metal MPs remaining on filters were observed for the second time by μ-XRF under parteral vacuum, and their positions on the filter were marked for the purpose of detecting their polymer composition on the same position on the filter by μ-FTIR. Since frequent and quick sample exchange can be conducted under parteral vacuum without stopping the vacuum pumping, the partial vacuum state was selected for time-saving during the

second μ-XRF observation rather than the full vacuum state. Considering the massive abundance and time-consuming detection for MPs of 10–53 μm, the polymer type detection was performed on metal MPs with size ranges of > 53 μm only.

4.2.3 Preparation of standard Cu-Zn-based APPs

To create calibration curve between metal concentration and corresponding Fluorescence X-ray intensity, the standard Cu-Zn-based APPs were prepared by mixing commercial Cu-Zn-based acrylic antifouling paint (named "Paint 3", R Copper Red, Nippon Paint, Ltd., Tokyo, Japan) with Ti-based PMMA marine coating (named "Paint 1", Dainippon Paint, Ltd., Osaka, Japan) by a volume ratio of 10:90. This mixed paint was then diluted by the Ti-based PMMA marine coating (Paint 1) exponentially for 7 times; finally 8 kinds of mixed paints with concentration gradients for Cu and Zn were obtained in total. The paints were identified as SS1, SS2, SS3, SS4, SS5, SS6, SS7 and SS8 with a Cu-Zn-based paint volume percentage of 10%, 5%, 2.5%, 1.25%, 0.625%, 0.312%, 0.156% and 0.0781%, respectively. These 8 kinds of mixed paints were evenly applied on baking paper, then peeled off into fragments after air-drying. These paint fragments were put into specialized crushing containers and immersed in liquid nitrogen for 5 min, then crushed into APPs through a freezing crusher (Freeze crusher μT-48, TAITEC, Saitama, Japan) using the vertical vibration of the crushing apparatus at 1200 rpm for 5 min. The pulverized APPs were sieved through a stainless-steel sieve cascade (φ10cm) (JIS Z 8801, Tokyo Screen, Japan) with mesh sizes of 500, 125 and 53 μm in turns. Thus, APPs of SS1–SS8 of size ranges of <53, 53–125, 125–500 and >500 μm were obtained.

4.2.4 Determination of Fluorescence X-ray intensity for Cu and Zn of standard APPs

The standard APPs of SS1–SS8 described in 2.5 with size ranges of <53, 53–125, 125–500 and >500 μm, 32 samples (4 sizes × 8 concentrations) in total, were stored in different dishes, respectively. Every APPs sample was taken out by micro spoon then distributed on a double-sided tape (1.5×1.5 cm) pasted onto a plastic cover. The Fluorescence X-ray intensity for Cu and Zn of each sample was determined by the "Poly Capillary" method of μ-XRF. Considering that the diameter of capillary for beam of Fluorescence X-ray was 100 μm, for samples of >500 and 125-500 μm, the particles surface can be completely covered within the irradiation range of Fluorescence X-rays from capillary. While for the samples of < 100 μm, part of the Fluorescence X-ray beam fails to penetrate the particles and falls into non-sample space. Thus, more particles of < 100 μm should be measured for obtaining sufficient Fluorescence X-ray intensity data with larger range of variation. Therefore, APPs of 5000, 500–5000, 500, 125–500, 130, 120, 110, 100, 90, 80, 70, 60, 50 μm was selected and the corresponding Fluorescence X-ray intensity was measured and recorded.

4.2.5 Determination of Cu and Zn concentration (mg/kg) of standard APPs by FLAAS

All plastic- and glassware were soaked in 1M HCl for at least 24 h before used then rinsed with UPW. About 50 mg of every made standard APPs (>500 μm) of SS1–SS8 were weighed by an electronic balance (HTR-80, Yushima Ltd., Japan) and then digested in 10 mL of aqua regia at 85 ℃ for 2 h in covered 100 ml Pyrex beakers [42]. After cooling, the contents (residual APPs and aqua regia) were transferred into

volumetric flasks and diluted to 25mL by 0.015M (0.1%) HNO_3, then filtered by PTFE filter (H100A047A, ADVANREC, 1 μm, φ47 mm). Considering the high concentrations for Cu and Zn, all digestates should be diluted to ensure that their absorbance (ABS) values for Cu and Zn fall lower than that of 40 ppb Cu solution and 3 ppm Zn solution in the calibration curve (described in 2.2). As such, 0.5 mL of the digestates of SS1–SS8 were diluted 4000, 2000, 2000, 500, 500, 200, 200, and 100 times respectively for the measurement of Cu ABS, and 50, 30, 30, 10, 5, 5, 0 and 0 times respectively for the measurement of Zn ABS. The diluted digestates of SS1–SS8 were identified as S1–S8 correspondingly.

The ABS values for Cu and Zn in the standard Cu and Zn solutions with different concentrations diluted by 0.1% HNO_3 were measured by flameless atomic absorption spectrophotometry (FLAAS) (Z-2710, Hitachi Ltd., Japan) to prepare the calibration curve. The ABS values for Cu and Zn in S1–S8 solutions were also measured by FLAAS, then the concentrations for Cu and Zn in S1–S8 solutions were calculated according to the calibration curve and their ABS values.

When measuring the ABS, about 20 μL of solution sample was injected into pyrotube HR with a graphite furnace, ABS was monitored at 324.8 nm of Cu with lamp current 7.5 mA and 307.6 nm of Zn with lamp current 5 mA. During the measuring process, the drying at 80-140 ℃ lasted for 40 s, the ashing at 600 ℃ for Cu and 300 ℃ for Zn lasted for 20 s, and the atomizing at 2400 °C for Cu and 2200 °C for Zn lasted for 5 s [134]. The measurement for every sample was repeated 3 times and the average values of ABS were recorded. Concentrations (mg/kg) for Cu and Zn in standard APPs of SS1–SS8 were calculated according to the concentrations for Cu and Zn in S1–S8, their dilution factor, the volume of digestates (25 mL) and the total quantities (about 50 mg) of APPs of SS1–SS8.

4.2.6 Determination of Cu and Zn concentrations (mg/kg) in metal MPs

For standard APPs of SS1–SS8, their calibration curves between metal (Cu and Zn) concentrations (mg/kg) and corresponding Fluorescence X-ray intensity (cps/mA) of APPs with different sizes (5000, 500-5000, 500, 125-500, 125, 130, 120, 110, 100, 90, 80, 70, 60, 50 μm) were created. Since the Fluorescence X-ray intensity values for Cu and Zn in metal MPs in Osaka Bay had been measured by μ-XRF, the corresponding concentrations for Cu and Zn in these metal MPs then could be calculated by these calibration curves. The relevant process of measurement of concentrations for Cu and Zn in standard APPs of SS1–SS8 and metal MPs in Osaka Bay is shown in Fig.S5.

4.2.7 Detection and identification of PMMA MPs by py-GC/MS

Samples of 10–53 μm in S-SML and bulk water were collected at Site 1, 4 and 8 on 24/10/2022 and they were analyzed with an 8890 GC System (Agilent) coupled to an electron ionization (EI) time-of-flight mass spectrometer JMS-T2000GC AccuTOF™ GC-Alpha (JEOL, Tokyo, Japan), equipped with a pyrolizer JHI-08 (Japan Analytical Industry Co., Ltd., Tokyo, Japan). Pyrolysis was performed at 590 ˚C for 10 sec. The pyrolizer was coupled with the split/split less injector, operated in split mode with a ratio of 1:100. The injector temperature of GC was set at 280 ˚C, as well as the pyrolysis interface temperature. A ZB-5ms fused-silica capillary column (5% phenyl – 95% dimethylpolysiloxane) of 30 m length x 0.25 mm internal diameter x 0.25 μm film thickness (Phenomenex Ltd, Macclesfield, UK) was used to separate the pyrolysis products in GC. The GC oven temperature was 40˚C (held 1 min), increased up to 300˚C

at a rate of 10˚C/min and held for 3 min. The total time of the chromatogram was 30 min. Helium gas (99.999%) was used as a carrier gas at a flow rate of 1 mL/min. The EI/FI source was set for EI/MS analysis, operating at 70 eV. Acquisition was performed in full MS mode (*m/z* 35–800) using CO_2 at *m/z* 43.990 as an internal standard as a *m/z* calibration agent. The PTFE filter was cut into 8 pieces. The MPs on the cut PTFE paper were analyzed by pyrolysis-GC/MS.

4.2.8 Data analysis

All the data analyses were performed in SPSS 19.0 (IBM, New York, NY, USA) and Origin 2021 (OriginLab, Northampton, MA, USA). The curves of polymer spectra were visualized by EZ OMNIC. All the figures were drawn in Excel and Origin 2021. Regarding statistical comparisons, for MPs with all kinds of metals, differences in their abundance at different sampling sites and zones both in S-SML and in bulk water were assessed by the Mann-Whitney U test and one-way ANOVA followed by Tamhane's T2 post-hoc test, while differences in abundance among different kinds of metal MPs were also assessed by Mann-Whitney U test. In addition, the correlations between several parameters of the metal MPs were examined by Pearson's correlation through Origin. Principal component analysis (PCA) was performed through Origin in order to describe the experimental system with a new set of reduced variables deriving from the initial parameters.

4.3 Results and Discussions

4.3.1 Polymer types of metal MPs

Considering that abundant PMMA MPs were detected, some samples already exmined via μ-FTIR were further selected and detected by pyrolysis-Gas chromatography/ Mass Spectrometry (py-GC/MS) for a more accurate qualitative analysis on the residual PMMA MPs as discribed in 4.2.7.

Taking the sample collected in Site 4 in S-SML as an example, tetrafluoroethylene, a pyrolysis product of the PTFE filter, was observed with *m/z* 99.994 for $[M]^{+\bullet}$, *m/z* 80.996 for $[M\text{-}F]^{+\bullet}$, *m/z* 61.997 for $[M\text{-}2F]^{+\bullet}$ for $[M\text{-}CF_2]^{+\bullet}$ at retention time (RT) 2.1 min in the chromatograms as shown in Fig.4-1 (a) and (b). The detection of tetrafluoroethylene from the PTFE filter background rather than MPs verified the accuracy of GC/MS analysis. A pyrolysis product MMA of PMMA, was observed at RT 3.5 min. In its mass spectrum, the *m/z* 100.053 for $[M]^{+\bullet}$, and its fragment ions *m/z* 99.044 for $[M\text{-}H]^{+\bullet}$, *m/z* 69.034 for $[M\text{-}CH_3O]^{+\bullet}$, and *m/z* 41.039 for $[C_3H_5]^{+\bullet}$ were detected in its mass spectrum as shown in Fig. 4-1 (c). At RT 2.9 min, pyrolysis product C_4H_6O of PMMA and its fragment ions were detected as shown in Fig. 4-1 (d). These RT, *m/z* values of the fragment ions, and its fragmentation pattern matched the results of pyrolysis-GC/MS of a standard PMMA. In addition, the pyrolysis product of PMMA from anthropogenic MPs were also similarly detected in the sample collected in Site 8 in S-SML, while they were not detected in other selected samples.

The qualitive detection of PMMA confirmed that some PMMA MPs were indeed lost due to the blowing of airflow under full vacuum during the first observation by μ-XRF, but some PMMA MPs still remained on the filters.

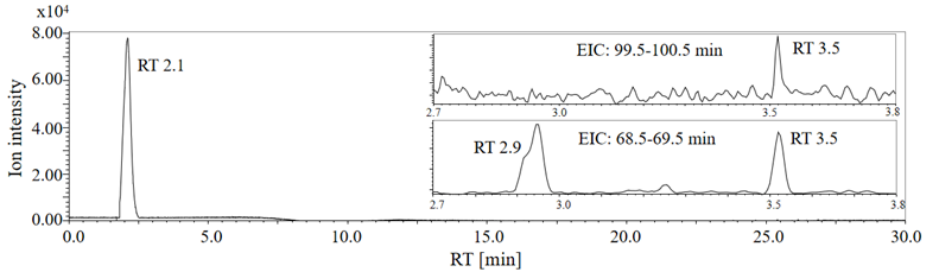

(a) GC/MS TIC

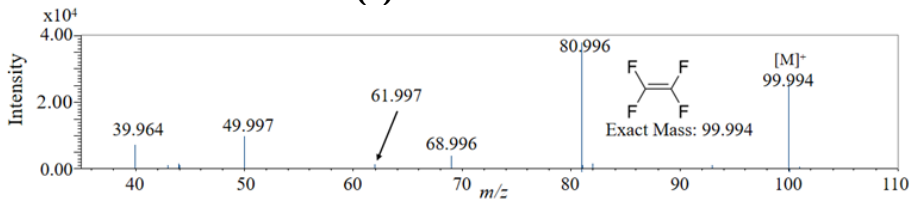

(b) Mass spectra at RT 2.1

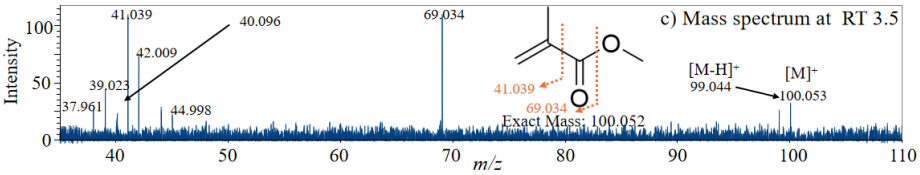

(c) Mass spectra at RT 3.5

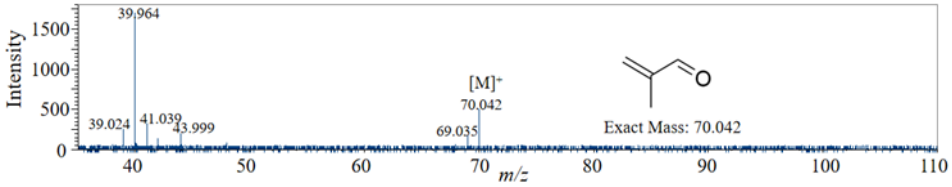

(d) Mass spectra at RT 2.9

Fig.4-1 Mass spectra of sample collected in Site 4 in S-SML on 24/10/2022

As described in 4.2.2, the polymer types of metal MPs were detected by μ-FTIR after being observed and positioned by μ-XRF. Since Cu and Zn are closely related to biocides in APPs, all the residual Cu, Cu-Zn and Zn MPs on filters were examined by μ-FITR to identify their polymer types to explore their polymeric association with APPs. For metal MPs with size ranges of > 53 μm, during the first observation under full vacuum, 190 items of Cu, Cu-Zn MPs and 106 items of Zn MPs were detected, while just 41 items of Cu, Cu-Zn MPs and 19 items of Zn MPs were detected on the filters during the second observation. This means that approximately 80% of Cu, Cu-Zn and Zn MPs were blown away and lost due to the airflow blowing under full vacuum. In addition, a certain number of Ti, Sn, Fe-Mn-Ni and Ba MPs were selected from massive residual metal MPs to measure their polymer composition to determine their association with microplastics and paint particles. The results (percentage of metal MPs containing each kind of polymer) are shown in Fig.4-2. For the metal MPs that had also their polymer type identified, information on their pictures and spectra measured by μ-XRF and μ-FTIR, and the corresponding Fluorescence X-ray intensity data for Cu-Zn-based MPs is shown in the database [135]. Among 41 items of Cu and Cu-Zn MPs, 35 items belonged to the acrylic resins and 3 items belonged to the PMMA resins. Since PMMA

is also categorized as an acrylic resin, it can be deduced that the acrylic resin-based microparticles accounted for 93% of total Cu-based MPs. At present, the acrylic resin-based self-polishing coatings are the most used ones in antifouling on ships; cuprous oxide (Cu_2O) is characterized as one of the main antifouling agents [136]. Therefore, some of the 38 items may well represent APPs that originated from the self-polishing antifouling paints on ships. 2 items of Cu-based MPs exhibited the polymer type PA6 and the PE-PP with a mixture of 4:1, which may originate from the antifouling paint on the experiment ship as described in 2.3.4.

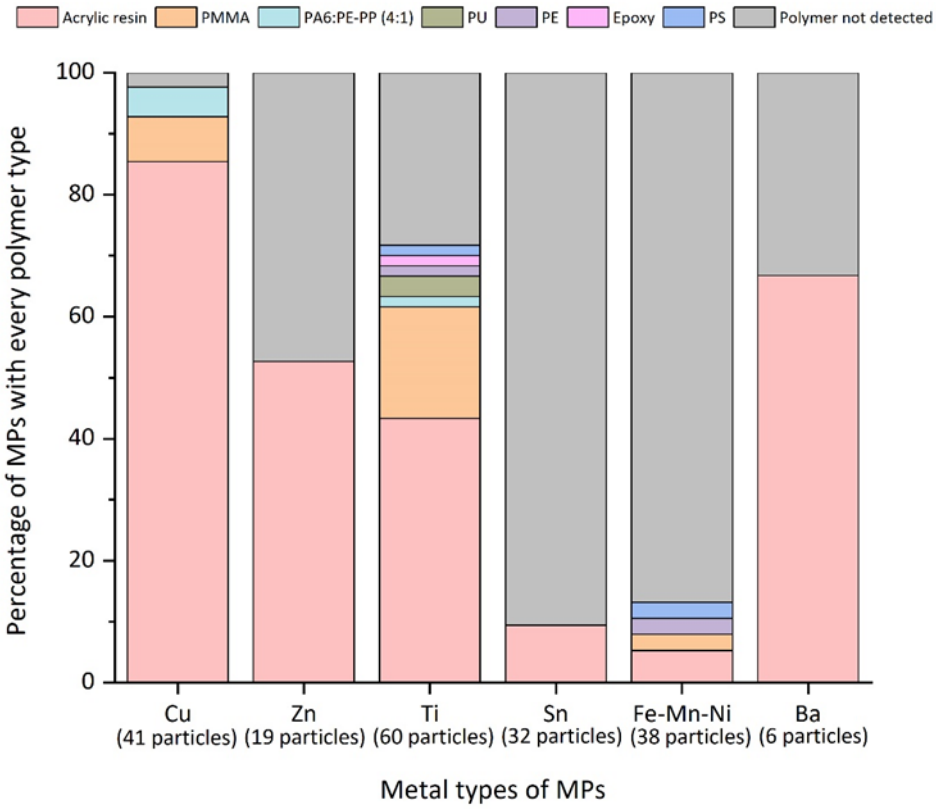

Fig.4-2 Percentage of microparticles with every polymer type accounted in every kind of metal MPs

Among 19 items of Zn MPs, 10 items belonged to the acrylic resins and accounted for 52.6% of all Zn MPs. Since the ban of tributyltin in antifouling paints, Zinc pyrithione (ZnPT) has become one of the most frequently used alternative biocides [137]. In addition, zinc acrylate resin is also one of the most useful resins used as polymeric matrix for antifouling paint [138]. In the current manufacturing process of acrylic antifouling paints in Japan, once the carbon group connecting two ester bonds is replaced by Zn, the hydrolyzed polymer of acrylic-zinc is formed and antifouling paints with excellent film renewal and antifouling properties can be obtained [139]. Besides, zinc oxide (ZnO) is used as a pigment or a booster of biocides in antifouling paints. To sum up, once related to APPs, the Zn MPs with acrylic polymeric matrix may reflect the biocides component of ZnPT, the copolymer composition of acrylic-zinc, and the ZnO used as booster or pigment in acrylic antifouling paints.

As shown in Fig.4-3, 4-4 and 4-5, the μ-XRF and μ-FTIR spectra of some Cu and Zn MPs with acrylic resins in Osaka Bay were contrasted with these of selected standard commercial Cu-Zn-based antifouling paints in Japanese paint market as shown in Tab.S1; the consistency of the compared spectra indicated the same metal and polymer

component of these anthropogenic MPs to those in antifouling paints.

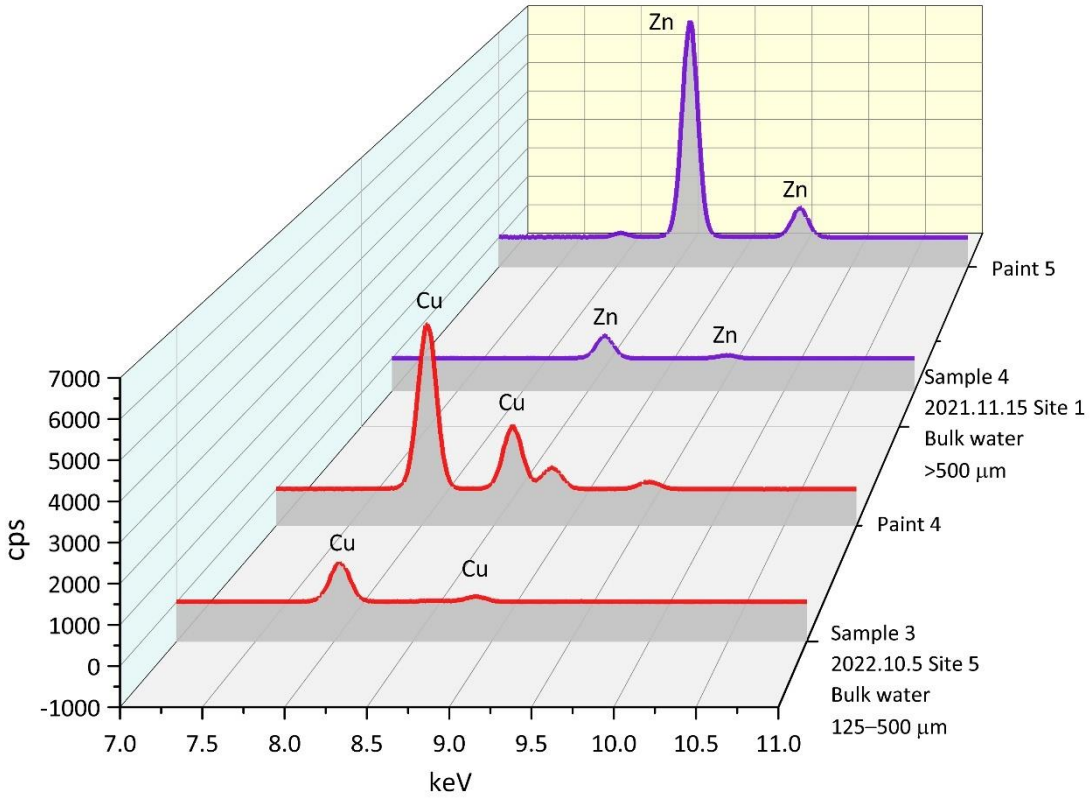

Fig. 4-3 Contrast of m-XRF spectra between Cu and Zn MPs (Sample 3 and Sample 4) in Osaka Bay and standard APPs (Paint 4 and Paint 5)

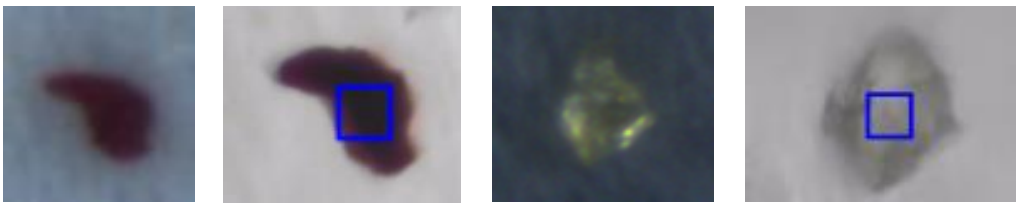

(a) **(b)** **(c)** **(d)**

Fig.4-4 μ-XRF and μ-FTIR pictures of Sample 3 (Cu MP) and Sample 4 (Zn MP) (a) Sample 3 μ-XRF (b) Sample 3 μ-FTIR (c) Sample 4 μ-XRF (d) Sample 4 μ-FTIR

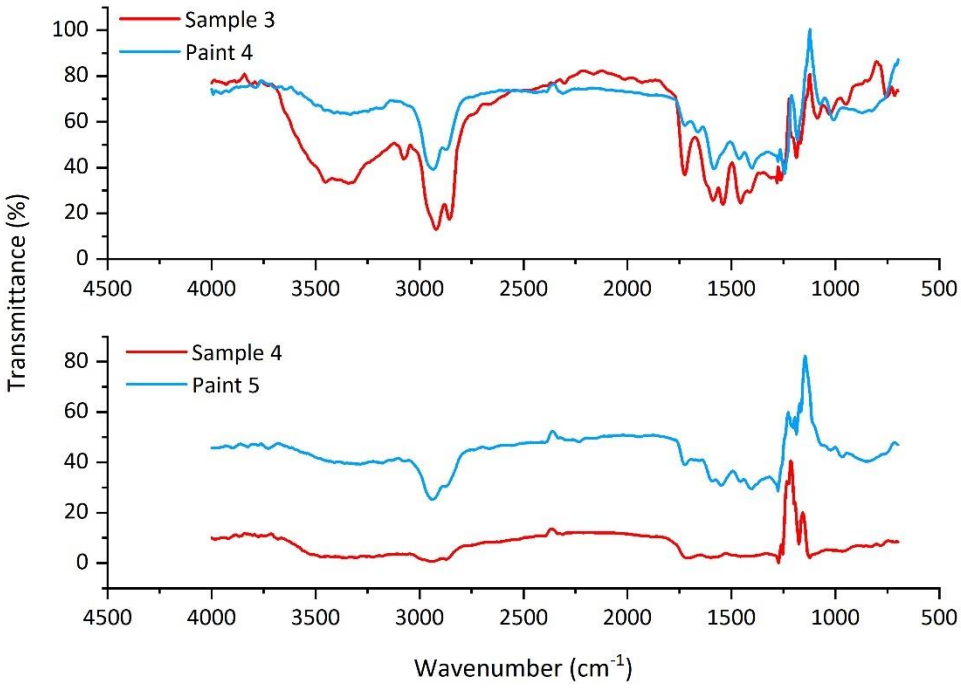

Fig.4-5 Contrast of μ-FTIR spectra between Cu and Zn MPs (Sample 3 and Sample 4) in Osaka Bay and standard APPs (Paint 4 and Paint 5)

Among 60 items of Ti MPs, 26 items belonging to the acrylic resins (43.4%) and 11 items belonging to the PMMA resins (18.3%) were found. For these items, terrestrial plastics and metal adsorption may be their potential sources, especially they may also originate from the protecting coatings on topside and superstructures of ships if an association with marine paints is assumed. In addition, PA6:PE-PP, PU, PE, Epoxy and PS types accounted for 1.7%, 3.3%, 1.7%, 1.7% and 1.7% in abundance among total Ti MPs, respectively. These polymers have also been widely used in the manufacturing of all kinds of plastic products, paints and coatings. Here only the paint-related potential sources of these Ti MPs are discussed. More than 70% of clear coating layers from original vehicle manufacturers contain PS [140]. PU coating is the most significant class of industrial paints related to outdoor painted sculptures [141]. Compared to other synthetic resins, epoxy resins dominate in the sector of anti-corrosion coatings due to their long-erm corrosion avoidance and chemical resistance [142]. Moreover, low-density polyethylene (LDPE) has also been used as binder for marine anticorrosive coatings [143]. Nanoparticles of TiO_2 are not used only as pigments but they also act as additives that improve mechanical strengths and the ability of anti-microbial, anti-corrosive and self-cleaning of properties [144]. Therefore, if we assume a paint particle origin, Ti MPs with polymeric matrix here may reflect a diverse sources of paints including the antifouling and anticorrosive paints used on surfaces of ships and marine structures in water environment, and the coatings on vehicle surface and buildings on land.

Among 32 items of Sn MPs, just 3 items belonging to the acrylic type MPs (9.38%) were identified and the polymer types of the rest of samples did not match with polymers data recorded in the library base of μ-FITR. Sn MPs without polymers seemed to occupy most of the proportion in marine environment.

Among 38 items of Fe-Mn-Ni MPs, 2 items of acrylic MPs (5.26%), 1 item of

PMMA MP (2.63%), 1 item of PE MP (2.63%) and 1 item of PS MP (2.63%) were detected. The rest of Fe-Mn-Ni MPs (86.85%) that did not show matching polymers may be inorganic metal MPs. Owing to the lower density of polymers compared to metals, Fe-Mn-Ni MPs without polymer components may present a relative higher density, which can lead their gathering in bulk water rather than in S-SML, further affecting their vertical distribution in the water column.

Among 6 items of Ba MPs, 4 items belonging to the acrylic resins (66.7%) were detected. Considering the least abundance of Ba MPs among all metal MPs, just 6 Ba MPs were discovered for the measurement of polymer types, while the high proportion of Ba MPs with acrylic resins may suggest that most Ba MPs floating in marine environment have polymeric matrix.

4.3.2 Cu and Zn concentrations (mg/kg) in metal MPs

Cu and Zn MPs with acrylic resins may reflect the presence of APPs, however, they may also derive from adsorption of metal ions onto aged microplastics from the surrounding water environment [128]. Therefore, concentrations for Cu and Zn in these MPs should be measured, and only acrylic MPs containing high concentrations for Cu or Zn may actually be characterized as APPs.

As described in 4.2.3, 4.2.4, 4.2.5 and 4.2.6, the calibration curve for standard APPs (SS1–SS8) between metal concentration (mg/kg) and Fluorescence X-ray intensity (cps/mA) is prepared for measuring the concentrations for Cu and Zn in the 41 items of Cu-based MPs and the 19 items of Zn MPs. For exploring whether the extraction of Cu and Zn by aqua regia can be affected by APPs sizes, SS1 APPs with size ranges of >500, 125–500, 53–125 and <53 μm were selected to measure their concentrations for Cu and Zn. The values of ABS for Cu and Zn in the digestates, the calculating process and concentrations for Cu and Zn in SS1 APPs with 4 size ranges are as shown in Tab.S2–6. Especially shown in Tab.S6, the concentrations for Cu and Zn extracted from SS1 APPs with different sizes presented no discrepancy between them ($p>0.05$). This verified that the APPs sizes cannot affect the extraction of Cu and Zn therein, therefore, only APPs of >500 μm for SS1–SS8 samples were selected to determine their concentrations for Cu and Zn. The corresponding values of ABS for Cu and Zn in digestates and the concentrations for Cu and Zn in SS1–SS8 APPs (>500 μm) are shown in Tab.S7–18. The average values of concentrations for Cu and Zn in SS1–SS8 (>500 μm) (Tab.S19) were used as the data in Y-axis of the calibration curve. Meanwhile, the Fluorescent X-ray intensity values for Cu and Zn in SS1–SS8 APPs with the size of 5mm, 500–5000, 500, 130–500, 130, 120, 110, 100, 90, 80, 70, 60 and 50 μm measured by μ-XRF (Tab.S20 and 21) were used as the data in X-axis of the calibration curve. Based on the values of concentrations for Cu and Zn and Fluorescent X-ray intensity for standard APPs of SS1-SS8 with different sizes, the calibration curve between their metal concentrations (mg/kg) and Fluorescent X-ray intensity values (cps/mA) were drawn as shown in Fig.4-6 and Fig.4-7.

For Cu, Cu-Zn MPs (41 items) and Zn MPs (19 items) larger than 50 μm, their Fluorescent X-ray intensity values were recorded in the database [135].

According to these Fluorescent X-ray intensity values and the calibration curves, their concentrations for Cu and Zn were calculated as shown in Tab.4-1 and 4-2. For one Cu or Zn MP, its Fluorescent X-ray intensity value was brought into two calibration curves whose size parameters was adjacently larger and smaller than that of the MP, then two corresponding metal concentration values were calculated and the average value was taken as the final concentration for Cu or Zn. The Cu concentration in 41

items Cu-based MPs ranged from 511–54,000 mg/kg in one MP, i.e. the mass percentage of Cu in MPs ranged from 0.05–5.4% w/w. Meanwhile, among 17 items of floating micro paint flakes (> 60 μm) found in the North Atlantic Ocean, their Cu concentration ranged from <52.9 to 6960 mg/kg in one flake (0.005–0.7% w/w) [133], which was lower than that in this study. Similarly, the Zn concentration in 19 items of Zn MPs in this stduy ranged from 95.1–13,200 mg/kg (<0.01–1.3% w/w) in one MP, which was higher than that the result of Zn concentration ranged from <38.2 to 37,400 mg/kg in one paint flake (<0.004–3.8% w/w) in the North Atlantic Ocean [133].

Until now there is no universal method to identify Cu and Zn MPs as APPs. For the 17 items of paint flakes in the North Atlantic Ocean, some alkyd or epoxy-based flakes with Cu concentrations > 824 mg/kg were identified as Cu-based APPs [133], according to which, 37 items acrylic MPs with Cu concentration >810 mg/kg in this study maybe also identified as Cu-based APPs. Although no relevant references were available for Zn MPs, some of the Zn MPs in this study maybe characterized as Zn-based APPs accordinng to their high Zn concentrations and acrylic resins that are always used as binders and polymeric matrix in antifouling paints.Significantly, high concentrations for Cu and Zn in metal MPs in this study seems to reflect the Cu-Zn-based biocides or pigments that already exist in APPs ranther than originate from metal absorption on aged microplastics from water.

Altogether, high concentrations of Cu and Zn in metal MPs in S-SML and bulk water in Osaka Bay were detected. Given the continuous leaching of Cu and Zn from metal MPs and their ecotoxicity to marine organisms, these metal MPs with high concentrations for Cu and Zn should be concerning. Furthermore, highly reliable and accurate concentrations for Cu and Zn were obatained through the calibration curve shown in Fig.4-6 and Fig.4-7, due to the commercial antifouling paints with similar whose polymeric matrix (acrylic resin) was the same as that of anthropogenic microparticles. This can provide insights for measurment of Cu and Zn concentrations in metal MPs in future research.

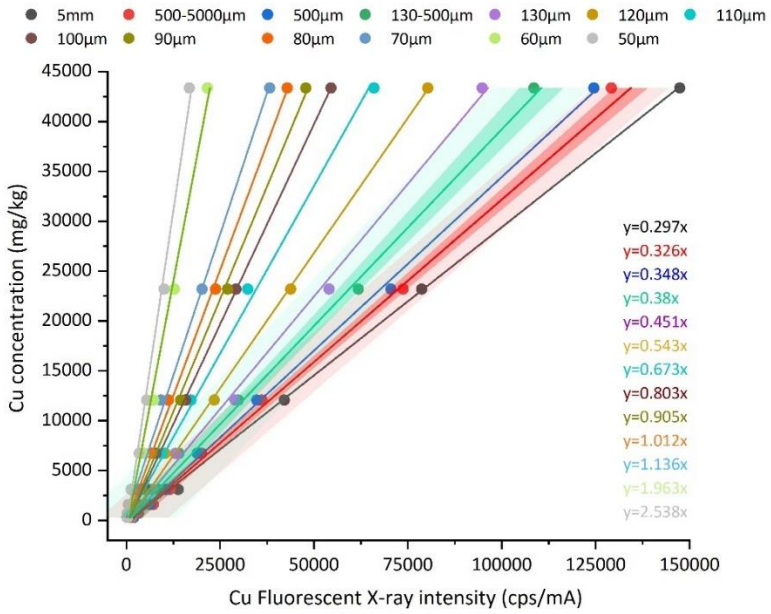

Fig. 4-6 Calibration curve between concentration and X-ray intensity for Cu in standard APPs (SS1–SS8) with different sizes

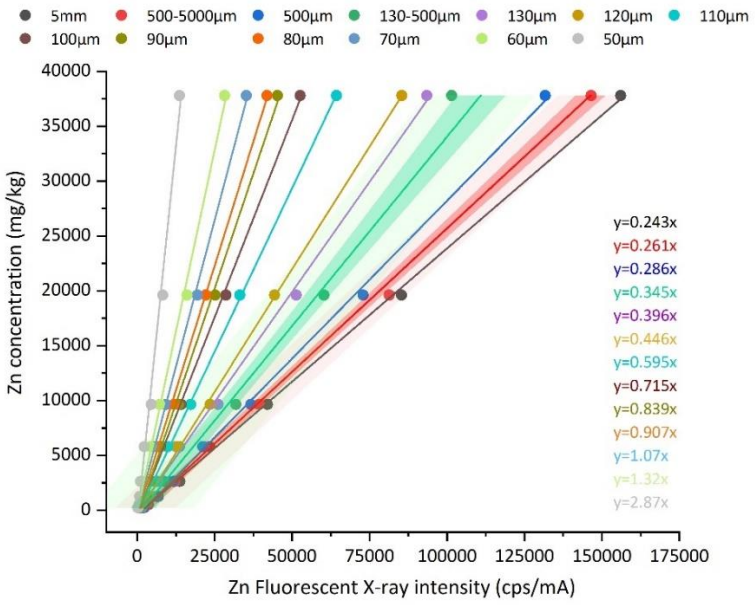

Fig.4-7 Calibration curve between concentration and X-ray intensity for Zn in standard APPs (SS1–SS8) with different sizes

Tab.4-1 Cu concentrations (mg/kg) in 41 items of Cu MPs

Depth	Size (μm)	Coastal area				Navigation routes			Center
		1	2	3	4	5	6	7	8
S-SML	>500	5,610	2,100 1,300	2,700		54,000 32,000 960 23,000 5,800 3,100 1,900 34,000 5,900			2,900 4,900 1,400
	125–500								
	53–125								
	>500			6,600 4,400 1,700		35,000 30,000 28,000 18,000 4,300 4,200 3,200 2,900 1,700 1,400 1,200 900 810 526 511		10,000	12,000
Bulk water	125–500								
	53–125			3,000	10,700			15,000 4,200 1,200	

Tab.4-2 Zn concentrations (mg/kg) in 19 items of Zn MPs

Depth	Size (μm)	Coastal area		Navigation routes				Center	
		1	2	3	4	5	6	7	8
S-SML	>500			1,090	635				1,090
	125–500				1,970				591
									718
									217
									95.1
	53–125	4,500			5,600				
Bulk water	>500	5,100	2,210						
	125–500							12,300	127
	53–125			7,080		13,200	3,950	1,200	
				10,200					

4.3.3 Percentage distribution of all metal MPs and their potential sources

The percentage distribution of all metal MPs among different sampling zones and depths was conducted according to their abundances. As shown in Fig.4-8, navigation routes contributed most of metal MPs loads with the percentage of 65.1%. Furthermore, 26.2% and just 8.7% of metal MPs originated from coastal area and from bay center respectively. Among all types of metal MPs, Fe-Mn-Ni MPs were the most abundant, accounting for 60.4%, while minor ones were Ti MPs (28.2%), Cu MPs (4.5%), Cu-Zn MPs (3.9%), Sn MPs (1.4%), Zn MPs (1.3%) and Ba MPs (0.3%). For Cu, Cu-Zn, Zn, Ti, Sn MPs, their abundances in both S-SML and bulk water were at a similar level, while the Fe-Mn-Ni MPs abundance in bulk water was about twice higher than that in S-SML. This is probably the main reason for the higher abundance level of all metal MPs in bulk water. Ba MPs was found in bulk water only.

It was also shown that 55.6% Cu MPs, 20.5% Cu-Zn MPs and 92.3% Zn MPs originated from navigation routes, so if some of these Cu-Zn-based MPs originate from antifouling paints due to shipping activities, their generation mechanism is discussed as follows. Most contemporary antifouling paints contain Cu(I)-based biocides (commonly cuprous oxide). Moreover, although zinc oxide is also used as the principal biocidal pigment sometimes, it is more generally used in combination with Cu(I) as a booster to increase the toxicity of the latter by 200-fold [33]. For contemporary self-polishing antifouling paints, during navigation, the soluble biocides are released to prevent the attachment of organisms to the coat surface. At the same time a new fresh area of coating is uncovered for subsequent release of biocides along with the continuous hydrolysis of the acrylic matrix depending on the shear of seawater flow [93]. The mechanical disturbance of coatings is one mechanism that can generate APPs [18], during which, theoretically the polymeric matrix of antifouling paint has been hydrolyzed, and the copolymer film becomes brittle accompanying the dissolution of biocides [91]. Considering that APPs are generated more passively with the general wear and tear (erosion) of hull [18], the brittle polymer matrix containing Cu and Zn-based biocides may fall off from the coating surface by the abrasion of seawater shear force, then further break into APPs. In addition, another mechanism of the formation of

APPs is the UV degradation of the binding polymer that leads to the weathering of coatings [18,145]. The weathering and abrasion of ship paints above the waterline can also generate APPs [133]. High salinity in seawater may increase the rate of the aging process for polymers compared with freshwater [146], therefore, antifouling paints above the waterline are prone to be weathered more easily when contacted with seawater then further break into APPs. In addition, the present results also show that about 40% Cu MPs, 64.1% Cu-Zn MPs and 7.69% Zn MPs originated from coastal area of the bay. In this case, if we assume that these MPs were APPs, their sources may be linked to repainting and cleaning of hulls in shipyards, especially for leisure boats where paint emissions are not well regulated. During the processes of scraping, sanding, stripping, sand-blasting and hydro-blasting of spent coatings for hull maintenances, significant quantities of toxic APPs are transported to aquatic environment [18]. These APPs floating in water cannot be hydrolyzed in relatively static seawater which does not impose shear stress; as such the residue may persist in the water environment for quite long. It is noted however that compared to navigation routes, coastal area contributed much fewer Cu and Zn MPs.

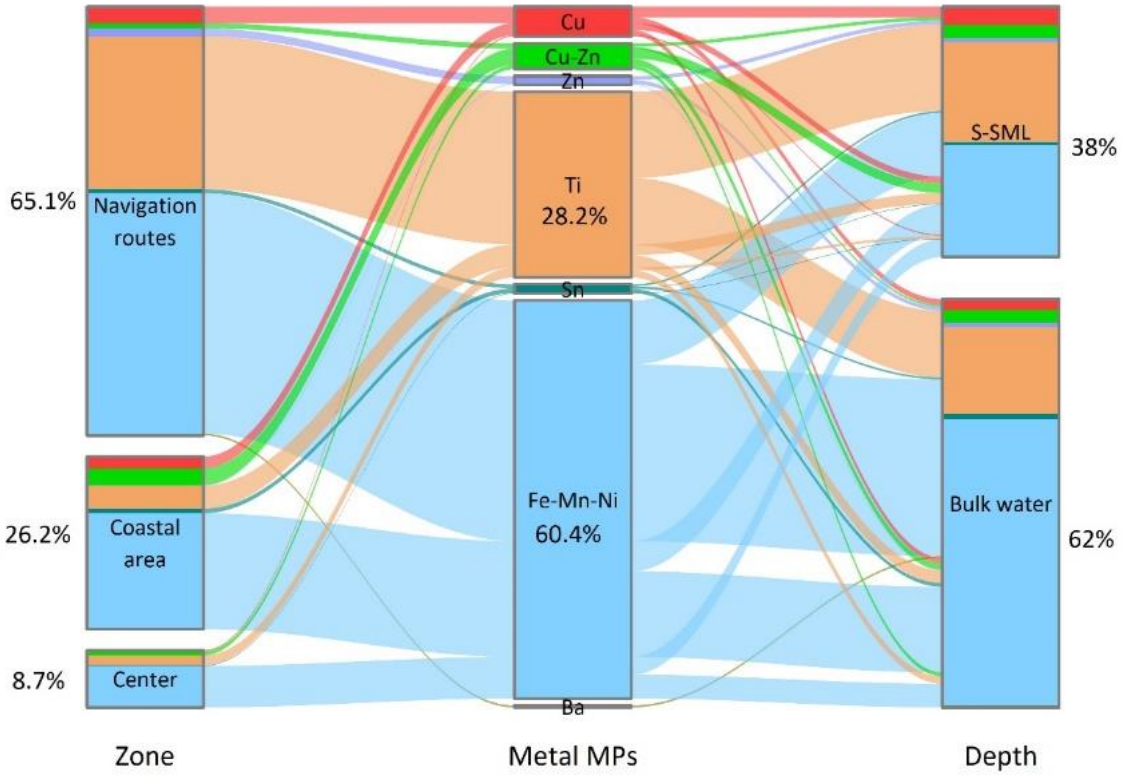

Fig.4-8 Alluvial diagram of the distribution of each kind of metal MPs in abundance at different sampling zones both in S-SML and bulk water

Most of Ti MPs (82.3% of total) also originated from the navigation routes. If associated with shipping activities, some of these MPs may derive from marine paints applied to the topside on ships. White color is used extensively on the superstructures of ships [147] and titanium dioxide (TiO_2) is applied in paint as a white pigment due to its high refractive index [144]. It is notable that the annual consumption of TiO_2 in the

production of paint is 75% greater than that of all other pigments put together [148]. Grey paints on the topside of hulls are also pigmented with TiO_2 [149], especially for admiralty ships in British navy [148]. Moreover, Rutile TiO_2 and Anatase TiO_2 are the main component of the titanium white pigment which is widely used in marine coatings in the contemporary Japanese paint market [150,151]. Marine sites are characterized by high humidity and salinity [152], which can make Ti-based marine paints fall off into seawater due to weathering more easily. Compared to antifouling paint that contain Cu and Zn as biocides, TiO_2 is less ecotoxic and more environmental-friendly since it is well embedded in the coating matrix and cannot leach easily [153]. Therefore, Ti MPs in water environment may produce fewer repercussions to aquatic biota. In addition, Ti with high concentration of 1046.01–175513.36 mg/g (dry weight) in sediments was detected in Lake Garda [73]. As shown in Fig.4-9, 4-10 and 4-11, the consistency of the compared spectra by μ-XRF and μ-FTIR indicated that Ti MPs had the same metal and polymer component as Ti-based marine and antifouling paints prevailing in Japanese paint market (Tab.S1), thus, some Ti MPs are likely to stem from marine paints.

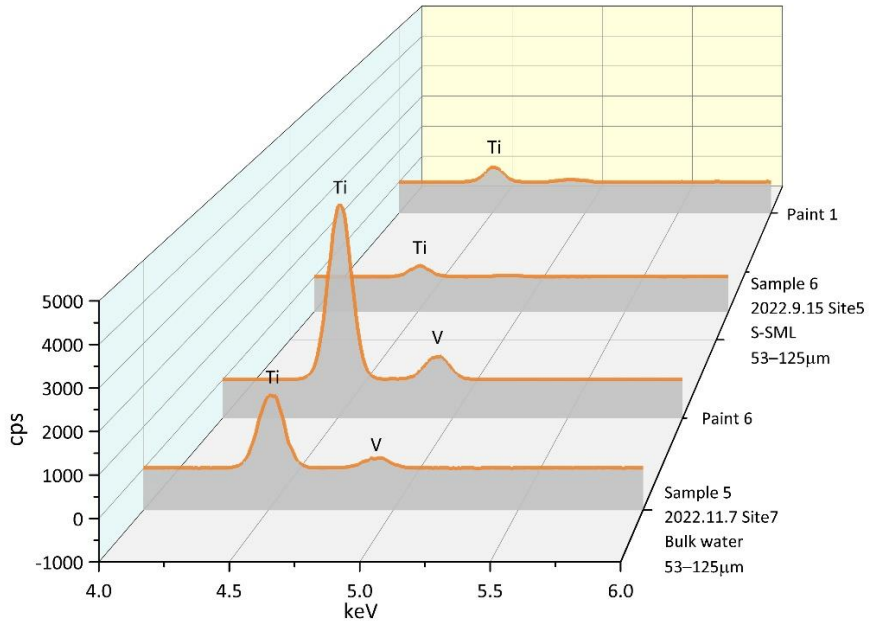

Fig.4-9 Contrast of μ-XRF spectra between Ti MPs (Sample 5 and Sample 6) in Osaka Bay and standard APPs (Paint 6 and Paint 1)

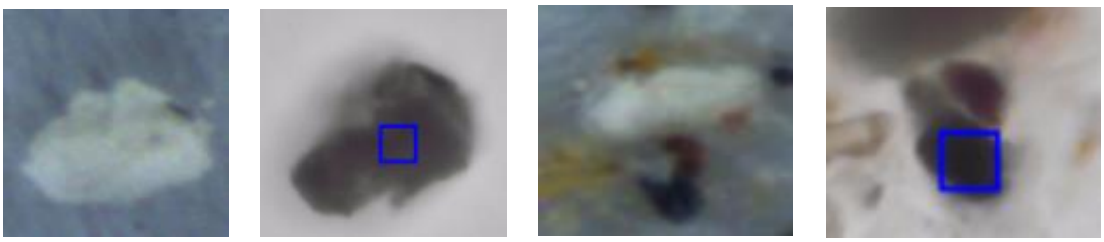

(a) **(b)** **(c)** **(d)**

Fig.4-10 μ-XRF and μ-FTIR pictures of Sample 5 (Ti MP) and Sample 6 (Ti MP) (a) Sample 5 μ-XRF (b) Sample 5 μ-FTIR (c) Sample 6 μ-XRF (d) Sample 6 μ-FTIR

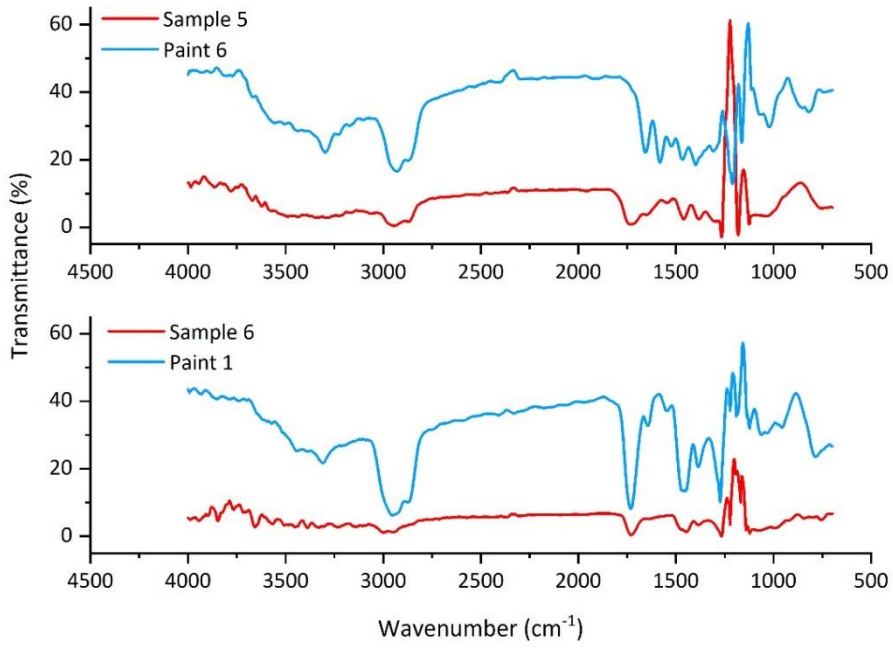

Fig.4-11 Contrast of μ-FTIR spectra between Ti MP (Sample 5 and Sample 6) in Osaka Bay and standard paint particles (Paint 6 and Paint 1)

Sn MPs from navigation routes and coastal areas accounted for 42.9% and 50%, respectively. Although Sn is also used as hardening catalyst in contemporary antifouling paints in Japan [154], given that most Sn MPs in this study do not have a polymeric matrix (Fig.4-2), the Sn detected in metal MPs seemed to not associate with APPs but rather with metal adsorption from the surrounding seawater. Organotin compounds, especially Tributyltin (TBT) had been used as antifouling biocides most widely before 1989 and they have been gradually regulated and finally banned for use on shipbuilding due to their adverse effects on marine organisms and repercussions on water environment [46]. However, in recent years, TBT with concentrations 4.4–28 ng/L in water samples at Tanabe Bay in Japan was detected and these levels are deemed toxic for gastropods in seawater [155]. Besides, Sn was also found in micro paint flakes in North Atlantic Ocean with the concentration ranged from 387 mg/kg to < 1900 mg/kg in one flake [133], and in plastics in sediments of Lake Garda (38.84–972.25 μg /g) in one plastic sample [73]. Thus, Sn MPs in this study may reflect the residual and adsorption of residual organotin formulations from historic applications of antifouling paints, and their hazardous and negative impacts on marine ecosystems may continuously exist.

Fe-Mn-Ni MPs contribution from navigation routes, coastal area and center was 60.4%, 29.1% and 10.5%, respectively. The abundance of Fe-Mn-Ni MPs in bulk water was about twice as high than that in S-SML. As shown in Fig.4-8, most Fe-Mn-Ni MPs without polymeric matrix are likely to deposit due to their higher density compared to microplastic then gathering in bulk water. Coupling of Fe and Mn in MPs prevailed in this study, and a similar Fe-Mn association was also observed in groundwater of Changchun city, China [156]. Both Fe and Mn are abundant elements in the earth crust, and the source of Fe-Mn nodules are mainly aquifer clay layers [156]. In addition, the

Fe-Mn MPs seem to be related with waste effluents from industries such as steel plants due to anthropogenic activities [157]. Thus, most of the Fe-Mn MPs in this study may have little connection with paint flakes and ship activities. However, polymer components such acrylic resins, PMMA, PS, PE and PVC were still detected in some Fe-Mn MPs. This shows a certain correlation between the Fe-Mn coupling and microplastics, which needs to be investigated further.

It is noteworthy that Ni is also coupled with Fe-Mn in some metal MPs in this study, and this seems to have not been reported in relevant research so far. Here, 2 items of Fe-Mn-based acrylic MPs also contained Ni simultaneously. Although this may have been caused by metal absorption, the possibility that these Fe-Mn-Ni MPs with acrylic matrix are associated with marine paints cannot be excluded. Mn and Ni visibly attached to paint fragments that were collected from a marine boat maintenance facility in Plymouth, England reflected the components of metallic base materials of the hulls [31]. In view of this, the co-occurrence of Ni with Fe-Mn in metal MPs with acrylic or other polymeric matrix may reflect the metallic substrates of hulls attached to antifouling or anticorrosive paints. It is known that carbon and alloy steels are widely used in shipping due to their good mechanical properties and low cost [158], and the surface modification technology is applied on these steel substrates to improve their mechanical performance, corrosion and wear resistance without affecting their comprehensive properties [159]. Laser beams are widely used in surface modification of many kinds of metals [160] utilizing the method of surface alloying and surface cladding [161]. The laser cladding technology has attracted great attention in recent decades and has been widely used to improve the surface properties of alloys [162]. At present, Fe-based and Ni-based alloy powders are mainly used in laser cladding technology to obtain the Fe and Ni-based composite alloy coatings combined with the alloy matrix [163], and Mn has also been added in laser cladding to improve the non-magnetic properties of the composite coatings [164]. In addition, Mn is also the main element in carbon steel with a mass percentage of 0.2%–1.5%. Once the protective coatings on hulls are worn and damaged due to impaction and aging, the base steel can come in contact with corrosive seawater, which then results in a continued corrosion attack to metallic materials [165]. The corroded metallic base materials containing Fe, Ni or Mn are removed and peeled off by the flowing seawater then they may break into metal MPs. It had been verified that Fe found in micro paint flakes in the North Atlantic Ocean may come from the corroded fragments of an underlying steel substrate of the hull [133]. Thus, a small portion of Fe-Mn-Ni MPs with polymeric matrix in this study may originate from the exfoliation of steel substrates of hulls that had been corroded by seawater, or from the metal absorption. This may explain why the most abundant loads of Fe-Mn-Ni MPs were found in navigation routes.

Finally, regarding Ba MPs, the lowest percentage originated from navigation routes and they were found only in the bulk water. Barium sulphate ($BaSO_4$) has been used as pigments [166] in historical TBT antifouling paint and extenders in antifouling [167] and anticorrosive paints [168]. Meanwhile, Ba has also been found in micro paint flakes in North Atlantic Ocean with a concentration of <1860 mg/kg to <30000 mg/kg in one flake [133], in antifouling paint fragments from a large marine boat maintenance facility in Plymouth, with a concentration of 1050 ± 89 mg/g in one fragment [31], and in plastics in sediments of Lake Garda with a concentration of 38.84–972.25 mg/g in one plastic sample [73]. As such, the Ba MPs at navigation routes in this study may also reflect the occurrence of microparticles of antifouling and anticorrosive paints.

4.3.4 Principle component analysis (PCA) of metal MPs

Although it is difficult to confirm the complex potential sources of these metals that originated from different anthropogenic and nature pathways, some associations among different metals may provide insights about the attributions of metal MPs through multivariate analysis. Principal component analysis (PCA) was performed as described, and the parameters examined were the abundance of each type of metal MPs at different sampling sites and zones both in S-SML and in bulk water among all samplings (22 collections for S-SML and 25 collections for bulk water). The PCA results of the loadings are shown in Fig.4-12. The three-factor solution explained 64.7% of the variance, where PC1 contributed 29.4% of the total variance with positive loadings of Cu and Zn, PC2 contributed 19.8% of the total variance with positive loadings of Ti and Sn, and PC3 contributed 15.5% of the total variance with positive loadings of Fe-Mn-Ni, Zn and Ba. A hypothesis on sources and spatial patterns of distribution of all the metal MPs in the study area can be proposed according to this analysis.

This study focuses on exploring the sources of metal MPs related to marine and antifouling paints, and therefore the results of PCA was explained based on the metal composition of the paints in the following discussion. The strong positive loadings of Cu and Cu-Zn on PC 1 undoubtedly reflected the occurrence of Cu-based APPs, which originated from the maintenance and cleaning in dry dock and shipyard and the navigating activities in shipping lane. PC2 was characterized by strong positive loadings of Ti and Sn; this may be linked to the common source of Ti and Sn in pigments and additives in marine paints. The positive loadings of Fe-Mn-Ni, Zn and Ba in PC3 indicated the source of metal MPs stemmed from the metallic base materials attached to paint component including corrosion inhibitors of zinc phosphate and extenders of barium sulphate. Overall, PCA analysis verified the hypothesis of the marine and antifouling paint-related source origins of the detected metal MPs.

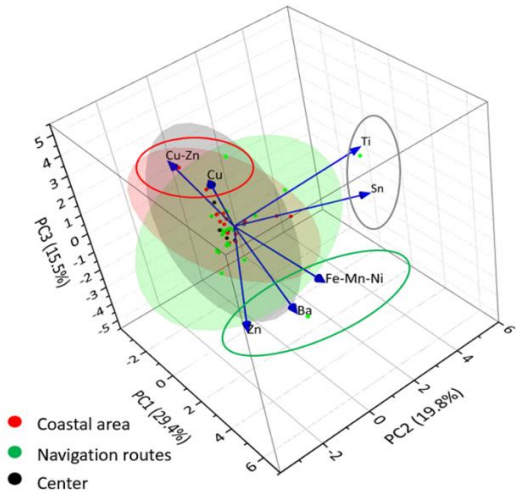

Fig.4-12 Principle component analysis (PCA) of all kinds of metal MPs in surface water

4.3.5 Co-occurrence pattern of metal MPs and microplastics

The abundance, size ranges, polymer types, distribution of microplastics in both S-SML and bulk water in Osaka Bay have been investigated. Based on this, the co-occurrence of metal MPs and microplastics in the same sampling sites was analyzed through Pearson's correlation analysis. As shown in Fig.4-13, there was no significant correlation between the abundance of any kind of metal MPs and the distance from land of each sampling site. In addition, the abundance of very kind of metal MPs in S-SML and bulk water presented no significant discrepancy (p>0.05). While metal MPs can still be captured and float in S-SML due to the surface tension therein even though metals always have a higher density than seawater. For Cu, Zn Ti, Sn and Fe-Mn-Ni MPs, there is a significant negative correlation between abundance and size decreased (R^2= -0.186 for Cu, -0.189 for Zn, -0.152 for Ti, -0.144 for Sn, -0.204 for Fe-Mn-Ni, respectively, p<0.05). Metal MPs of smaller sizes are more, in relation to total microparticles numbers and their loads are prone to increase as they decompose into smaller microparticles. Furthermore, for Cu, Zn, Ti and Sn MPs, their abundance was positive correlated to the abundance of polymer containing microplastics (R^2= 0.358 for Cu, 0.244 for Zn, 0.438 for Ti, 0.183 for Sn, respectively, p<0.05), which revealed their associations with microplastics. The Pearson correlation showed the co-occurrence pattern between metal MPs and microplastics. This may indicate that some of the existing Cu, Zn, Ti and Sn MPs may represent the debris from antifouling and marine paints and coatings. On the other hand, it may also demonstrate metal adsorption on microplastics, which corroborates the function of microplastics as pollutant carriers. This might be especially true for Sn-related to Tributyltin in historical antifouling paint formulations-which once adsorbed on microplastics, may continue to impact marine organisms.

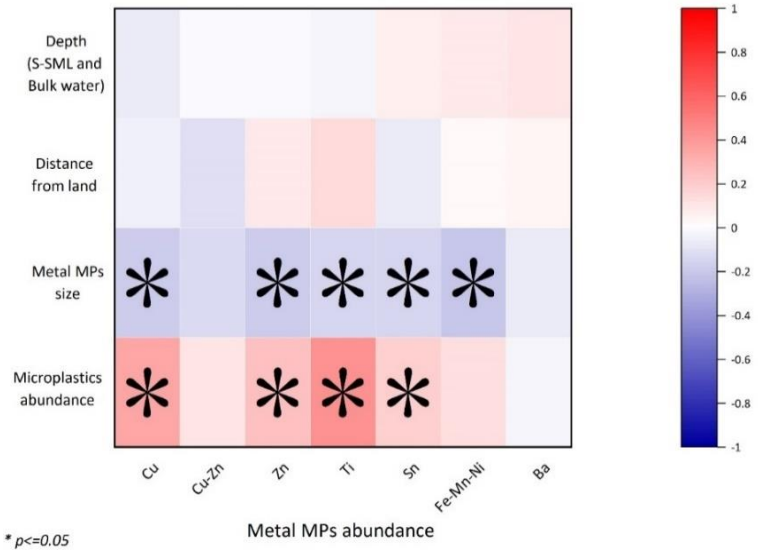

Fig. 4-13 Pearson's correlation analysis between metal MPs abundance and microplastics abundance, metal MPs sizes, distance from land and depth (S-SML and bulk water)

The correlation between each kind of metal MPs abundance and abundance of microplastics with each polymer type was also assessed as shown in Fig.4-14. Considering the overwhelming abundance PMMA MPs, acrylic resins were also classified as PMMA MPs. However, Cu MPs with acrylic resins did not present positive correlation with PMMA MPs abundance; this may be because we did not specially record acrylic resins abundance in the previous study. Most notably, there was a strong positive correlation between PMMA MPs and Ti MPs in abundance (R^2=0.3, p<0.05). This illustrates that these Ti MPs also exhibit a PMMA polymeric matrix, this can be also verified in Fig.4-2, where PMMA polymeric MPs accounted for about 60% in total Ti MPs. The high degree of co-occurrence of Ti and PMMA in microparticles may reveal the pollution caused by Ti-based acrylic paints due to complex pathways and sources, including paints from terrestrial paints from exterior of buildings or from marine and antifouling paints in ocean. In addition, PS MPs also presented a positive correlation with Ti and Sn MPs. PS MPs are widely used in coatings in vehicle manufacturing, but they are also contained in terrestrial road marking paints, which is considered as a significant source of paint fragment and debris in several Japanese cities [169]. Therefore, the high correlation between Ti and Sn MPs and PS MPs may reflect the application of Ti pigment and Sn hardening catalysts in road marking paints. Regarding adsorption of metals on microplastics, given that the PMMA, PS and PET are common types of microplastics in marine environments, whether they are more likely to serve as carriers for metal adsorption needs to be determined in future research.

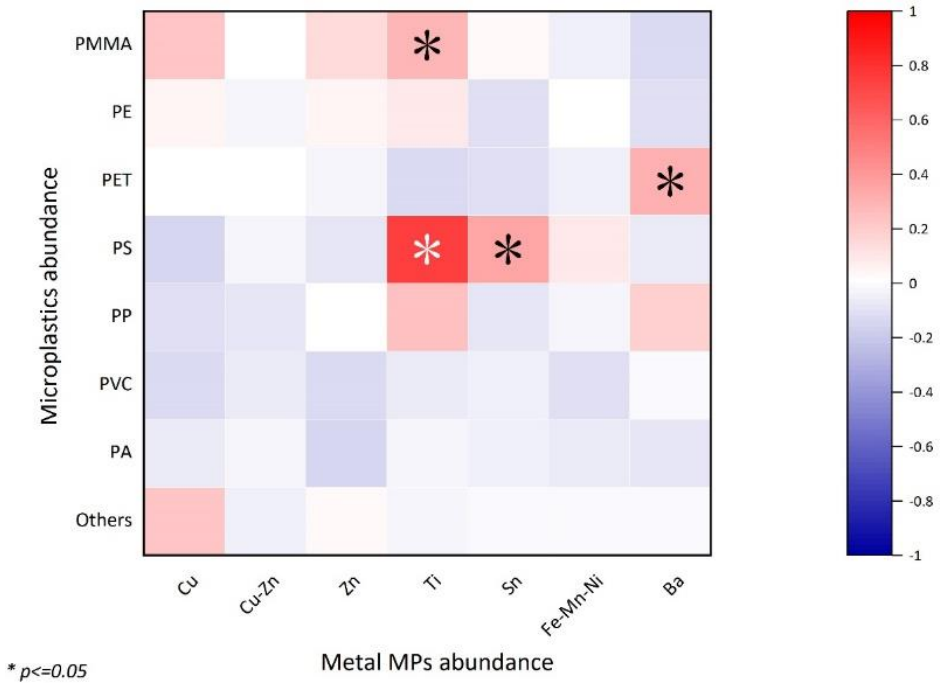

Fig.4-14 Pearson's correlation analysis between metal MPs abundance and abundance of microplastics with every kind of polymer type

Significantly, until now, the identification on microplastics mainly focus on their polymer types, while their metal components are neglected. Considering that microplastics always play a role as a vector of heavy metals, the identification on metal components on microplastics is helpful for deepening the understanding of the function of microplastics as pollutant carriers. Moreover, the measurement of metal concentrations in microplastics contributes to distinguish APPs and other paint MPs from ordinary microplastics. Compared to traditional microplastics, APPs with higher eco-toxicity due to metal-based biocides should be more valued and emphasized and their identification method can be perfected by importing the metal analysis in microplastics. Otherwise, the imperfection of the microplastic binding substance database may affect the identification results on some APPs and other paint-related microparticles.

4.4 Conclusions

Our research investigated the co-occurrence of microplastics and metal MPs in the S-SML in Osaka Bay for the first time. Notably, most Cu-Zn-based MPs exhibited a polymeric matrix of acrylic resins that are widely used as binders in antifouling paints. Given the application of Cu and Zn as biocides in antifouling paints, some acrylic MPs containing high concentrations of Cu and Zn may originate from antifouling paints and their pollution potential should be investigated. Metal MPs were always positively correlated with microplastics abundance. Moreover, Ti MPs exhibited diversity in their polymeric matrix and presented positive correlation with PMMA microplastics abundance, which may be related to the Ti-based marine paints. Coupling between Ni and Fe-Mn in some acrylic MPs may reflect the substrates of hulls attached to antifouling or anticorrosive paint flakes. These results provide new insights in understanding the paint-related sources of metal MPs with acrylic matrix. Significantly, highly reliable and accurate concentrations for Cu and Zn in MPs were measured by calibration curves obtained from standard paint particles with similar matrix based on μ-XRF and FLAAS [135].

Chapter V
Ultraviolet C accelerated weathering effect on the generation of antifouling paint particles in artificial seawater

5.1 Introduction

Some Cu-Zn-based APPs have been identified in surface seawater in Osaka Bay in this study. The polymeric matrix of these APPs were always acrylic resins. The acrylic binders used in antifouling paints started in 1950–1960, and the self-polishing acrylic antifouling paints were firstly used in 1974–1985 [91]. In theory, once contacted with seawater these self-polishing APPs started to dissolve due to the hydrophobic of acrylic binders depending on the shear of seawater flow [93]. Most antifouling paints formulas are belonged to self-polishing category in Japanese antifouling paint market [34]. APPs found in this study may be remained due to the loss of hydrolysis which was caused by the weakening of seawater shear stress. However, the real situation of the exfoliation and residual of APPs in seawater should be still explored to determine their generation mechanism.

APPs in sea-water encounter various impacts, such as the irradiation of radiation of ultraviolet (UV), the abrasion of wave under different wave velocity, and the fluctuation of temperature, pH and salinities. Wherein the UV-exposure as a primary weathering factor can weaken the polymer structure and increase its hydrophilicity [141], which can further facilitate the release of additives behind the polymer surface, certainly including metal biocides in APPs. Compared with non-weathered ones, the concentration of heavy metals was several times higher in the leachates of weathered APPs and contributed to the increased toxicity to the Green Algae [41]. Furthermore, once irradiated by solar UV, polymeric materials of plastics are prone to fragmentation due to photo-oxidation and subsequent secondary micro- or nanoparticles have become an emerging class of pollutants [170], which can also cause paints to decompose into smaller sizes. For antifouling paints that are frequently exposed to ultraviolet radiation near the waterline, once they fall off from the hulls and become APPs in seawater, the previous UV weathering may affect the size reduction and metal leaching of these APPs, while there is a lack of relevant research currently.

Although the UV-C with the wavelength between 200 and 280 nm has been absorbed by ozone layer and cannot reach the earth surface just like the UV-A and UV-B, it has been manufactured artificially to be used for sterilization and disinfection of appliance surface widely. Whilst, the application of UV-C has been successfully utilized for the prevention of biofouling in seawater systems and on instruments and sensors and is beginning to be explored for application on the ship hulls [171]. Of particular concern, once applied to the antifouling of ship hull statically berthing in port or dock,

UV-C used to control biofouling also irradiates APPs falling off from the hull surface simultaneously, which may also increase the release of the metal concentration and toxicity from those APPs. Nevertheless, there is no research to investigate the corresponding repercussions of these APPs irradiated by the UV-C, nor to judge how the related toxicity and leached metal concentration is magnified compared with the pristine APPs. In addition, UVC has also been used in the relevant experiments on APPs to accelerate the weathering process [40].

Thus, the purpose of this study is to (1) identify the exfoliation and residual of APPs from hulls in seawater through the accelerated weathering by UVC, (2) explore the UVC weathering on APPs size change and metal leaching in artificial seawater. Thus, the generation of APPs fell from self-polishing contemporary antifouling paints on hulls can be confirmed.

5.2 Materials and Methods

5.2.1 Preparation of weathered APPs samples

The Cu-Zn-based acrylic antifouling paint (Paint 3) were brushed on the Q235 steel disc with diameter of 50 mm. Considering that the carbon steel has been widely used in the shipbuilding, the Q235 steel, a commonly used carbon steel, was selected to simulate the process of antifouling paint falling off from the hull of the ship. After dried, these painted Q235 steel samples were irradiated by UVC with intensity of 1.55 mW/cm^2 for 1–6 weeks respectively. These weathered painted Q235 steels were then immersed into 300 mL artificial seawater (pH 7.95, EC 4.6 mS/cm) at the rotating speed of 360 rpm for 72 hours. After that the artificial seawater was filtered and APPs were retained on the PTFE filter (POPMF-1000, 10 μm, Wintec, Kobe, Japan) with diameters of 47mm. The relevant processes of generating APPs are shown in Fig.S6.

Tab. 5-1 Mass (g) of every kind of sample

Sample	UVC weathered period (weeks)						
	0	1	2	3	4	5	6
Q235 steel	45.7012	45.1065	45.6325	45.7188	45.81	45.696	45.6386
Painted-steel	48.4086	46.1607	48.6695	46.5093	46.3879	46.3879	46.5062
Paint	2.7074	1.0542	3.037	0.7905	0.8035	0.6919	0.8676

5.2.2 Identification of APPs on filters

APPs on filters were identified by the X-Ray Fluorescence Spectrometry (μ-XRF: XGT-900, HORIBA, Kyoto, Japan) and their abundance and sizes were automatically detected. The maximum APPs abundance that μ-XRF can detect at one time is 300 items, while the abundance of small-sized APPs is too large to be identified in one time. In view of this, just APPs with size of >150 μm were detected and recorded.

5.2.3 Measurement of concentration of Cu and Zn in artificial seawater

The dissolved Cu and Zn that leached from the weathered antifouling paints were concentrated by the Nobias-Chelate resin (PA1L, Hitachi, Tokyo, Japan) through the automatic solid-phase extraction device. Firstly, the Nobias-Chelate resin was filled by acetone for 5 minutes, then rinsed by 10 mL HNO_3 (1M), 10 mL UPW and 10 mL acetic acid (0.1M), respectively. Secondly, 30 mL artificial seawater added with 1.5 mL acetic acid (2 M) passed through the rinsed Nobias-Chelate resin, and the dissolved Cu and Zn was concentrated in the Nobias-Chelate resin, then 10 mL UPW was used to rinse the resin. Thirdly, the Cu and Zn concentrated in the Nobias-Chelate resin were extracted by 3 mL HNO_3 (1M), and the dissolved Cu and Zn in 30mL artificial seawater were concentrated in 3mL of leachate. The leachate was diluted by 50 times and 2 times for measuring the concentration of Cu and Zn by the flameless atomic absorption spectrophotometry (FLAAS) (Z-2710, Hitachi Ltd., Japan) described by 4.2.5, respectively.

5.3 Results and Discussions

5.3.1 Concentrations of Cu-Zn-based APPs fell off from painted Q235 steel samples

As shown in Fig.5-1, the Cu-Zn-based APPs with red color indeed fell off from the painted-steel samples. The concentrations of Cu-Zn-APPs fell off from every kind of painted-Q235 steels in artificial seawater are shown in Fig.5-2. Painted-steel samples which were not weathered by UVC generated least abundance of APPs (>150 μm) of 343.28 items/L/g, i.e., 1 g antifouling paints generated 343.28 items APPs in 1 L artificial seawater. The APPs concentrations that fell from the painted-steel samples continuously raised as the increasing of UVC weathered period until the 4th week. APPs in artificial seawater had the highest concentration of 15714.58 items/kg for the painted-steel sample weathered by UVC for 4 weeks. This may illustrate that paints are more likely to decompose and broke into APPs of smaller sizes after weathered by UVC, which was caused by the weaken of polymer structure due to UVC irradiation. Although APPs (>150 μm) concentration decreased for painted-steel samples weathered by UVC for 5 weeks and 6 weeks, this may because that longer UV weathering periods made more paints break into APPs smaller than 150 μm. As shown in Fig.5-3, APPs with size of 150–200 μm always accounted for most proportion among APPs with size range of >150 μm, and APPs with smaller sizes always presented advantages in abundance.

Fig.5-1 The abundance of Cu-Zn-based APPs (>150 μm) fell from painted-steel samples

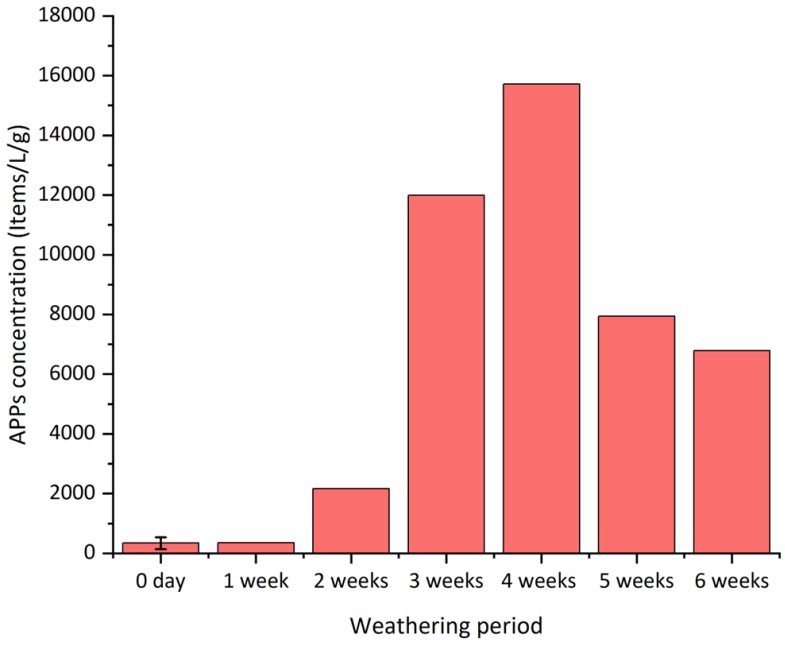

Fig.5-2 The abundance of APPs (>150 μm) fell from painted-steel samples weathered by UVC with different periods

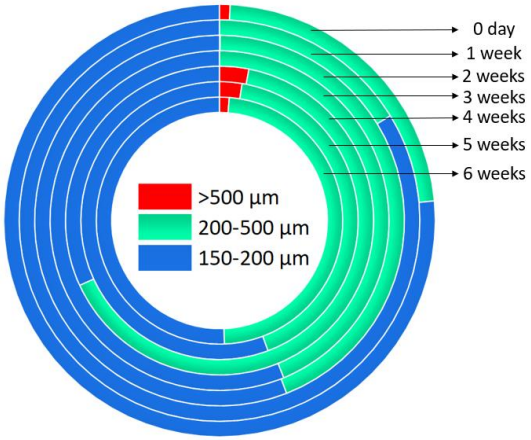

Fig.5-3 The size distribution of APPs (>150 μm) which fell from painted-steel samples weathered by UVC with different periods

5.3.2 Concentrations of dissolved Cu and Zn leached from APPs in artificial seawater

As shown in Fig.5-4 and 5-5, the dissolved Cu and Zn concentration in artificial seawater leached from APPs (>150 μm) which fell from painted-steel samples weathered by UVC with different periods were recorded, and the highest of concentrations for Cu (643 ppb/g) and for Zn (1103.82 ppb/g) in 300 mL artificial seawater were detected for painted-steel samples weathered by UVC for 4 weeks and 6 weeks, respectively. Antifouling paints weathered by UVC from 3 weeks to 6 weeks always presented higher dissolved Cu and Zn concentrations in the artificial seawater. This may suggest that metal biocides are more easily leached from weathered APPs due to the polymeric matrix was weakened due to UV.

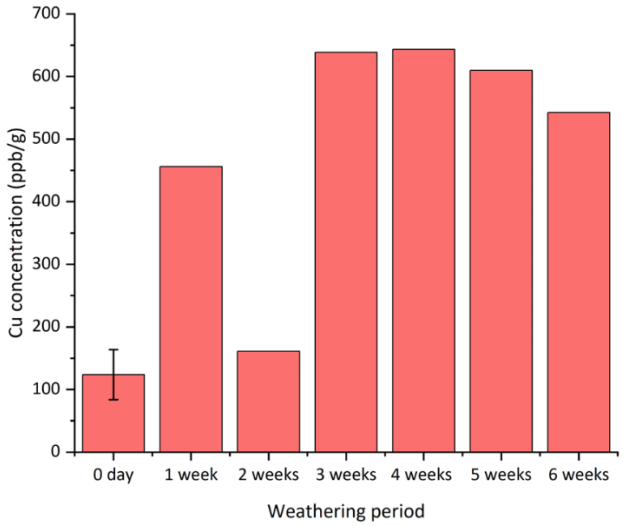

Fig.5-4 Dissolved Cu concentration leached from APPs (>150 μm) which fell from painted-steel samples weathered by UVC with different periods

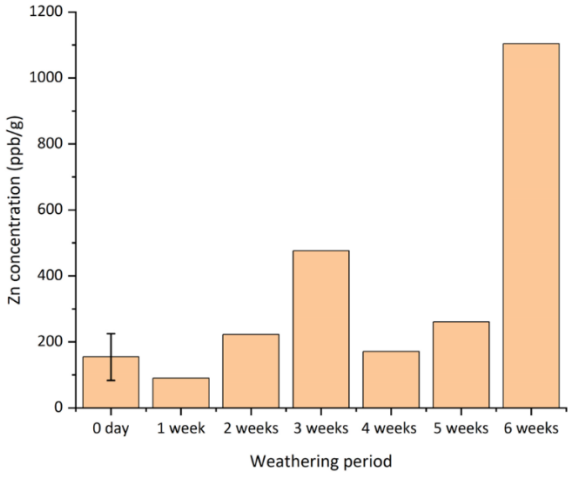

Fig.5-5 Dissolved Zn concentration leached from APPs (>150 μm) which fell from painted-steel samples weathered by UVC with different periods

5.4 Conclusions

APPs were generated from antifouling paints on the surface of carbon steels and remained in the artificial seawater. Paints are more likely to decompose and broke into APPs of smaller sizes after weathered by UVC, which was caused by the weaken of polymer structure due to UVC irradiation. Cu and Zn-based biocides were more easily leached from APPs whose weathered period were longer.

Chapter VI
Conclusions

In order to understand the pollution situation of microplastics and antifouling paint particles (APPs) in the surface seawater in Osaka Bay, the occurrence and distribution of microplastics and microparticles containing heavy metals (metal MPs) were investigated in sea-surface microlayer (S-SML) and bulk water (1m depth) among different sampling zones including coastal areas, navigation routes and center of the bay. This is the first to research the co-occurrence of microplastics and metal MPs, which highlighted the pollution of marine and antifouling paints and provided some theoretical guidance for controlling microplastics pollution. Some new and notable results have been obtained during this study, which are summarized as follows:

1. The average abundance of microplastics at navigation routes was 1360 ± 1050 items/kg in S-SML, about 20 times higher than that of 68.3 ± 49.3 items/kg in bulk water (p<0.05), was relatively high in relation to worldwide values. Especially in S-SML, microplastics abundance at navigation routes was significantly higher than that at the coastal area (p<0.05) and at the center (p<0.05), which may be attributed to the marine and antifouling paints generated from shipping activities.
2. Microplastics were classified in four size categories: 10–53, 53–125, 125–500, and >500 μm, which accounted for 81.2%, 11.1%, 4.45%, and 3.25% in the S-SML, and for 62.2%, 19.8%, 12%, and 6% in bulk water evenly among all sampling sites, respectively. As microplastic sizes increased, their relative abundances decreased.
3. Approximately 11 kinds of polymer types of microplastics were detected, i.e., acrylic resins mainly represented by Polymethyl methacrylate (PMMA), Polypropylene (PP), Polyethylene (PE), Polyester (PET), Polystyrene (PS), Nylon (PA), Polyvinyl chloride (PVC), Polyurethane (PU), Polycarbonate (PC), Ethylene-vinyl acetate copolymer (EVA) and Epoxy. PMMA accounted for the highest proportions of microplastics in both S-SML and bulk water, with 95.1% and 45.6%, respectively.
4. The average abundance of PMMA microplastics in S-SML was 1310 items/kg along navigation routes, which is significantly higher than that of 362 items/kg in the coastal area (p<0.05) and 230 items/kg at the bay center (p<0.05). Specially, the abundance of PMMA microplastics with a size of 10–53 μm along the navigation routes was significantly higher than that in the coastal area (p < 0.05) and at the bay center (p < 0.05).
5. PMMA microplastics abundance in the S-SML was significantly larger than that in bulk water (p<0.05), while non-PMMA microplastics of exhibited a similar abundance level of less than 16 items/kg in both S-SML and bulk water among coastal areas, navigation routes and center of bay. Abundant PMMA microplastics should be responsible for the abundant loads of microplastics. In total, PMMA

microplastics with a size of 10–53 μm along the navigation routes in the S-SML dominated the whole microplastics loads in Osaka Bay.

6. 7 main kinds of metal components were detected in microparticles both in S-SML and bulk water, i.e., Cu, Cu and Zn (Cu-Zn), Zn, Ti, Sn, Fe and Mn or Ni (Fe-Mn-Ni) and Ba. Metal MPs have a relatively uniform distribution in abundance in surface seawater among all sampling sites. Fe-Mn-Ni MPs abundance was significantly higher than that of Ti MPs ($p<0.05$) and of other metal MPs ($p<0.01$), meanwhile, Ti MPs abundance was also significantly higher than that of Cu, Cu-Zn, Zn, Sn and Ba MPs ($p<0.01$). Metal MPs with size range of 10–53 μm always accounted for more than 80% in total abundance.
7. The navigation routes contributed most of metal MPs loads with the percentage of 65.1%. Furthermore, 26.2% and just 8.7% of metal MPs originated from coastal area and from bay center respectively. Among all types of metal MPs, Fe-Mn-Ni MPs which may originate from carbon steel substrate in hull subsurface and heavy fuel oil in ship engine during shipping activities, were the most abundant, accounting for 60.4%, while minor ones were Ti MPs (28.2%), Cu MPs (4.5%), Cu-Zn MPs (3.9%), Sn MPs (1.4%), Zn MPs (1.3%) and Ba MPs (0.3%).
8. The polymer type for 97.8 % of Cu and Cu-Zn MPs (41 samples) and 52.6 % of Zn MPs (19 samples) was acrylic resins which are widely used as binders in contemporary antifouling paints for ships; concentrations of 511–54,000 mg/kg for Cu and 95.1–13,200 mg/kg for Zn were found in these metal MPs. The high metal concentrations found the co-existence of acrylic polymers point towards an origin from APPs which are stemmed from the maintenance, cleaning and navigation of shipping activities. To quantify Cu and Zn concentrations in these microparticles based on X-ray fluorescence spectroscopy (μ-XRF), calibration curves obtained from standard paint particles containing different Cu and Zn concentrations and different particle sizes made with similar matrix used in commercial antifouling paint were firstly established, according to which highly reliable Cu and Zn concentrations in metal MPs were obtained combined with the flameless atomic absorption spectrophotometry (FLAAS).
9. For Cu, Zn, Ti and Sn MPs, their abundance was positive correlated to the abundance of polymer containing microplastics (R^2= 0.358 for Cu, 0.244 for Zn, 0.438 for Ti, 0.183 for Sn, respectively, $p<0.05$), which revealed their associations with microplastics. There was a strong positive correlation between PMMA MPs and Ti MPs in abundance ($R^2=0.3$, $p<0.05$). Considering that PMMA microparticles containing Ti have the similar μ-FTIR spectra with that of marine paint microparticles, the marine paints used on upside and superstructure of ship hulls are seen as one source of these abundant floating PMMA microplastics.
10. APPs were generated from antifouling paints on the surface of carbon steels and remained in the artificial seawater. Paints are more likely to decompose and broke into APPs of smaller sizes after weathered by UVC, which was caused by the weaken of polymer structure due to UVC irradiation. Cu and Zn-based biocides were more easily leached from APPs whose weathered period were longer.

Reference

[1] Cole, M., Lindeque, P., Halsband, C., Galloway, T.S., 2011. Microplastics as contaminants in the marine environment: A review. Mar Pollut Bull 62, 2588-2597.
[2] Andrady, A.L., 2011. Microplastics in the Marine Environment. Mar Pollut Bull 62, 1596-1605.
[3] Barnes, D.K.A., Galgani, F., Thompson, R.C., Barlaz, M., 2009. Accumulation and fragmentation of plastic debris in global environments. Phil Trans Soc B 364, 1985-1998.
[4] Lebreton, L., Slat, B., Ferrari, F., Sainte-Rose, B., Aitken, J., Marthouse, R., Hajbane, S., Cunsolo, S., Schwarz, A., Levivier, A., Noble, K., Debeljak, P., Maral, H., Schoeneich-Argent, R., Brambini, R., Reisser, J., 2018. Evidence that the Great Pacifc Garbage Patch is rapidly accumulating plastic. Sci Rep 8, 4666.
[5] Zitko, V., Hanlon, M., 1991. Another source of pollution by plastics: skin cleansers with plastic scrubbers. Mar Pollut Bull 22, 41-42.
[6] Gregory, M.R., 1996. Plastic 'scrubbers' in hand cleansers: a further (and minor) source for marine pollution identified. Mar Pollut Bull 32, 867-871.
[7] Browne, M.A., Galloway, T., Thompson, R., 2007. Microplastic-an emerging contaminant of potential concern? Integr Environ Asses 3, 559-561.
[8] Luo, H.W., Liu, C.Y., He, D.Q., Xu, J., Sun., J.Q., Li, J., Pan, X.L., 2022. Environmental behaviors of microplastics in aquatic systems: A systematic review on degradation, adsorption, toxicity and biofilm under aging conditions. J Hazard Mat 423, 126915.
[9] Yeo, B.G., Takada, H., Yamashita, R., Okazaki, Y., Uchida, K., Tokai, T., Tanaka, K., Trenholm, N., 2019. PCBs and PBDEs in microplastic particles and zooplankton in open water in the Pacifific Ocean and around the coast of Japan. Mar Pollut Bull 151, 110806.
[10] Miller, M.E., Hamann, M., Kroon, F.J., 2020. Bioaccumulation and biomagnification of microplastics in marine organisms: A review and meta-analysis of current data. PloS ONE 15(10), 0240792.
[11] Wu, D., Feng, Y.D., Wang, R., Jiang, J., Guan, Q.Q., Yang, X., Wei, H.C., Xia, Y.K., Luo, Y.M., 2023. Pigment microparticles and microplastics found in human thrombi based on Raman spectral evidence. J Adv Res 49, 141-150.
[12] Zhang, N., Li, Y.B., He, H.R., Zhang, J.F., Ma, G.S., 2021. You are what you eat: Microplastics in the feces of young men living in Beijing. Sci Total Environ 767, 144345.
[13] Van Cauwenberghe, L., Janssen, C.R., 2014. Microplastics in bivalves cultured for human consumption. Environ Pollut 193, 65-70.
[14] Arthur, C., Baker, J., Bamford, H., 2009. Proceedings of the international research workshop on the occurrence, effects and fate of microplastic marine debris. Sept 9–11, 2008, NOAA Technical Memorandum NOS-OR&R30.
[15] Gaylarde, C.C., Neto, J.A.B., Fonseca, E.M.d., 2021. Paint fragments as polluting

microplastics: A brief review. Mar Pollut Bull 162, 111847.
[16] OSPAR Commission, 2010. Guideline for monitoring marine litter on the beaches in the OSPAR maritime area. OSPAR Commission, London.
[17] IMO, 2019. Hull Scrapings and Marine Coatings as a Source of Microplastics. International Maritime Organization, London, UK.
https://wwwcdn.imo.org/localresources/en/OurWork/Environment/Documents/Hull%20Scrapings%20final%20report.pdf
[18] Turner, A., 2021. Paint particles in the marine environment: An overlooked component of microplastics. Water Res X 12, 100110.
[19] Lacerda, A., Rodrigues, L., Sebille E., Rodrigues, F., Ribeiro, L., Secchi, E.R., Kessler, F., Proietti, M.C., 2019. Plastics in sea surface waters around the Antarctic Peninsula. Sci Rep 9, 3977.
[20] Lima, A.R.A., Costa, M.F., Barletta, M., 2014. Distribution patterns of microplastics within the plankton of a tropical estuary. Environ Res 132, 146–155.
[21] Suaria, G., Avio, C.G., Mineo, A., Lattin, G.L., Magaldi, M.G., Belmonte, G., Moore, C.J., Regoli, F., Aliani, S., 2016. The Mediterranean Plastic Soup: synthetic polymers in Mediterranean surface waters. Sci Rep 9, 37551.
[22] Ivar do Sul, J.A., Costa, M.F., Fillmann, G., 2014. Microplastics in the pelagic environment around oceanic islands of the Western Tropical Atlantic Ocean. Water Air Soil Pollut 225, 2004.
[23] Öztekin, A., Bat, L., 2017. Microlitter pollution in sea water: a preliminary study from Sinop Sarikum coast of the southern Black Sea. Turkish J Fish Aquatic Sciences 17, 1431–1440.
[24] Aliabad, M.K., Nassiri, M., Kor, K., 2019. Microplastics in the surface seawaters of Chabahar Bay, Gulf of Oman (Makran coasts). Mar Pollut Bull 143, 125–133.
[25] Wang, T., Zou, X.Q., Li, B.J., Yao, Y.L., Zang, Z., Li, Y.L., Yu, W.W., Wang, W.Z., 2019. Preliminary study of the source apportionment and diversity of microplastics: Taking floating microplastics in the South China Sea as an example. Environ Pollut 245, 965–974.
[26] Wang, T., Li, B.J., Yu, W.W., Zou, X.Q., 2021. Microplastic pollution and quantitative source apportionment in the Jiangsu coastal area, China. Mar Pollut Bull 166, 112237.
[27] Dibke, C., Fischer, M., Scholz-Böttcher, B.M., 2021. Microplastic Mass Concentrations and Distribution in German Bight Waters by Pyrolysis−Gas Chromatography−Mass Spectrometry/Thermochemolysis Reveal Potential Impact of Marine Coatings: Do Ships Leave Skid Marks? Environ Sci Technol 55, 2285–2295.
[28] Song, Y.K., Hong, S.H., Jang, M., Kang, J.H., Kwon, O.Y., Han, G.M., Shim, W.J., 2014. Large Accumulation of Micro-sized Synthetic Polymer Particles in the Sea Surface Microlayer. Environ Sci Technol 48, 9014–9021.
[29] Evans, S.M., Birchenough, A.C., Brancato, M.S., 2000. The TBT ban: out of the frying pan into the fire? Mar Pollut Bull 40, 204–211.
[30] Muller-Karanassos, C., Turner, A., Arundel, W., Vance, T., Lindeque, P.K., Cole, M., 2019. Antifouling paint particles in intertidal estuarine sediments from southwest England and their ingestion by the harbour ragworm, *Hediste diversicolor*. Environ

Pollut 249, 163–170.
[31] Singh, N., Turner, A., 2009. Trace metals in antifouling paint particles and their heterogeneous contamination of coastal sediments. Mar Pollut Bull 58, 559–564.
[32] Cuong, D.T., Karuppiah, S., Obbard, J.P., 2008. Distribution of heavy metals in the dissolved and suspended phase of the sea-surface microlayer, seawater column and in sediments of Singapore's coastal environment. Environ Monit Assess 138, 255–272.
[33] Turner, A., 2010. Marine pollution from antifouling paint particles. Mar Pollut Bull 60, 559–564.
[34] Okamura, H., 2024. Anthropogenic microparticles floating in seawater (Chapter 8). In: Harino, Kojima and Onduka (Ed.), Change of Antifouling Biocides for a Long Time and Impact for Aquatic Organisms (In Japanese). Kouseisha Kouseikaku, Tokyo, pp. 154-171.
[35] Paz-Villarraga, C.A., Castro, Í.B., Fillmann, G., 2022. Biocides in antifouling paint formulations currently registered for use. Environ Sci Pollut Res 29, 30090–30101.
[36] Castro, Í.B., Iannacone, J., Santos, S., Fillmann, G., 2018. TBT is still a matter of concern in Peru. Chemosphere 205:253–259.
[37] Bowman, J.C., Readman, J.W., Zhou, J.L., 2003. Seasonal variability in the concentrations of Irgarol 1051 in Brighton Marina, UK; including the impact of dredging. Mar Pollut Bull 46:444–451.
[38] Chen, Q., Allgeier, A., Yin, D., Hollert, H., 2019. Leaching of endocrine disrupting chemicals from marine microplastics and mesoplastics under common life stress conditions. Environ Int 130, 104938.
[39] Kholodovych, V., Welsh, W.J., 2007. Thermal-Oxidative Stability and Degradation of Polymers. In: Mark, J.E. (Ed.), Physical Properties of Polymers Handbook. Springer, New York, USA, pp. 927–938.
[40] Simon, M., Vianello, A., Shashoua, Y., Vollertsen, J., 2021. Accelerated weathering affects the chemical and physical properties of marine antifouling paint microplastics and their identification by ATR-FTIR spectroscopy. Chemosphere 274, 129749.
[41] Simon, M., Hartmann, B.N., Vollertsen, J., 2021. Accelerated weathering increases the release of toxic leachates from microplastic particles as demonstrated through altered toxicity to the green algae raphidocelis subcapitata. Toxics 9, 185.
[42] Holmes, L., Turner, A., 2009. Leaching of hydrophobic Cu and Zn from discarded marine antifouling paint residues: Evidence for transchelation of metal pyrithiones. Environ Pollut 157, 3440–3444.
[43] Cresswell, T., Richards, J. P., Glegg, G. A., Readman, J. W., 2006. The Impact of Legislation on the Usage and Environmental Concentrations of Irgarol 1051 in UK Coastal Waters. Mar. Pollut. Bull., 52,1169–1175.
[44] Schmidt, J.M., 1999. Anaerobic Aquatic Metabolism of 14C-Irgarol1051. 1992 ABC Report 38885. Analytical Bio-Chemistry Laboratories, Inc. Columbia, MO. [In: Hall Jr., L.W., Giddings, J.M. Solomon, K.R., Balcomb, R. (Eds.), An Ecological Risk Assessment for the Use of Irgarol 1051 as an Algaecide for Antifouling Paints, special issue]. Crit Rev Toxicol 29, 367–437.
[45] Thomas, K.V., McHugh, M., Hilton, M., Waldock, M., 2003. Increased persistence of antifouling paint biocides when associated with paint particles. Envrion Pollut 123, 153–161.

[46] Hasan, C.K., Turner, A., Readman, J., Frickers, T., 2014. Environmental Risks Associated with Booster Biocides Leaching from Spent Anti-Fouling Paint Particles in Coastal Environments. Envrion Pollut 123, 153–161.
[47] Li, J., Liu, H., & Chen, J. P., 2018. Microplastics in freshwater systems: a review on occurrence, environmental effects, and methods for microplastics detection. Water Res 137, 362–374.
[48] Besseling, E., Wang, B., Lürling, M., & Koelmans, A. A., 2014. Nanoplastic affects growth of S. obliquus and reproduction of D. magna. Environ Sci Technol, 48(20), 12336–12343.
[49] Zhang, C., Chen, X., Wang, J., & Tan, L., 2017. Toxic effects of microplastic on marine microalgae Skeletonema costatum: interactions between microplastic and algae. Environ Pollut 220, 1282–1288.
[50] Sjollema, S. B., Redondo-Hasselerharm, P., Leslie, H. A., Kraak, M. H., & Vethaak, A. D., 2016. Do plastic particles affect microalgal photosynthesis and growth? Aquat Toxicol 170, 259–261.
[51] Rosenkranz, P., Chaudhry, Q., Stone, V., & Fernandes, T. F., 2009. A comparison of nanoparticle and fine particle uptake by Daphnia magna. Environ Toxicol Chem 28(10), 2142–2149.
[52] Alimba, C. G., Faggio, C., 2019. Microplastics in the marine environment: current trends in environmental pollution and mechanisms of toxicological profle. Environ Toxicol Phar 68, 61–74.
[53] Waring, R. H., Harris, R. M., & Mitchell, S. C. (2018). Plastic contamination of the food chain: a threat to human health? Maturitas, 115, 64–68.
[54] Deng, Y., Zhang, Y., Lemos, B., & Ren, H., 2017. Tissue accumulation of microplastics in mice and biomarker responses suggest widespread health risks of exposure. Sci Rep 7, 46687.
[55] Lu, L., Wan, Z., Luo, T., Fu, Z., & Jin, Y., 2018. Polystyrene microplastics induce gut microbiota dysbiosis and hepatic lipid metabolism disorder in mice. Sci Total Environ 631, 449–458.
[56] Jin, Y., Lu, L., Tu, W., Luo, T., & Fu, Z., 2019. Impacts of polystyrene microplastic on the gut barrier, microbiota and metabolism of mice. Sci Total Environ 649, 308–317.
[57] Dris, R., Gasperi, J., Mirande, C., Mandin, C., Guerrouache, M., Langlois, V., & Tassin, B., 2017. A first overview of textile fibers, including microplastics, in indoor and outdoor environments. Environ Pollut 221, 453–458.
[58] Alzieu, C., Thibaud, Y., Heral, M., Boutier, B., 1980. Risk assessment of using anti fouling coatings in shellfish farming areas. Rev des Trav l'Institut des Pech. Marit 44, 305–348.
[59] Floch, H., Deschiens, R., Lecorroller, Y., 1964. On the elective molluscicidal action of cuprous oxide, metallic copper and cuprous chloride. Bull Soc Pathol Exot Filiales 57, 124–138.
[60] Mochida, K., Ito, K., Harino, H., Kakuno, A., Fujii, K., 2006. Acute toxicity of pyrithione antifouling biocides and joint toxicity with copper to red sea bream (*Pagrus major*) and toy shrimp (*Heptacarpus futilirostris*). Environ Toxicol Chem 25, 3058–3064.
[61] Amara, I., Miled, W., Slama, R.B., Ladhari, N., 2018. Antifouling processes and toxicity effects of antifouling paints on marine environment. A review. Environ Toxicol

Phar 57, 115–130.
[62] Lehmann, M., Häusl, F., Gekle, S., 2023. Modeling of vertical microplastic transport by rising bubbles. Microplast. Nanoplast 3, 4.
[63] Ye, S., Andrady, A.L., 1991. Fouling of floating plastic debris under Biscayne Bay exposure conditions. Mar Pollut Bull 22, 608–613.
[64] Cunliffe, M., Engel, A., Frka, S., Gasparovic, B., Guitart, C., Murrell, J.C., Salter, M., Stolle, C., Goddard, R.U., Wurl, O., 2013. Sea surface microlayers: A unified physicochemical and biological perspective of the air−ocean interface. Prog Oceangr 109, 104–116.
[65] Meeker, J.D., Sathyanarayana, S., Swan, S.H., 2009. Phthalates and other additives in plastics: human exposure and associated health outcomes. Philos Trans R So Lond B Biol Sci 364 (1526), 2097–2113.
[66] Mato, Y., Isobe, T., Takada, H., Kanehiro, H., Ohtake, C., Kaminuma, T., 2001. Plastic resin pellets as a transport medium for toxic chemicals in the marine environment. Environ Sci Technol 35, 318–324.
[67] Brennecke, D., Duarte, B., Paiva, F., Caçador, I., Canning-Clode, J., 2016. Microplastics as vector for heavy metal contamination from the marine environment. Estuar Coast Shelf Sci 178, 189–195.
[68] Rochman, C.M., Hentschel, B.T., Teh, S.J., 2014. Long-term sorption of metals is similar among plastic types: implications for plastic debris in aquatic environments. PLoS One 9, e85433.
[69] Cai, X.Y., Chen, H.L., Huang, B., Lu, J.B., 2022. Analysis on advances and characteristics of microplastic pollution in China's lake ecosystems. Ecotox Environ Safe 232, 113254.
[70] Pan, Z., Guo, H.G, Chen, H.Z., Wang, S.M., Sun, X.W., Zou, Q.P., Zhang, Y.B., Lin, H., Cai, S.Z., Huang, J., 2019. Microplastics in the Northwestern Pacific: Abundance, distribution, and characteristics. Sci Total Environ 650, 1913–1922.
[71] Zhang, Q., Xu, E.G., Li, J., Chen, Q., Ma, L., Zeng, E.Y., Shi, H., 2020. A review of microplastics in table salt, drinking water, and air: direct human exposure. Environ Sci Technol 54 (7), 3740–3751.
[72] Cai, M.G., He, H.X., Liu, M.Y., Li, S.W., Tang, G.W., Wang, W.M., Huang, P., Wei, G., Lin, Y., Chen, B., et al, 2018. Lost but can't be neglected: Huge quantities of small microplastics hide in the South China Sea. Sci Total Environ 633, 1206–1216.
[73] Imhof, H.K., Laforsch, C., Wiesheu, A.C., Schmid, J., Anger, P.M., Niessner, R., Ivleva, N.P., 2016. Pigments and plastic in limnetic ecosystems: A qualitative and quantitative study on microparticles of different size classes. Water Res 98, 64–74.
[74] Baldwin, A.K., Spanjer, A.R., Rosen, M.R., Thom, T., 2020. Microplastics in lake mead national recreation area, USA: Occurrence and biological uptake. PLoS ONE 15, e0228896.
[75] Wang, Z., Su, B., Xu, X., Di, D., Huang, H., Mei, K., Dahlgren, R.A., Zhang, M., Shang, X., 2018. Preferential accumulation of small (<300 μm) microplastics in the sediments of a coastal plain river network in eastern China. Water Res 144, 393–401.
[76] Nishiyama, K., Yano, T., Suzuki, H., Iida, H., 1991. Meteorology and Oceanography in the Seto Inland Sea. Mar Pollut Bull 23, 5–9.
[77] Chang, P.H., Guo, X.Y., Takeoka, H., 2009. A numerical study of the seasonal circulation in the Seto Inland Sea, Japan. J Oceanogr 65, 721–736.

[78] Chae, D.H.; Kim, I.S.; Kim, S.K.; Song, Y.K.; Shim, W.J., 2015. Abundance and Distribution Characteristics of Microplastics in Surface Seawaters of the Incheon/Kyeonggi Coastal Region. Arch Environ Contam Toxicol 69, 267–278.
[79] Cincinelli, A., Scopetani, C., Chelazzi, D., Lombardini, E., Martellini, T., Katsoyiannis, A., Fossi, M.C., Corsolini, S., 2017. Microplastic in the surface waters of the Ross Sea (Antarctica): Occurrence, distribution and characterization by FTIR. Chemosphere 175, 391–400.
[80] Yamamoto, T., Kitamaru, T., Matsuda, O., 1996. River inputs of fresh water, total nitrogen and total phosphorus into the Seto Island Sea. J Fac Appl Biol Sci Hiroshima Univ 35, 81–104.
[81] Hoshika, A., Tanimoto, T., Mishima, Y., 1999. Current and material transport at Tomogashima Strait, Japan. J Oceanogr 55, 427–437.
[82] So, W.K., Ghan, K., Not, C., 2018. Abundance of plastic microbeads in Hong Kong coastal water. Mar Pollut Bull 133, 500–505.
[83] Kalčíková, G., Aličˇ, B., Skalar, T., Bundschuh, M., Gotvajn, A.Ž, 2017. Wastewater treatment plant effluents as source of cosmetic polyethylene microbeads to freshwater. Chemosphere 188, 25–31.
[84] Ryan, P.G., 2015. Does size and buoyancy affect the long-distance transport of floating debris? Environ Res Lett 10, 084019.
[85] Krelling, A.P., Souza, M.M., Williams, A.T., Turra, A., 2017. Transboundary movement of marine litter in an estuarine gradient: Evaluating sources and sinks using hydrodynamic modelling and ground truthing estimates. Mar Pollut Bull 119, 48–63.
[86] Zhang, H., 2017. Transport of microplastics in coastal seas. Estuar Coast Shelf Sci 199, 74–86.
[87] Enders, K., Lenz, R., Stedmon, C.A., Nielsen, T.G., 2015. Abundance, size and polymer composition of marine microplastics ≥10 μm in the Atlantic Ocean and their modelled vertical distribution. Mar Pollut Bull 100, 70–81.
[88] Raita, G., Takashi, I, 2015. Poly (methyl methacrylate) (PMMA). In Encyclopedia of Polymeric Nanomaterials, Kobayashi, S. and Müllen, K., Eds., Springer: Berlin/Heidelberg, Germany.
[89] Madhuraj, P.K., Appu, J.B., Amal, R., Riya, K.A., Abhinab, B., Suja, P.D., 2022. Machine learning aided meta-analysis of microplastic polymer composition in global marine environment. J Hazard Mat 440, 129801.
[90] González-Reyna, M.A., Espinosa-Medina, M.A., Rodrigo Esparza, A.R., Hernández-Martinez, A.R., Maya-Cornejo, J., Estévez, M., 2021. Anticorrosive Effect of the Size of Silica Nanoparticles on PMMA-Based Hybrid Coatings. J Mater Eng Perform 30,1054−1065.
[91] Almeida, E., Diamantino, T.C., Soua, O., 2007. Marine paints: The particular case of antifouling paints. Prog Org Coat 59, 2–20.
[92] Tsuboi, M., Yoshikawa, E., Arimura, H., Kozono, S., Nakamura, N., 2001. Silyl (Meth)acrylate Copolymer-Based Antifouling Marine Coating Composition. Japan Patent JP2001081147, 27 March 2001. (In Japanese)
[93] Lejars, M., Margaillan, A., Bressy, C., 2020. Siloxy Silylester Methacrylate Diblock Copolymer-Based Coatings with Tunable Erosion and Marine Antifouling Properties. Appl Polym Mater 2, 3291–3300.
[94] Howell, D., Behrends, B., 2006. A methodology for evaluating biocide release rate,

surface roughness and leach layer formation in a TBT-free, self-polishing antifouling coating. Biofouling 22, 303–315.
[95] Kii, S., Dam-Johansen, K., Weinell, C.E., Pedersen, M.S., 2002. Seawater-Soluble Pigments and Their Potential Use in Self-Polishing Antifouling Paints: Simulation Based Screening Tool. Prog Org Coat 45, 423–434.
[96] Sha, J., Chen, R., Yu, J., Liu, Q., Liu, J., Zhu, J., Liu, P., Li, R., Wang, J., 2023. Dynamic multi-level micro-structured antifouling surfaces by combining quaternary ammonium modified GO with self-polishing copolymers. Carbon 201, 1038–1047.
[97] Sha, J., Liu, X., Chen, R., Yu, J., Liu, Q., Liu, J., Zhu, J., Liu, P., Li, R., Wang, J., 2023. Surface hydrolysis-anchored eugenol self-polishing marine antifouling coating. J Colloid Interface Sci 637, 67–75.
[98] Hayes, J., Golden, M., Smith, G.D., 2007. From Formulation to Finished Product: Causes and Potential Cures for Conservation Concerns in Acrylic Emulsion Paints. In Modern Paints Uncovered, 2nd ed.; Leamer, T., Smithen, P., Kruger, J.W., Schilling, M.R., Eds., Getty Conservation Institute: Los Angeles, CA, USA, pp. 58–65.
[99] Erlebacher, J.D., Brown, E., Mecklenburg, M.F., Tumosa, C.S., 1992. The Effects of Temperature and Relative Humidity on the Mechanical Properties of Modern Painting Materials. MRS Online Proc Libr 267, 359–370.
[100] Mansourpanah, Y., Habili, E.M., 2013. Preparation and modification of thin film PA membranes with improved antifouling property using acrylic acid and UV irradiation. J Membr Sci 430, 158–166.
[101] Geyer, R., Jambeck, J.R., Law, K.L., 2017. Production, use, and fate of all plastics ever made. Adv Sci 3, 1700782.
[102] Kelly, M.R., Lant, N.J., Kurr, M., Burgess, J.G., 2019. Importance of water-volume on the release of microplastic fibers from laundry. Environ Sci Technol 53, 11735–11744.
[103] Park, C.H., Kang, Y.K., Seung-Soon, I., 2004. Biodegradability of cellulose fabrics. J Appl Polym 94, 248–253.
[104] Siracusa, V., Rocculi, P., Romani, S., Dalla Rosa, M., 2008. Biodegradable polymers for food packaging: A review. Trends Food Sci Technol 19, 634–643.
[105] Yu, D., Peng, X.B., Wang, J.P., Wang, J.D., Bao, K., 2016. Occurrence of microplastics in the beach sand of the Chinese inner sea: The Bohai Sea. Environ Pollut 214, 722–730.
[106] Zhao, D., Ran, J.M., Teng, W., Liu, J., Liu, Y.L., Yin, X.N., 2018. Microplastic pollution in sediments from the Bohai Sea and the Yellow Sea, China. Sci Total Environ 640–641, 637–645.
[107] Song, Y.K., Hong, S.H., Jang, M., Han, G.M., Shim, W.G., 2015. Occurrence and Distribution of Microplastics in the Sea Surface Microlayer in Jinhae Bay, South Korea. Arch Environ Contam Toxicol 69, 279–287.
[108] Stead, J.L., Cundy, A.B., Hudson, M.D., Thompson, C.E.L., Williams, I.D., Russell, A.E., Pabortsava, K., 2020. Identification of tidal trapping of microplastics in a temperate salt marsh system using sea surface microlayer sampling. Sci Rep10, 14147.
[109] Miller, R.Z., Watts, A.J., Winslow, B.O., Galloway, T.S., Barrows, A.P., 2017. Mountains to the sea: River study of plastic and non-plastic microfiber pollution in the northeast USA. Mar Pollut Bull 124, 245–251.
[110] Gray, A.D., Werta, H., Leads, R.R., Weinstein, J.E., 2018. Microplastic in two

South Carolina Estuaries: Occurrence, distribution, and composition. Mar Pollut Bull 128, 223–233.
[111] Taha, Z.D., Amin, R.M., Anuar, S.T., Nasser, A.A.A., Sohaimi, E.S., 2021. Microplastics in seawater and zooplankton: A case study from Terengganu estuary and offshore waters, Malaysia. Sci Total Environ 786, 147466.
[112] Prarat, P., Hongsawat, P., 2022. Microplastic pollution in surface seawater and beach sand from the shore of Rayong province, Thailand: Distribution, characterization, and ecological risk assessment. Mar Pollut Bull 174, 113–200.
[113] Zhou, M., Yanai, H., Yap, C.K., Emmanouil, C., Okamura, H., 2023. Anthropogenic Microparticles in Sea-Surface Microlayer in Osaka Bay, Japan. J Xenobiot 13, 685–703.
[114] Beyer, J., Trannum, H.C., Bakke, T., Hodson, P.V., Collier, T.K., 2016. Environmental effects of the Deepwater Horizon oil spill: a review. Mar Pollut Bull 110, 28–51.
[115] Wu, H.F., Zhang, X.Y., Wang, Q., Li, L.Z., Ji, C.L., Liu, X.L., Zhao, J.M., Yin, X.L., 2013. A metabolomics investigation on arsenic-induced toxicological effects in the clam Ruditapes philippinarum under different salinities. Ecotoxicol Environ Saf 90, 1–6.
[116] Gale, N.L., Adams, C.D., Wixson, B.G., Loftin, K.A., Huang, Y.W., 2004. Lead, zinc, copper, and cadmium in fish and sediments from the big river and flat river creek of Missouri's old lead belt. Environ Geochem Health 26 (1), 37–49.
[117] Beltrame, M., De Marco, S., Marcovecchio, J., 2009. Dissolved and particulate heavy metals distribution in coastal lagoons. A case study from Mar Chiquita Lagoon, Argentina. Estuar Coast Shelf Sci 85, 45–56.
[118] Papagiannis, I., Kagalou, I., Leonardos, J., Petridis, D., Kalfakakou, V., 2004. Copper and zinc in four freshwater fish species from Lake Pamvotis (Greece). Environ Int 30 (3), 357–362.
[119] Crump, K.L., Trudeau, V.L., 2009. Mercury-induced reproductive impairment in fish. Environ Toxicol Chem 28 (5), 895–907.
[120] Meng, W., Qin, Y., Zheng, B., Zhang, L., 2008. Heavy metal pollution in Tianjin Bohai Bay, China. J Environ Sci 20, 814–819.
[121] Tulcan, R., Ouyang, W., Lin, C., He, M., Wang, B., 2021. Vanadium pollution and health risks in marine ecosystems: anthropogenic sources over natural contributions. Water Res. 207, 117838.
[122] Wang, Q., Li, H., Zhang, Y., Wang, X., Zhang, C., Xiao, K., Qu, W., 2019. Evaluations of submarine groundwater discharge and associated heavy metal fluxes in Bohai Bay, China. Sci Total Environ 695, 133873
[123] Wang, J., Liu, R.H., Yu, P., Tang, A.K., Xu, L.Q., Wang, J.Y., 2012. Study on the Pollution Characteristics of Heavy Metals in Seawater of Jinzhou Bay. Procedia Environ Sci 13, 1507–1516.
[124] Zhang, A., Wang, L.L., Zhao, S.L., Yang, X.L., Zhao, Q., Zhang, X.H., Yuan, X.T., 2017. Heavy metals in seawater and sediments from the northern Liaodong Bay of China: Levels, distribution and potential risks. Reg Stud Mar Sci 11, 32–42.
[125] Piotrowicz, S.R., Ray, B.J., Hoffman, G.L., Duce, R.A., 1972. Trace Metal Enrichment in the Sea-Surface Microlayer. J Geophys Res 77, 5243–5254.
[126] Marina-Montes, C., Pérez-Arribas, L.V., Escudero, M., Anzano, J., Cáceres, J.O.,

2020. Heavy metal transport and evolution of atmospheric aerosols in the Antarctic region. Sci Total Environ 721,137702.
[127] Sadiq, M., 1992. Toxic Metal Chemistry in Marine Environments. Marcel Dekker, New York.
[128] Vedolin, M.C., Teophilo, C.Y.S., Turra, A., Figueira, R.C.L., 2018. Spatial variability in the concentrations of metal in beached microplastics. Mar Pollut Bull 129, 487–493.
[129] Jasna, M.L., Jelena, L., Pero, T., Dubravka, B.V., Jasna, Š., 2018. Levels of trace metals on microplastic particles in beach sediments of the island of Vis, Adriatic Sea, Croatia. Mar Pollut Bull 137, 231–236.
[130] Liu, H., Ding, C.L., Zhang, G.C., Guo, Y.Y., Song, Y.Y., Thangaraj, S., Zhang, X.D., Sun, J., 2023. Dissolved and particulate heavy metal pollution status in seawater and sedimentary heavy metals of the Bohai Bay. Mar Environ Pollut 191, 106158.
[131] Mueller, L., Jakobi, G., Czech, H., Stengel, B., Orasche, J., Arteaga-Salas, J.M., Karg, E., Elsasser, M., Sippula, O., Streibel, T., Slowik, J.G., Prevot, A.S.H., Jokiniemi, J., Rabe, R., Harndorf, H., Michalke, B., Schnelle-Kreis, J., Zimmermann, R., 2015. Characteristics and temporal evolution of particulate emissions from a ship diesel engine. Appl Energ 155, 204–217.
[132] Zając, G., Szyszlak-Bargłowicz, J., Słowik, T., Kuranc, A., Kamińska, A., 2015. Designation of Chosen Heavy Metals in Used Engine Oils Using the XRF Method. Pol J Environ Stud 24 (5), 2277–2283.
[133] Turner, A., Ostle, C., Wootton, M., 2022. Occurrence and chemical characteristics of microplastic paint flakes in the North Atlantic Ocean. Sci Total Environ 806, 150375.
[134] Okamura, H., Kano, K., Yap, C.K., Emmanouil, C., 2022. Floating particles with high copper concentration in the sea-surface microlayer. Environ Sci Pollut Res 29, 29535–29542.
[135] Zhou, M., Osaka, I., Hashimoto, K., Yap, C.K., Emmanouil, C., Nakano, T., Okamura, H., 2024. Co-occurrence of microplastics and microparticles containing Cu and Zn and other heavy metals in sea-surface microlayer in Osaka Bay, Japan. J Hazard Mater 480, 136085.
[136] Zhang, H., Kong, F., Chen, Y., Zhao, X., Tang, Y., Zuo, Y., 2023. Degradation of Two Anti-Corrosion and Anti-Fouling Coating Systems in Simulated Diurnal Cycling Immersion. Coatings 13, 389.
[137] Soon, Z.Y., Jung, J.H., Jang, M., Kang, J.H., Jang, M.C., Lee, J.S., Kim, M., 2019. Zinc Pyrithione (ZnPT) as an Antifouling Biocide in the Marine Environment—a Literature Review of Its Toxicity, Environmental Fates, and Analytical Methods. Water Air Soil Poll 230, 310.
[138] Ni, C.H., Feng, K., Li, X., Zhao, H.Z., Yu, L.M., 2020. Study on the preparation and properties of new environmentally friendly antifouling acrylic metal salt resins containing indole derivative group. Prog Org Coat 148, 105824.
[139] Tanino, S., Hayashi, Y., 2018. Antifouling Coating Composition, Antifouling Coating Film, Base Material Provided with Antifouling Coating Film, Method for Product Same, and Antifouling Method WO2018/003136, 1 April 2018. (In Japanese)
[140] Yang, S.H., Shen, J.Y., Chang, M.S., Wu, G.J., 2012. Quantification of vehicle paint components containing polystyrene using pyrolysis-gas chromatography/mass spectrometry. Anal Methods 4, 1989–1995.

[141] Defeyt, C., Langenbacher, J., Rivenc, R., 2017. Polyurethane coatings used in twentieth century outdoor painted sculptures. Part I: comparative study of various systems by means of ATR-FTIR spectroscopy. Herit Sci 5, 11.
[142] Aggarwal, L.K., Thapliyal, P.C., Karade, S.R., 2007. Anticorrosive properties of the epoxy–cardanol resin-based paints. Prog Org Coat 59, 76–80.
[143] Singh, S.K., Tambe, S.P., Raja, V.S., Kumar, D., 2007. Thermally sprayable polyethylene coatings for marine environment. Prog Org Coat 60, 186–193.
[144] Chen, M.C., Koh, P.W., Ponnusamy, V.K., Lee, S.L., 2022. Titanium dioxide and other nanomaterials based antimicrobial additives in functional paints and coatings: Review. Prog Org Coat 163, 106660.
[145] Bejgarn, S., MacLeod, M., Bogdal, C., Breitholtz, M., 2015. Toxicity of leachate from weathering plastics: an exploratory screening study with *Nitocra spinipes*. Chemosphere 132, 114e119.
[146] Hanun, J.N., Hassan, F., Jiang, J.J., 2021. Occurrence, fate, and sorption behavior of contaminants of emerging concern to microplastics: Influence of the weathering/aging process. J Environ Chem Eng 9, 106290.
[147] Banfield, T.A., 1955. Anti-Corrosion Methods and Materials. In The Painting of Ships, 2(10). British Paints Ltd., British.
[148] Information Research Ltd., A Profile of the European Paint Industry 7th ed., 1986, pp. 13.
[149] Hamilton, A.D.C., 1957. Modern marine paints. Corrosion Technology 11, 5–8.
[150] Itou, S., 2010. Introduction to Pigments. J Jpn Soc Colour Mater 83 (7), 308–316.
[151] Sato, A., 2013. Painting of Marine Coatings - Basic Points to Pay Attention to in Painting of Marine Coatings. J JIME 48 (1), 94–99.
[152] Guerguer, M., Naaman,e S., Edfouf, Z., Raccurt, O., Bouaouine, H., 2021. Chemical Degradation and Color Changes of Paint Protective Coatings Used in Solar Glass Mirrors. Coatings 11,476.
[153] Szeto, W., Leung, M.K.H., Leung, D.Y.C., 2021. Recent developments of titanium dioxide materials for aquatic antifouling application. J Mar Sci Technol 26, 301–321.
[154] Waku, H., 2021. Composition of antifouling paint. Would Intellectual Property Organization WO2021/033705 A1, 25 February 2021. (In Japanese)
[155] Harino, H., Yamato, S., 2021. Distribution of antifouling biocides in a coastal area of Tanabe Bay, Japan. J Mar Biol Assoc UK 101, 49–59.
[156] Adeyeye, O., Xiao, C.L., Zhang, Z.H., Liang, X.J., 2020. State, source and triggering mechanism of iron and manganese pollution in groundwater of Changchun, Northeastern China. Environ Monit Assess 192, 619.
[157] Kar, D., Sur, P., Mandal, T., Saha, T., Kole, R.K., 2008. Assessment of heavy metal pollution in surface water. Int J Environ Sci Tech 5(1), 119–124.
[158] Bhandari, J., Khan, F., Abbassi, R., Garaniya, V., 2015. Modelling of pitting corrosion in marine and offshore steel structures – a technical review. J Loss Prev Process Ind 37, 39–62.
[159] Gronostajski, Z., Kaszuba, M., Widomski, P., Smolik, J., Ziemba, J., 2019. Analysis of wear mechanisms of hot forging tools protected with hybrid layers performed by nitriding and PVD coatings deposition. Wear 420–421, 269–280.
[160] Tian, Y.S., Chen, C.Z., Li, S.T., Huo, Q.H., 2005. Research progress on laser

surface modification of titanium alloys. Appl Surf Sci 242, 177–184.
[161] Damborenea, J., 1998. Surface modification of metals by high power lasers. Surf Coat Tech 100–101, 377–382.
[162] Tian, J.Y., Xu, P., Chen, J.H., Liu, Q.B., 2019. Microstructure and phase transformation behaviour of a Fe/Mn/Si/Cr/Ni alloy coating by laser cladding. Opt Laser Eng 122, 97–104.
[163] Gao, S.L., Liang. J., Zhou. J.S., 2022. Evolution in microstructure features and properties of Mo-containing Fe-Cr-Ni-B-Si composite coatings by laser cladding. Mater Charact 188,111926.
[164] Yang, J.X., Miao, X.H., Wang, X.B., Yang, F., 2014. Influence of Mn additions on the microstructure and magnetic properties of FeNiCr/60% WC composite coating produced by laser cladding. Int J Refract Met H 46, 58–64.
[165] Zayed, A., Garbatov, Y., Guedes Soares, C., 2018. Corrosion degradation of ship hull steel plates accounting for local environmental conditions. Ocean Eng 163, 299–316.
[166] Amir, N.S., Yusof, N.Z., Ismail, R., 2021. Green and Sustainable Antibiofouling Coatings: A Review. Earth Env Sci 685, 012023.
[167] Oikonomou, E.K., Iatridi, Z., Moschakou, M., Damigos, P., Bokias, B., Kallitsis, J.K., 2012. Development of Cu^{2+}- and/or phosphonium-based polymeric biocidal materials and their potential application in antifouling paints. Prog Org Coat 75, 190–199.
[168] Amo, B., Blustein, G., P´erez, M., Garc´ıa, M., Dey´a, M., Stupak, M., Romagnoli, R., 2008. A multipurpose compound for protective coatings. Colloid Surface A 324, 58–64.
[169] Kitahara, K.I., Nakata, H., 2020. Plastic additives as tracers of microplastic sources in Japanese road dusts. Sci Total Environ 736, 139694.
[170] Andrady, A.L., Barnes, P.W., Bornman, J.F, 2022. Oxidation and fragmentation of plastics in a changing environment; from UV-radiation to biological degradation. Sci Total Environ 851, 158022.
[171] Salters, B., Piola, R., 2017. UVC Light for antifouling. Mar Technol Soc J 51,59–70.

Supplementary Materials

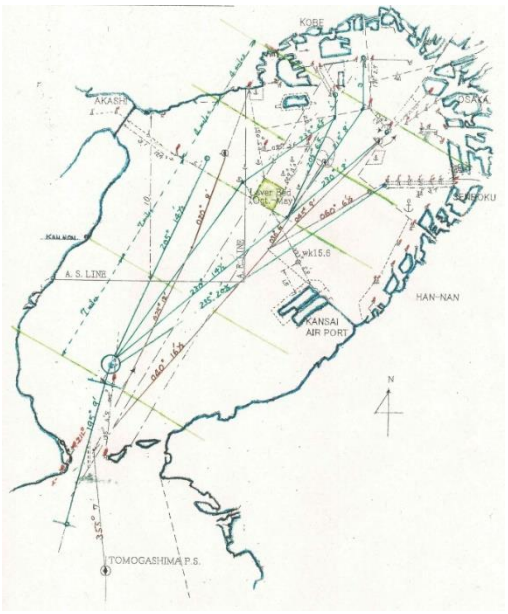

Fig.S1 Navigation routes in Osaka Bay (Protected by Professor Shoji Fujimoto)

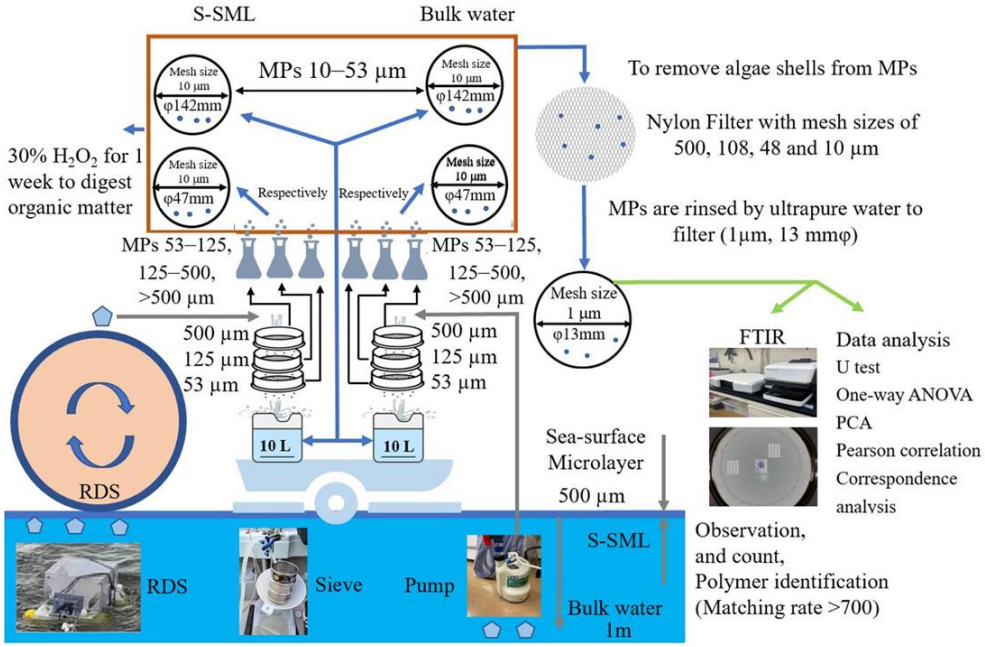

Fig.S2 Relevant filtering and dealing process of laboratory treatment for identifying microplastics

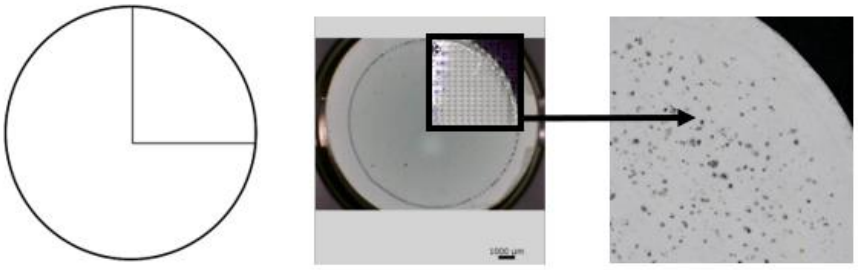

(a)

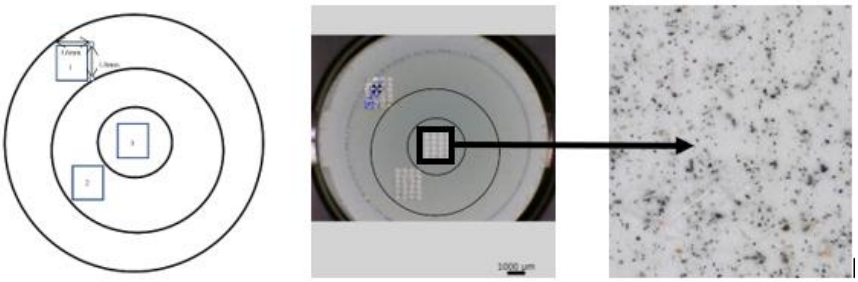

(b)

Fig.S3 Observing method of MPs on filters (a) MPs of >500, 125–500 and 53–125 μm (b) MPs of 10–53 μm

Tab.S1 Parameter of two kinds of selected marine paint and antifouling paints

No.	Paint name	Manufacture	Polymer Type	Metal
Paint 1	Sea Blue Ace paint for outer side and superstructures	Dainippon Paint Co., Ltd	PMMA	Ti
Paint 2	CCP Cleaning	Kanae paint Co., Ltd.	Acrylic resin	Cu, Zn
Paint 3	R Copper Red	Nippon Paint Co., Ltd	Acrylic resin	Cu, Zn
Paint 4	Seagull Alpha Red	Tohpe Co., Ltd	Acrylic resin	Cu, Zn
Paint 5	Alfrex Red	Dainippon PaintCo., Ltd	PMMA	Zn
Paint 6	Sea Blue Ace antifouling paint	Dainippon Paint Co., Ltd	PMMA	Ti, Zn

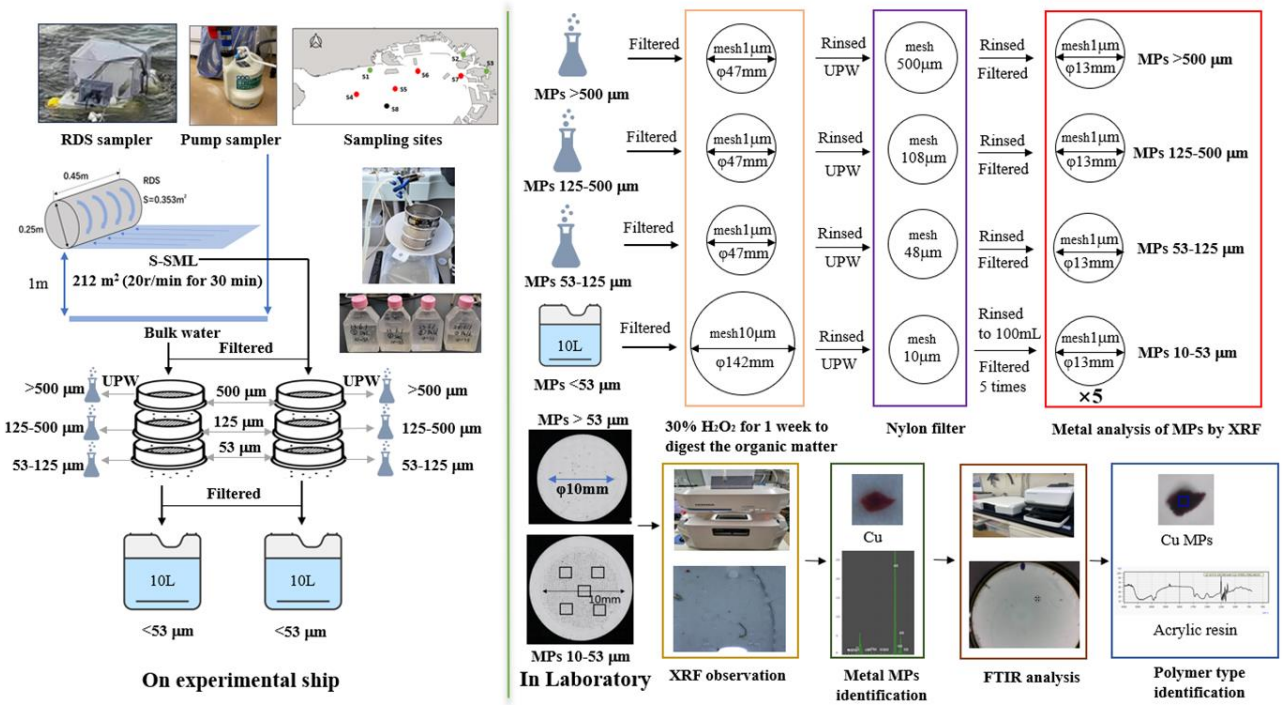

Fig.S4 Relevant water sampling and laboratory treatment for identifying metal MPs

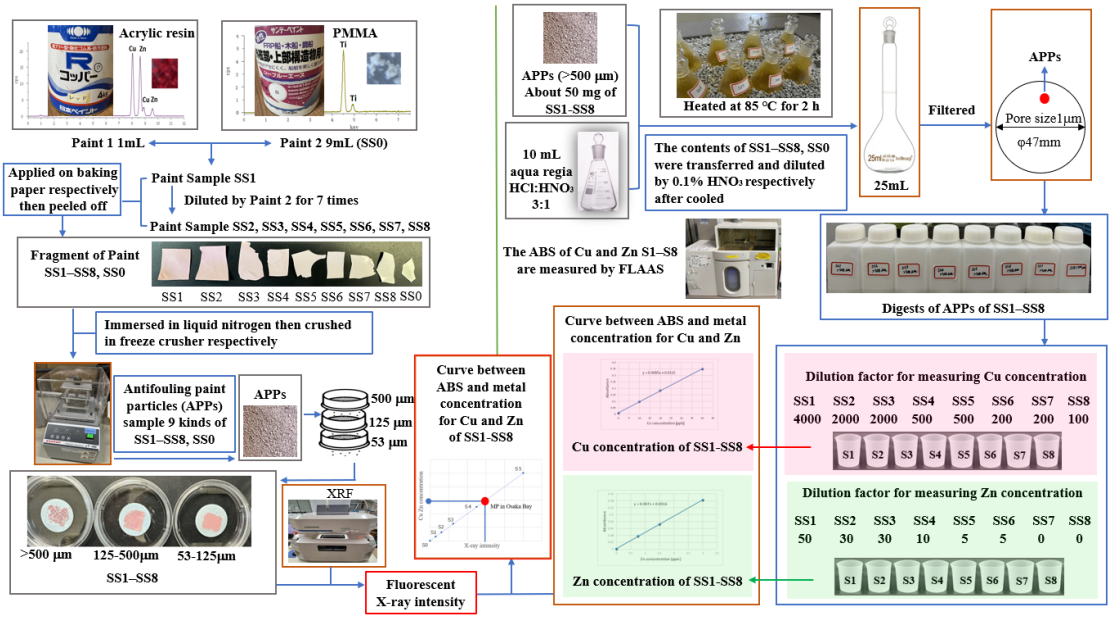

Fig.S5 Relevant process of measurement of Cu and Zn concentration in standard APPs and Metal MPs in Osaka Bay

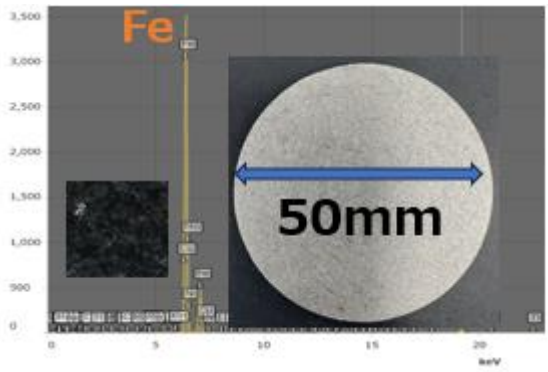

(a) Q235 steel disc and its m-XRF spectra

(b) Painted-Q235 steed

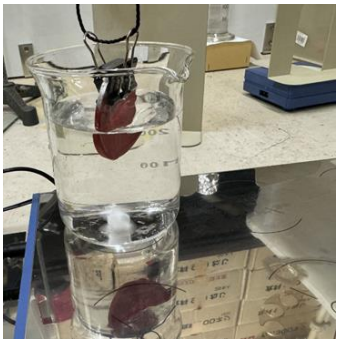

(c) APPs generation device in artificial seawater

Fig.S6 Relevant process of generating APPs from painted-Q235 steel in artificial seawater

Tab.S2 Cu ABS of SS1 APPs samples after digested in aqua regia

APPs sample	Size (μm)	Sequence	Mass (mg)	Dilution factor	Diluted Sample	Absorbance (ABS)	ABS1	ABS2	ABS3
					ultrapure water	0.0003	0.0003	0.0002	0.0004
					0.015M(0.1%) HNO_3	0.0082	0.0079	0.0086	0.0081
-	-	-	-	-	Cu solution(10ppb)	0.0785	0.0769	0.0795	0.0791
					Cu solution(20ppb)	0.1582	0.1567	0.1602	0.1577
					Cu solution(40ppb)	0.3389	0.3286	0.3578	0.3303
					ultrapure water	0.0005	0.0006	0.0005	0.0004
SS1-1-1	>500		59.1		S1-1-1	0.2274	0.2319	0.2246	0.2256
SS1-1-2	125-500	1	57.3	4000	S1-1-2	0.1953	0.1929	0.1967	0.1964
SS1-1-3	53-125		59.2		S1-1-3	0.2162	0.2127	0.2164	0.2195
SS1-1-4	<53		59.8		S1-1-4	0.2008	0.1978	0.2023	0.2022
					ultrapure water	0.0003	0.0003	0.0004	0.0004
					0.015M(0.1%) HNO_3	0.009	0.0079	0.0086	0.0106
-	-	-	-	-	Cu solution(10ppb)	0.0837	0.0769	0.0795	0.0948
					Cu solution(20ppb)	0.1677	0.1567	0.1602	0.1861
					Cu solution(40ppb)	0.3482	0.3286	0.3578	0.3582
					ultrapure water	0.0002	0.0003	0.0002	0.0002
SS1-2-1	>500	2	52.1	4000	S1-2-1	0.2063	0.2051	0.2072	0.2066
SS1-2-2	125-500	2	50.3	4000	S1-2-2	0.1566	0.1566	0.1565	0.1566
					ultrapure water	0.0003	0.0003	0.0004	0.0001
					0.015M(0.1%) HNO_3	0.0091	0.0125	0.0054	0.0095
-	-	-	-	-	Cu solution(10ppb)	0.0978	0.0935	0.0804	0.1194
					Cu solution(20ppb)	0.1845	0.1849	0.1576	0.211
					Cu solution(40ppb)	0.35	0.422	0.3485	0.2785
					ultrapure water	0.0002	0.0003	0.0002	0.0002
SS1-2-3	53-125	2	50.7		S1-2-3	0.2655	0.2484	0.2938	0.2542
SS1-2-4	<53		52		S1-2-4	0.1752	0.1756	0.1735	0.1765
SS1-3-1	>500		51.1	4000	S1-3-1	0.202	0.2008	0.2027	0.2025
SS1-3-2	125-500	3	51.2		S1-3-2	0.2584	0.2539	0.2594	0.2618
SS1-3-3	53-125		51.3		S1-3-3	0.236	0.2338	0.2405	0.2337
SS1-3-4	<53		50.3		S1-3-4	0.1821	0.1825	0.1789	0.185

Tab.S3 Cu concentrations in SS1 APPs with different sizes

Diluted digestates	Absorbance (ABS)	Cu concentration (ppb) in diluted digests (calculated by the calibration curve between ABS and standard Cu solution	Diluted factor	Cu concentration (ppb) in undiluted digests (calculated by multiplying the diluted factor by Cu concentration in diluted digests)	Volume of undiluted digests (mL)	Cu mass leached from APPs in undiluted digests (μg)	APPs samples	Size (μm)	Sequence	Mass of APPs samples (mg)	Cu concentration (mg/kg) in APPs samples (calculated by using Cu mass leached from APPs in undiluted digests dividing the mass of APPs)
S1-1-1	0.2274	27.4		109000		2740	SS1-1-1	>500		59.1	46300
S1-1-2	0.1953	23.5		94000		2350	SS1-1-2	125-500	1	57.3	41000
S1-1-3	0.2162	26.0		104000		2600	SS1-1-3	53-125		59.2	44000
S1-1-4	0.2008	24.2		96700		2420	SS1-1-4	<53		59.8	40400
S1-2-1	0.2063	23.9		95800		2390	SS1-2-1	>500		52.1	46000
S1-2-2	0.1566	18.1	4000	72400	25	1810	SS1-2-2	125-500	2	50.3	36000
S1-2-3	0.2655	29.9		120000		2990	SS1-2-3	53-125		50.7	58900
S1-2-4	0.1752	19.3		77000		1930	SS1-2-4	<53		52	37000
S1-3-1	0.202	22.4		89600		2240	SS1-3-1	>500		51.1	43900
S1-3-2	0.2584	29.0		116000		2900	SS1-3-2	125-500	3	51.2	56700
S1-3-3	0.236	26.4		106000		2640	SS1-3-3	53-125		51.3	51500
S1-3-4	0.1821	20.1		80300		2007	SS1-3-4	<53		50.3	39900

Tab.S4 Zn ABS of SS1 APP samples after digested in aqua regia

APPs sample	Size (μm)	Sequence	Mass (mg)	Dilution factor	Diluted Sample	Absorbance (ABS)	ABS1	ABS2	ABS3
					ultrapure water	0.0004	0.0005	0.0005	0.0003
					0.015M(0.1%) HNO_3	0.0007	0.001	0.0005	0.0006
-	-	-	-	-	Zn solution(0.75ppm)	0.038	0.0411	0.0333	0.0395
					Zn solution(1.5ppm)	0.0721	0.0736	0.0728	0.0699
					Zn solution(3ppb)	0.1422	0.1401	0.142	0.1446
					ultrapure water	0.0653	0.0663	0.0644	0.0651
SS1-1-1	>500		59.1		S1-1-1	0.0644	0.0654	0.0642	0.0637
SS1-1-2	125-500	1	57.3		S1-1-2	0.0635	0.0631	0.0633	0.064
SS1-1-3	53-125		59.2		S1-1-3	0.0709	0.0693	0.0714	0.0719
SS1-1-4	<53		59.8		S1-1-4	0.0734	0.07978	0.07023	0.07022
SS1-2-3	53-125	2	50.7		S1-2-3	0.0671	0.0689	0.0666	0.0659
SS1-2-4	<53		52	50	S1-2-4	0.0741	0.0744	0.0741	0.0739
SS1-3-1	>500		51.1		S1-3-1	0.0708	0.0708	0.0706	0.0709
SS1-3-2	125-500	3	51.2		S1-3-2	0.069	0.0696	0.0693	0.0682
SS1-3-3	53-125		51.3		S1-3-3	0.0662	0.0657	0.0669	0.066
SS1-3-4	<53		50.3		S1-3-4	0.0648	0.0661	0.0641	0.0643
					ultrapure water	0.0008	0.0009	0.0006	0.0009
					0.015M(0.1%) HNO_3	0.0005	0.0001	0.0005	0.001
-	-	-	-	-	Zn solution(0.75ppm)	0.0311	0.032	0.0317	0.0295
					Zn solution(1.5ppm)	0.0757	0.0768	0.0753	0.075
					Zn solution(3ppb)	0.1456	0.1434	0.1506	0.1427
					ultrapure water	0.0008	0.0009	0.0008	0.0007
SS1-2-1	>500	2	52.1	50	S1-2-1	0.0763	0.0771	0.0758	0.076
					ultrapure water	0.0008	0.0007	0.001	0.0007
					0.015M(0.1%) HNO_3	0.0008	0.0011	0.0006	0.0007
-	-	-	-	-	Zn solution(0.75ppm)	0.033	0.0324	0.0331	0.0334
					Zn solution(1.5ppm)	0.0554	0.0548	0.0567	0.0547
					Zn solution(3ppb)	0.1173	0.1205	0.1189	0.1125
					ultrapure water	0.0005	0.0005	0.0004	0.0006
SS1-2-2	125-500	2	50.3	50	S1-2-2	0.0614	0.0592	0.0626	0.0625

Tab.S5 Zn concentrations in SS1 APPs with different sizes

Diluted digestates	Absorbance (ABS)	Zn concentration (ppb) in diluted digests (calculated by the calibration curve between ABS and standard Cu solution	Diluted factor	Zn concentration (ppb) in undiluted digests (calculated by multiplying the diluted factor by Zn concentration in diluted digests)	Volume of undiluted digests (mL)	Zn mass leached from APPs in undiluted digests (μg)	APPs samples	Size (μm)	Sequence	Mass of APPs samples (mg)	Zn concentration (mg/kg) in APPs samples (calculated by using Zn mass leached from APPs in undiluted digests dividing the mass of APPs)
S1-1-1	0.0644	1340		66800		1670	SS1-1-1	>500		59.1	28300
S1-1-2	0.0635	1320		65900		1650	SS1-1-2	125-500	1	57.3	28700
S1-1-3	0.0709	1470		73700		1840	SS1-1-3	53-125		59.2	31100
S1-1-4	0.0734	1530		76400		1910	SS1-1-4	<53		59.8	31900
S1-2-1	0.0763	1580		78900		1970	SS1-2-1	>500		52.1	37900
S1-2-2	0.0614	1570	50	78500	25	1960	SS1-2-2	125-500	2	50.3	39000
S1-2-3	0.0671	1390		69700		1740	SS1-2-3	53-125		50.7	34400
S1-2-4	0.0741	1540		77100		1930	SS1-2-4	<53		52	37100
S1-3-1	0.0708	1470		73600		1840	SS1-3-1	>500		51.1	36000
S1-3-2	0.069	1430		71700		1790	SS1-3-2	125-500	3	51.2	35000
S1-3-3	0.0662	1370		68700		1720	SS1-3-3	53-125		51.3	33500
S1-3-4	0.0648	1340		67200		1680	SS1-3-4	<53		50.3	33400

Tab.S6 Cu and Zn concentrations in standard APPs of SS1 with different sizes

No.	Sample	Size (μm)	APPs Mass	Cu concentration (mg/kg)	Average Cu concentration (mg/kg)	Sig.	Zn concentration (mg/kg)	Average Zn concentration (mg/kg)	Sig.
	S1-1-1	>500	59.1	46300			28300		
1	S1-1-2	125-500	57.3	41000			28700		
	S1-1-3	53-125	59.2	44000			31100		
	S1-1-4	<53	59.8	40400			31900		
	S1-2-1	>500	52.1	46000	45100±6990	p>0.05	37900	33900±3250	p>0.05
2	S1-2-2	125-500	50.3	36000		(ANOVA)	39000		(ANOVA)
	S1-2-3	53-125	50.7	58900			34400		
	S1-2-4	<53	52	37000			37000		
	S1-3-1	>500	51.1	43900			36000		
3	S1-3-2	125-500	51.2	56700			35000		
	S1-3-3	53-125	51.3	51500			33500		
	S1-3-4	<53	50.3	39900			33400		

Tab.S7 Cu ABS of SS1–SS8 APPs of >500 μm after digested in aqua regia for the first time

No.	APPs sample	Cu-Zn volume percentage compared with Ti in APPs	Mass (mg)	Processing method	Dilution factor	Sample	Absorbance (ABS)	ABS1	ABS2	ABS3
1	-	-	-	-	-	ultrapure water	0.0003	0.0003	0.0003	0.0004
2				Standard Cu solution (1000 mg/L) was diluted to 100 mg /L with 0.1% HNO_3, then further diluted to make Cu concentrations of 40, 20, and 10ppb		0.015M(0.1%) HNO_3	0.0106	0.0107	0.0105	0.0103
3						Cu solution(10ppb)	0.0948	0.0965	0.0967	0.0912
4						Cu solution(20ppb)	0.1861	0.1859	0.1849	0.1874
5						Cu solution(40ppb)	0.3582	0.3555	0.338	0.3811
6	SS1	10%	52.1	APPs were heated in 10 mL Aqua regia at 85℃ for 2h, the content then was diluted to 25 mL by 0.015M HNO_3, after which these digests were filtered and diluted by 0.015M HNO_3 to different multiples	4000	S1	0.2063	0.2051	0.2072	0.2066
7	SS2	5%	51.2		2000	S2	0.2109	0.2095	0.2123	0.2108
8	SS3	2.5%	51.9		2000	S3	0.1055	0.1043	0.1055	0.1067
9	SS4	1.25%	51.5		500	S4	0.2242	0.2228	0.2246	0.2251
10	SS5	0.625%	51.1		500	S5	0.1059	0.1055	0.1061	0.1061
11	SS6	0.313%	51.6		200	S6	0.1501	0.1498	0.1497	0.1508
12	SS7	0.156%	50.9		200	S7	0.0767	0.0765	0.077	0.0766
13	SS8	0.0781%	51.9		100	S8	0.0557	0.0563	0.0549	0.0559
14	-	-	-	-	-	ultrapure water	0.0002	0.0003	0.0002	0.0002

Tab.S8 Cu concentrations in SS1–SS8 APPs of >500 μm measured for the first time

Diluted digestates	Absorbance (ABS)	Cu concentration (ppb) in diluted digests (calculated by the calibration curve between ABS and standard Cu solution	Diluted factor	Cu concentration (ppb) in undiluted digests (calculated by multiplying the diluted factor by Cu concentration in diluted digests)	Volume of undiluted digests (mL)	Cu mass leached from APPs in undiluted digests (μg)	APPs samples	Mass of APPs samples (mg)	Cu concentration (mg/kg) in APPs samples (calculated by using Cu mass leached from APPs in undiluted digests dividing the mass of APPs)
S1	0.2063	22.6	4000	90300	25	2230	SS1	52.1	43300
S2	0.2109	23.1	2000	4620	25	1160	SS2	51.2	22600
S3	0.1055	11	2000	22000	25	549	SS3	51.9	10600
S4	0.2242	24.6	500	12300	25	310	SS4	51.5	5980
S5	0.1059	11	500	5520	25	138	SS5	51.1	2700
S6	0.1501	16.1	200	3220	25	80.6	SS6	51.6	1560
S7	0.0767	7.69	200	1530	25	38.4	SS7	50.9	754
S8	0.0557	5.26	100	526	25	13.2	SS8	51.9	254

Tab.S9 Cu ABS of SS1–SS8 APPs of >500 μm after digested in aqua regia for the second time

No.	APPs sample	Cu-Zn volume percentage compared with Ti in APPs	Mass (mg)	Processing method	Dilution factor	Sample	Absorbance (ABS)	ABS1	ABS2	ABS3
1	-	-	-	-	-	ultrapure water	0.0003	0.0002	0.0004	0.0002
2				Standard Cu solution (1000 mg/L) was diluted to 100 mg /L with 0.1% HNO_3, then further diluted to make Cu concentrations of 40, 20, and 10ppb		0.015M(0.1%) HNO_3	0.0102	0.0129	0.0091	0.0086
3						Cu solution(10ppb)	0.0861	0.0855	0.0865	0.0864
4						Cu solution(20ppb)	0.1583	0.1567	0.1601	0.1581
5						Cu solution(40ppb)	0.2963	0.296	0.2964	0.2965
6	SS1	10%	50.3	APPs were heated in 10 mL Aqua regia at 85℃ for 2h, the content then was diluted to 25 mL by 0.015M HNO_3, after which these digests were filtered and diluted by 0.015M HNO_3 to different multiples	4000	S1	0.1566	0.1566	0.1565	0.1566
7	SS2	5%	51.9		2000	S2	0.1848	0.1757	0.1897	0.1889
8	SS3	2.5%	50.4		2000	S3	0.0909	0.0914	0.0904	0.0909
9	SS4	1.25%	50.5		500	S4	0.1954	0.1886	0.1972	0.2004
10	SS5	0.625%	51.7		500	S5	0.1049	0.1054	0.1040	0.1052
11	SS6	0.313%	50.9		200	S6	0.1275	0.129	0.1269	0.1265
12	SS7	0.156%	52		200	S7	0.063	0.0628	0.0615	0.0647
13	SS8	0.0781%	50.8		100	S8	0.0513	0.0515	0.0515	0.0508
14	-	-	-	-	-	ultrapure water	0.0003	0.0001	0.0003	0.0004

Tab.S10 Cu concentrations in SS1–SS8 APPs of >500 μm measured for the second time

Diluted digestates	Absorbance (ABS)	Cu concentration (ppb) in diluted digests (calculated by the calibration curve between ABS and standard Cu solution	Diluted factor	Cu concentration (ppb) in undiluted digests (calculated by multiplying the diluted factor by Cu concentration in diluted digests)	Volume of undiluted digests (mL)	Cu mass leached from APPs in undiluted digests (μg)	APPs samples	Mass of APPs samples (mg)	Cu concentration (mg/kg) in APPs samples (calculated by using Cu mass leached from APPs in undiluted digests dividing the mass of APPs)
S1	0.1566	20.2	4000	80900	25	202	SS1	50.3	40200
S2	0.1848	24.2	2000	48400	25	1210	SS2	51.9	23300
S3	0.0909	11	2000	21900	25	548	SS3	50.4	10900
S4	0.1954	25.7	500	12800	25	321	SS4	50.5	6350
S5	0.1049	12.9	500	6470	25	162	SS5	51.7	3130
S6	0.1275	16.1	200	323	25	80.6	SS6	50.9	1580
S7	0.063	7.04	200	1410	25	35.2	SS7	52	677
S8	0.0513	5.39	100	539	25	13.5	SS8	50.8	265

Tab.S11 Cu ABS of SS1–SS8 APPs of >500 μm after digested in aqua regia for the third time

No.	APPs sample	Cu-Zn volume percentage compared with Ti in APPs	Mass (mg)	Processing method	Dilution factor	Sample	Absorbance (ABS)	ABS1	ABS2	ABS3
1	-	-	-	-	-	ultrapure water	0.0003	0.0003	0.0003	0.0002
2				Standard Cu solution (1000 mg/L) was diluted to 100 mg /L with 0.1% HNO_3, then further diluted to make Cu concentrations of 40, 20, and 10ppb		0.015M(0.1%) HNO_3	0.0087	0.0087	0.0096	0.0078
3						Cu solution(10ppb)	0.0946	0.0949	0.0942	0.0946
4						Cu solution(20ppb)	0.1822	0.1825	0.1824	0.1817
5						Cu solution(40ppb)	0.3656	0.3668	0.3643	0.3658
6	SS1	10%	55.9	APPs were heated in 10 mL Aqua regia at 85℃ for 2h, the content then was diluted to 25 mL by 0.015M HNO_3, after which these digests were filtered and diluted by 0.015M HNO_3 to different multiples	4000	S1	0.2381	0.2417	0.2368	0.2357
7	SS2	5%	55.6		2000	S2	0.2407	0.2429	0.2412	0.2381
8	SS3	2.5%	51.7		2000	S3	0.1418	0.1422	0.1417	0.1414
9	SS4	1.25%	50.1		500	S4	0.2873	0.293	0.2843	0.2847
10	SS5	0.625%	50.8		500	S5	0.1321	0.1292	0.1336	0.1336
11	SS6	0.313%	50.2		200	S6	0.1515	0.1488	0.1551	0.1506
12	SS7	0.156%	58		200	S7	0.0777	0.0762	0.07062	0.088628
13	SS8	0.0781%	50.8		100	S8	0.0751	0.0761	0.0776	0.0716
14	-	-	-	-	-	ultrapure water	0.0003	0.0003	0.0003	0.0002

Tab.S12 Cu concentrations in SS1–SS8 APPs of >500 μm measured for the third time

Diluted digestates	Absorbance (ABS)	Cu concentration (ppb) in diluted digests (calculated by the calibration curve between ABS and standard Cu solution	Diluted factor	Cu concentration (ppb) in undiluted digests (calculated by multiplying the diluted factor by Cu concentration in diluted digests)	Volume of undiluted digests (mL)	Cu mass leached from APPs in undiluted digests (μg)	APPs samples	Mass of APPs samples (mg)	Cu concentration (mg/kg) in APPs samples (calculated by using Cu mass leached from APPs in undiluted digests dividing the mass of APPs)
S1	0.2381	26	4000	104000	25	2600	SS1	55.9	46600
S2	0.2407	26.3	2000	52700	25	1320	SS2	55.6	23700
S3	0.1418	15.2	2000	30400	25	761	SS3	51.7	14700
S4	0.2873	31.6	500	15800	25	394	SS4	50.1	7870
S5	0.1321	14.1	500	7060	25	177	SS5	50.8	3470
S6	0.1515	16.3	200	3260	25	81.5	SS6	50.2	1620
S7	0.0777	8.01	200	1600	25	40.1	SS7	58	690
S8	0.0751	7.72	100	772	25	19.3	SS8	56.8	339

Tab.S13 Zn ABS of SS1–SS8 APPs of >500 μm after digested in aqua regia for the first time

No.	APPs sample	Cu-Zn volume percentage compared with Ti in APPs	Mass (mg)	Processing method	Dilution factor	Sample	Absorbance (ABS)	ABS1	ABS2	ABS3
1	-	-	-	-	-	ultrapure water	0.0008	0.0009	0.0006	0.0009
2				Standard Zn solution (1000 mg/L) was diluted to 100 mg /L with 0.1% HNO3, then further diluted to make Zn concentrations of 3, 1.5, and 0.75 ppm		0.015M(0.1%) HNO3	0.0008	0.001	0.0005	0.009
3						Zn solution(0.75ppm)	0.0311	0.032	0.0317	0.0295
4						Zn solution(1.5ppm)	0.0757	0.0768	0.0753	0.075
5						Zn solution(3ppm)	0.1456	0.1434	0.1506	0.1427
6	SS1	10%	52.1	APPs were heated in 10 mL Aqua regia at 85℃ for 2h, the content then was diluted to 25 mL by 0.015M HNO3, after which these digests were filtered and diluted by 0.015M HNO3 to different multiples	50	S1	0.0763	0.0771	0.0758	0.076
7	SS2	5%	51.2		30	S2	0.0659	0.0656	0.0663	0.0658
8	SS3	2.5%	51.9		30	S3	0.0342	0.0348	0.0342	0.0337
9	SS4	1.25%	51.5		10	S4	0.0544	0.0552	0.0543	0.0536
10	SS5	0.625%	51.1		5	S5	0.051	0.0521	0.0514	0.0495
11	SS6	0.313%	51.6		5	S6	0.0243	0.0243	0.0244	0.0241
12	SS7	0.156%	50.9		0	S7	0.0518	0.0512	0.0516	0.0527
13	SS8	0.0781%	51.9		0	S8	0.0239	0.0235	0.0243	0.024
14	-	-	-	-	-	ultrapure water	0.0008	0.0009	0.0008	0.0007

Tab.S14 Zn concentrations in SS1–SS8 APPs of >500 μm measured for the first time

Diluted digestates	Absorbance (ABS)	Zn concentration (ppb) in diluted digests (calculated by the calibration curve between ABS and standard Zn solution)	Diluted factor	Zn concentration (ppb) in undiluted digests (calculated by multiplying the diluted factor by Cu concentration in diluted digests)	Volume of undiluted digests (mL)	Zn mass leached from APPs in undiluted digests (μg)	APPs samples	Mass of APPs samples (mg)	Zn concentration (mg/kg) in APPs samples (calculated by using Cu mass leached from APPs in undiluted digests dividing the mass of APPs)
S1	0.0763	1580	50	79000	25	1970	SS1	52.1	37900
S2	0.0659	1370	30	41000	25	1030	SS2	51.2	20030
S3	0.0342	720	30	21600	25	540	SS3	51.9	10400
S4	0.0544	1130	10	11300	25	283	SS4	51.5	5500
S5	0.051	1060	5	5320	25	133	SS5	51.1	2600
S6	0.0243	518	5	2590	25	64.8	SS6	51.6	1260
S7	0.0518	1080	0	1080	25	27	SS7	50.9	530
S8	0.0239	510	0	510	25	12.8	SS8	51.9	245

Tab.S15 Zn ABS of SS1–SS8 APPs of >500 μm after digested in aqua regia for the second time

No.	APPs sample	Cu-Zn volume percentage compared with Ti in APPs	Mass (mg)	Processing method	Dilution factor	Sample	Absorbance (ABS)	ABS1	ABS2	ABS3
1	-	-	-	-	-	ultrapure water	0.0008	0.0007	0.001	0.0007
2				Standard Zn solution (1000 mg/L) was diluted to 100 mg /L with 0.1% HNO_3, then further diluted to make Zn concentrations of 3, 1.5, and 0.75 ppm		0.015M(0.1%) HNO_3	0.0008	0.0011	0.0006	0.0007
3						Zn solution(0.75ppm)	0.033	0.0324	0.0331	0.0334
4						Zn solution(1.5ppm)	0.0554	0.0548	0.0567	0.0547
5						Zn solution(3ppm)	0.1173	0.1205	0.1189	0.1125
6	SS1	10%	50.3	APPs were heated in 10 mL Aqua regia at 85℃ for 2h, the content then was diluted to 25 mL by 0.015M HNO_3, after which these digests were filtered and diluted by 0.015M HNO_3 to different multiples	50	S1	0.0614	0.0592	0.0626	0.0625
7	SS2	5%	51.9		30	S2	0.0586	0.0595	0.0576	0.0587
8	SS3	2.5%	50.4		30	S3	0.0257	0.0255	0.0255	0.0261
9	SS4	1.25%	50.5		10	S4	0.0468	0.0436	0.0452	0.0516
10	SS5	0.625%	51.7		5	S5	0.0469	0.0452	0.0423	0.0532
11	SS6	0.313%	50.9		5	S6	0.0218	0.0197	0.0273	0.0184
12	SS7	0.156%	52		0	S7	0.041	0.047	0.0359	0.0401
13	SS8	0.0781%	50.8		0	S8	0.018	0.0141	0.0144	0.0255
14	-	-	-	-	-	ultrapure water	0.0005	0.0005	0.0004	0.0006

Tab.S16 Zn concentrations in SS1–SS8 APPs of >500 μm measured for the second time

Diluted digestates	Absorbance (ABS)	Zn concentration (ppb) in diluted digests (calculated by the calibration curve between ABS and standard Zn solution)	Diluted factor	Zn concentration (ppb) in undiluted digests (calculated by multiplying the diluted factor by Cu concentration in diluted digests)	Volume of undiluted digests (mL)	Zn mass leached from APPs in undiluted digests (μg)	APPs samples	Mass of APPs samples (mg)	Zn concentration (mg/kg) in APPs samples (calculated by using Cu mass leached from APPs in undiluted digests dividing the mass of APPs)
S1	0.0614	1570	50	7850	25	1960	SS1	50.3	39000
S2	0.0586	1500	30	44900	25	1120	SS2	51.9	21600
S3	0.0257	637	30	19100	25	477	SS3	50.4	9480
S4	0.0468	1190	10	11900	25	296	SS4	50.5	5880
S5	0.0469	1190	5	5950	25	148	SS5	51.7	2880
S6	0.0218	535	5	2680	25	66.9	SS6	50.9	1310
S7	0.041	1040	0	1040	25	25.9	SS7	52	498
S8	0.018	436	0	436	25	10.9	SS8	50.8	214

Tab.S17 Zn ABS of SS1–SS8 APPs of >500 μm after digested in aqua regia for the third time

No.	APPs sample	Cu-Zn volume percentage compared with Ti in APPs	Mass (mg)	Processing method	Dilution factor	Sample	Absorbance (ABS)	ABS1	ABS2	ABS3
1	-	-	-	-	-	ultrapure water	0.0005	0.0006	0.0004	0.0005
2				Standard Zn solution (1000 mg/L) was diluted to 100 mg /L with 0.1% HNO_3, then further diluted to make Zn concentrations of 3, 1.5, and 0.75 ppm		0.015M(0.1%) HNO_3	0.0008	0.0008	0.0007	0.0009
3						Zn solution(0.75ppm)	0.0379	0.0369	0.0381	0.0386
4						Zn solution(1.5ppm)	0.08	0.0791	0.0802	0.0807
5						Zn solution(3ppm)	0.1577	0.1547	0.1596	0.1589
6	SS1	10%	55.9	APPs were heated in 10 mL Aqua regia at 85℃ for 2h, the content then was diluted to 25 mL by 0.015M HNO_3, after which these digests were filtered and diluted by 0.015M HNO_3 to different multiples	50	S1	0.086	0.0846	0.0867	0.0867
7	SS2	5%	55.6		30	S2	0.0686	0.0645	0.0642	0.0771
8	SS3	2.5%	51.7		30	S3	0.0329	0.0296	0.0376	0.0314
9	SS4	1.25%	50.1		10	S4	0.063	0.0592	0.068	0.0618
10	SS5	0.625%	50.8		5	S5	0.0519	0.0448	0.0551	0.0559
11	SS6	0.313%	50.2		5	S6	0.0265	0.0118	0.0301	0.0375
12	SS7	0.156%	58		0	S7	0.0593	0.057	0.058	0.0629
13	SS8	0.0781%	50.8		0	S8	0.0245	0.024	0.0223	0.0272
14	-	-	-	-	-	ultrapure water	0.0006	0.0007	0.0005	0.0007

Tab.S18 Zn concentrations in SS1–SS8 APPs of >500 μm measured for the third time

Diluted digestates	Absorbance (ABS)	Zn concentration (ppb) in diluted digests (calculated by the calibration curve between ABS and standard Zn solution)	Diluted factor	Zn concentration (ppb) in undiluted digests (calculated by multiplying the diluted factor by Cu concentration in diluted digests)	Volume of undiluted digests (mL)	Zn mass leached from APPs in undiluted digests (μg)	APPs samples	Mass of APPs samples (mg)	Zn concentration (mg/kg) in APPs samples (calculated by using Cu mass leached from APPs in undiluted digests dividing the mass of APPs)
S1	0.086	1630	50	81700	25	2040	SS1	55.9	36500
S2	0.0686	1300	30	39100	25	977	SS2	55.6	17600
S3	0.0329	623	30	18700	25	468	SS3	51.7	9050
S4	0.063	1200	10	12000	25	299	SS4	50.1	5970
S5	0.0519	984	5	4920	25	123	SS5	50.8	2420
S6	0.0265	502	5	2510	25	62.7	SS6	50.2	1230
S7	0.0593	1130	0	1120	25	28.1	SS7	58	485
S8	0.0245	464	0	464	25	11.6	SS8	50.8	228

Tab.S19 Concentrations of Cu and Zn (mg/kg) in SS1-SS8 standard APPs > 500 μm

Standard APPs samples	Cu concentration (mg/kg)					Zn concentration (mg/kg)				
	1st	2nd	3rd	Average	Std	1st	2nd	3rd	Average	Std
SS1	43300	40200	46600	43400	2590	37900	39000	36500	37800	1020
SS2	22600	23300	23700	23200	462	20000	21600	17600	19800	1670
SS3	10600	10900	14700	12100	1870	10400	9480	9050	9650	568
SS4	5980	6350	7870	6730	818	5500	5880	5970	5780	203
SS5	2700	3130	3470	3100	315	2600	2880	2420	2630	190
SS6	1560	1580	1620	1590	24.7	1230	1310	1230	1260	35.2
SS7	754	677	690	707	33.7	530	498	485	504	18.9
SS8	254	265	339	286	37.7	245	214	228	229	12.6

Tab.S20 Average of Cu X-ray intensity values of SS1-SS8 standard APPs with different sizes

APP	X-ray intensity value (cps/mA)												
	5mm	500-5000μm	500 μm	130-500 μm	130 μm	120 μm	110 μm	100 μm	90 μm	80 μm	70 μm	60 μm	50 μm
SS1	147000	129000	125000	109000	94800	80300	66000	54500	47800	42800	38200	21600	16800
SS2	78700	73800	70500	61800	54100	43800	323000	292000	27000	23800	20200	12900	10100
SS3	42100	36200	34800	29800	289000	23400	17200	15800	14500	11200	9220	7310	5440
SS4	20080	19500	18900	14000	13100	10400	9390	7890	6760	6610	4710	4570	3440.
SS5	13900	11700	10700	8670	6190	713	5910	5210	4200	3070	2900	1270	1240
SS6	7210	7110	6370	4840	3030	4560	33000	2510	2200	1200	1470	10000	549
SS7	328	2830	2350	2150	2060	1430	1280	1208	1100	924	757	645	249
SS8	1950	1900	1790	1490	1260	900	729	722	596	565	335	274	209

Tab.S21 Average of Zn X-ray intensity value of SS1-SS8 standard APPs with different sizes

APP	X-ray intensity value (cps/mA)												
	5mm	500-5000μm	500 μm	130-500 μm	130 μm	120 μm	110 μm	100 μm	90 μm	80 μm	70 μm	60 μm	50 μm
SS1	156000	147000	132000	102000	93500	85400	64400	52600	453009	41900	35200	28300	13700
SS2	85300	81400	72900	60300	51300	44400	33100	28700	25200	22200	19400	16100	8290
SS3	42100	39400	36700	31900	26100	23600	17300	14300	13300	11900	9280	7340	4580
SS4	23400	21600	21200	13700	12500	13100	9900	7620	73401	6350	4980	4300	2250
SS5	13900	12200	11600	8780	6680	6320	6050	4210	4200	2860	28202	2120	1100
SS6	6860	6420	6310	4050	3310	4460	3040	2580	2460	2300	1450	882	852
SS7	3600	3090	2460	2020	1510	1780	1340	1190	1070	783	665	617	495
SS8	1730	2320	2010	1600	1160	770	746	610	459	420	362	328	204

Acknowledgments

I would like to give my heartfelt and faithful thanks to all of them who spared their valuable time, knowledge, interests and supports on my study and work during my doctoral course.

First of all, I wish to express my sincere thanks, respects and show my deep sense of gratitude to my research advisor Professor Hideo Okamura, Research Center for Inland Seas, Kobe University, Japan, for guiding me with deep interest, constant encouragement, precious advices, advanced experiment methods and providing new ideas in the research field with lots of patience throughout all my study period.

I also owe my special thanks and deep appreciate to my associate advisor Professor Takeshi Nakano, Graduate School of Maritime Sciences, Kobe University, Japan, for his valuable direction, forward looking suggestions, especially his warm care and kindness which give me the warmth and strength to move forward.

I would like to show my heartfelt thanks to Professor Shoji Fujimoto, Professor Kazuyo Yamaji, Professor Hiroki Hotta, Graduate School of Maritime Sciences, Kobe University, Japan, Doctor Christina Emmanouil, Aristotle University of Thessaloniki, Greece, for their carefully and patiently reviewing for my doctoral thesis and providing valuable suggestions.

I wish to express my most heartily thanks to Professor Issey Osaka, Toyama Prefectural University, Japan, Professor Chee Kong Yap, Universiti Putra Malaysia, Malaysia, for their guidance and assistance on my experiment and paper writing.

We would like to thank Professor Koji Hamasaki, The University of Tokyo, Japan, for helping us making the RDS-KU1 to collect samples from the S-SML. I also thank Captain Katsumi Aoyama and Keisuke Kitajima, Kobe University Training Ship HAKUO, Japan, for helping us to collect the seawater sampling.

I acknowledge my special gratefulness to Professor Yoshifumi Horie, Professor Christopher Andre Gomez, Professor Bradak-hayashi Balazs, Professor Haruko, Okada, Graduate School of Maritime Sciences, Kobe University, Japan, and Professor Caixiang Gu, Shanghai Maritime University, China, for their kindness, guidance, encouragements and providing valuable suggestions in my research as well as my life.

Acknowledgments are also made to our lab members and colleagues, Doctor Miho Nomura, who provided detailed guidance on experiment methods and operation of experimental equipment, Mr. Hirofumi Yanai, who completed the complex experiments together as my experiment partner, and Mr. Akinori Nakamura, Mr. Kensuke Mitsunaga, Mr. Sou Takeuchi, Mr. Ryosuke Nozaki, Mr. Yuto Chihaya, Miss Ayaka, Sawada, Mr. Yusei Matsuo and Miss Saki Fujimoto, for their kind helps.

Especially, I wish to show my deepest appreciates, thanks and love to my parents in heaven, I am grateful for their great love and support for me. I will try my best to go ahead with the strength and courage they have given me.

I would also like to thank my dear auntie Senior Engineer Congxiao Zhou, Shanghai Maritime University, China and her husband Professor Xiuzhong Xu, Shanghai Maritime University, China. Thanks for their care and encouragement for me,

which has become the bright and beautiful light that illuminates my life.

A lot of thanks and appreciates are expressed to my important and lovely dear friend Doctor Dongping Shen, Graduate School of Maritime Sciences, Kobe University, Japan. Thanks for his kindness and friendship towards me in my daily life, as well as his wise advice when I was confused, which will always illuminate the direction for me to move forward. Hoping our friendship and linkage can continue forever.

I also appreciate for my dear friend Mr. Guobin Wang, who gave me warmth, care and help when I was in difficulties and darkness. Thanks to his kindness and friendship, I have gained the courage and strength to face difficulties. Looking forward to a friendship that can cross stages of our lives.

I really want to thank my dear student and friend Mr. Jiahang Li, who always supports and encourages me with his smile, care, and sincerity and shares the pleasure and happiness during my work and study period. May our friendship be everlasting.

I am truly grateful for the encourage, care and support from my dear friend, Doctor Hongze Liu, Graduate School of Maritime Sciences, Kobe University, Japan.

I would like to thank my friends in Graduate School of Maritime Sciences, Kobe University, Japan, Doctor Miao Zhang, who always provides delicious dinner, Mr. Yanpeng Song and Mr. Jiale Liu, who always make my daily life pleasure and fun, Mr. Zhimeng Wang, Mr. Tianyang Li, Mr. Haoran Zhou, Mr. Yiming Zhang and Miss Hao Jiang, who always enjoy and share wonderful campus life with me.

Finally, I would like to thank Japanese government and Kobe University for award of SPRING for my research, study, and life during the doctoral period, and award of Umeki Foundation for conference travel supports. I also want to thank my motherland China and the Chinese government for providing me with a support of wisdom, freedom, and prosperity.

Papers Published and Submitted

1. **Mi Zhou**, Hirofumi Yanai, Chee Kong Yap, Christina Emmanouil and Hideo Okamura. (2023) Anthropogenic Microparticles in Sea-Surface Microlayer in Osaka Bay, Japan. *Journal of Xenobiotics*, 13: 685–703.
   DOI: org/10.3390/jox13040044
2. **Mi Zhou**, Issey Osaka, Kotaro Hashimoto, Chee Kong Yap, Christina Emmanouil, Takeshi Nakano and Hideo Okamura. (2024) Co-occurrence of microplastics and microparticles containing Cu and Zn and other heavy metals in sea-surface microlayer in Osaka Bay, Japan. *Journal of Hazardous Materials*, 480: 136085.
   DOI: org/10.1016/j.jhazmat.2024.136085
3. **Mi Zhou** and Hideo Okamura. (2024) Microparticles containing heavy metals floating in the sea-surface microlayer in Osaka Bay, Japan. (In Japanese). Journal of The Japan Institute of Marine Engineering, 59 (5): 548–552.
   DOI: org/10.5988/jime.59.548